

This is to certify that the

thesis entitled

THE TEMPERATURE DEPENDENCE OF THE RESISTIVITY

THE NOBLE METALS FROM 0.03 TO 9 K

presented by

STEVEN DALE STEENWYK

has been accepted towards fulfillment of the requirements for

PH.D. degree in PHYSICS

Date November 10, 1980

O-7639



OVERDUE FINES: 25¢ per day per item

RETURNING LIBRARY MATERIALS:

Place in book return to remove charge from circulation records

THE TEMPERATURE DEPENDENCE OF THE RESISTIVITY THE NOBLE METALS FROM 0.03 to 9 K

by

STEVEN DALE STEENWYK

A DISSERTATION

Submitted to
Michigan State University
in partial fulfillment of the requirements
for the degree of

DOCTOR OF PHILOSOPHY

Department of Physics

ABSTRACT

THE TEMPERATURE DEPENDENCE OF THE RESISTIVITY OF THE NOBLE METALS FROM 0.03 TO 9 K

bу

STEVEN DALE STEENWYK

We present here a thorough investigation of the temperature dependent resistivity $\rho(T)$ of the noble metals for temperatures from 0.3 K - 9 K. We experimentally determine the magnitude of electronelectron scattering contributions as well as the magnitude and mathematical form of the phonon contribution and its variation with strain and impurity content. We review the basics of the relevant theory including some of the recent calculations of the contribution from various scattering mechanisms, specifically, scattering of electrons by other electrons and by phonons. We consider at length the fundamental effects of the dominant contributors to the residual resistivity, impurity and dislocation scattering, in light of the anisotropy in k-space of the relaxation time determined by these mechanisms. We performed measurements of the resistivity to a precision of one ppm on samples ranging from extremely pure single crystals of Cu and Ag to dilute polycrystalline alloys of Cu with Ag. The techniques required to prepare such samples and to make very high precision measurements are discussed. In particular, treatment is given to some of the unique problems faced in using a SQUID based measuring system on samples of nano-ohm resistance with special attention paid to the use of superconducting chokes and transformers to control the electrical response

time of the circuit. The results of our measurements give substantial verification of the calculations of the e-e scattering contribution to $\rho(T)$. Of special interest is the serendipitious verification of the theory of Bermann, Kaveh and Wiser † explaining the origin of the T⁴ behavior we had observed in the earliest work. This theory reproduces a nearly T⁴ behavior by a combination of electron-electron and electronphonon scattering. Our data fit their equations very well. While we expected to find, and indeed did find, the effect of dislocation to be a reduction in the phonon scattering, we did not anticipate their prediction that dislocations would increase the electron-electron contribution. Our measurements provide convincing verification of this prediction. Finally, we believe we have succeeded in isolating the e-e contribution to copper at very low temperatures (T < 1 K), but have also uncovered some peculiar behavior at the very lowest temperatures. This includes a shoulder in the resistivity of very pure Ag and a very low temperature resistance minimum in Cu.

⁺A. Bermann, M. Kaveh and N. Wiser, J. Phys. F <u>10</u>, L71 (1980).

TO MY WIFE, NANCY,

WHOSE PATIENT AND LOVING SUPPORT

SUSTAINED ME

ACKNOWLEDGEMENTS

I am sincerely grateful to Professor Peter A. Schroeder for his guidance and assistance during the experimental work, and the writing of this dissertation. I shall particularly remember his willingness to forgo his professor's prerogatives to take part in experimental runs even at inconvient hours. I am very glad for the opportunity to work with Dr. John A. Rowlands on the strained copper experiments, and thankful for our many enlightening discussions. I am grateful to Dr. William P. Pratt, Jr. for his cheerful advice, especially concerning experimental techniques. I sincerely appreciate the assistance of my fellow student Vernon Heinen for his assistance in running the dilution refrigerator. I an indebted to my typist Delores Sullivan for the fine work and the extra effort made to meet a tight deadline. I gratefully acknowledge the financial support of the National Science Foundation during my entire term of study. I wish to thank John and Laurey Zwart and my wife, Nancy, for their assistance with some of the figures and John especially for taking care of a number of details in my absence.

TABLE OF CONTENTS

			Pa	.ge
LIST	OF T	ABLES	•	vi
LIST	OF F	IGURES	. v	ii
CHAPTI	ER			
I.	BAC	KGROUND AND THEORY		1
	Α.	Some General Aspects		2
	В.	Specific Scattering Mechanisms		11
		1) Impurity Scattering		11
		2) Phonon Scattering		13
		3) Scattering by Dislocations	•	20
		4) Electron-Electron Scattering	•	22
	c.	Concurrent Scattering Mechanisms	•	26
	D.	A Review of Experimental and Theoretical Literature	•	38
		1) Some Experimental Results		39
		2) Theoretical Developments		55
		3) Determinations of Relaxation Time Anisotrophy .		63
II.	EXP	ERIMENTAL METHOD AND APPARATUS	•	68
	Α.	The SQUID Null Detector System	•	68
	В.	Special Problems with Very Low Resistance Samples .	•	75
		1) Contact Resistance		75
		2) Response Time Control with Superconducting		
		Transformans and Chokes		70

CHAPTER			
		3) Enhanced Noise Pickup 84	
	C.	Design and Construction of a He ⁴ Cryostat	
		1) Mechanical Construction 85	
		2) SQUIDs and Standard Resistors 89	
		3) Thermometry	
	D.	Sample Preparation	
III.	RES	ULTS	
	Α.	A Study of the Sample Dependence of BT^4 103	
	В.	Analysis in Terms of the Theory of Bergmann, Kaveh and Wiser	
		1) Reanalysis of Published Data	
		2) Analysis of New Data for Strained Cu 119	
	c.	Electron-Electron Scattering	
	D.	Anomolous Behavior at Ultra-low Temperatures 131	
	Sum	mary and Conclusion	
APPENDICES			
	A	THERMOELECTRIC RATIO MEASUREMENTS ON STRAINED Cu 137	
	В	DERIVATION OF USEFUL EXPRESSIONS FOR SUPERCONDUCTING TRANSFORMERS AND PARALLEL INDUCTORS USED IN SQUID CIRCUITS	
	С	THERMOMETRY PROGRAM FOR HP67 PROGRAMMABLE CALCULATOR . 147	
REFERENCES			

LIST OF TABLES

Table			Page
1.1	Some published experimental results for Ag	•	. 42
1.2	Some published experimental results for Au		. 44
1.3	Some published experimental results for Cu	•	. 45
1.4	Theoretical estimates of the e-e contribution to the resistivity	•	. 59
1.5	Relaxation time ratio for scattering by phonons in Cu	•	. 66
1.6	Relaxation time ratio for dislocation scattering in Cu	•	. 67
2.1	Source and purity of sample materials	•	. 96
2.2	Sample information		. 9 8
3.1	Reanalysis of published data in terms of Equations (3.8) and (3.9)		. 117
3.2	Typical fits to various equations for Cu lla	•	. 121
3.3	Fitting parameter for $CuAg^2$ $u(\rho_0 = 3.49534 \text{ n}\Omega\text{cm})$. 122
3.4	Values of the fitting parameters A, A', C, C' and N for strained samples		. 124

LIST OF FIGURES

Figure			Pa	age
1.1(a)	A noble metal Fermi surface within the first Brillouin zone	•	•	5
1.1(b)	Cross section of the individual Fermi surface of each metal. ⁴	•	•	5
1.2	A simplified noble metal Fermi surface (solid line) displaced from its equilibrium position (dotted line) by an electric field. The region between the dotted and dashed lines is the schematic form of the electron distribution function for (a) an isotropic relaxation time and (b) an anisotropic relaxation time	•	•	9
1.3	A simplified Fermi surface showing variation of angular change in velocity for a fixed $ \vec{q} $		•	16
1.4	Intersection of Debye phonon sphere with Fermi surface showing locus of possible final states which grows as T^2	•	•	18
1.5	Cross section of an edge dislocation with dislocation line normal to the page		•	21
1.6	Scattering from extended strain field around dislocation core showing predominance of small angle events			21
1.7	Fermi distribution function with $\mathbf{E}_{\mathbf{F}}$ set to zero		•	25
1.8	Schematic representation of the thermal shell about a spherical Fermi surface (see text for discussion).	•	•	25
1.9	Schematic representation of the two-band model for impurity and phonon scattering. The height of resistors in a branch is inversely related to the Fermi surface area times Fermi velocity for that band. The length of a resistor is inversely related to the relaxation time for the represented mechanism	•	•	32

Figure		P	age
1.10	Schematic representation of two-band model including dislocation scattering. Conventions are the same as for Fig. 1.9	•	31
2.1(a)	Standard SQUID null detector circuit showing fixed temperature reference resistor $R_{\rm r}$	•	70
2.1(b)	Sample and reference mounted for differential method		70
2.2	Set up to measure contact resistance using constant current source I, ammeter A, and sensitive voltmeter V		77
2.3	Two ways to lower the effective inductance. (a) Use of an inductance L_p in parallel with the SQUID coil L_s . (b) Use of a superconducting D.C. transformer	•	80
2.4	Semi-schematic drawing of cryostat and dewar assembly.		87
2.5	Semi-schematic drawing of the tail section of the cryostat	•	88
2.6	Top: Mounting of SQUIDs and standard resistors. Bottom: Terminal strip connections sample must be connected to appropriate terminals on main strip	•	90
2.7	Various sample geometries: (a) linear geometry, circular cross section with spot welded arms; (b) linear geometry, rectangular cross section with milled arms; (c) tuning fork geometry, semicircular cross section, cuts made with spark cutter form cylindrical ingot		100
3.1	ρ vs. \widetilde{T}^4 for Ag 3 and Cu 6 (note, the ordinate for Au 3 should be multiplied by 0.9)	•	104
3.2	$\rho(T) = (\rho_{Total} - \rho_{o}) \text{ vs. } T^4 \text{ for annealed and strained}$ states of Cu II and CuAg 2. The strained Cu II and CuAg 2 shown are examples of the worst and the best precision in this series of runs	•	106
3.3	B vs. ρ_0 for Cu and dilute <u>Cu</u> Ag alloys in annealed (open symbols) and strained (solid symbols) states with strain shown in percent. See text for explanation of various lines and curves		107
3.4	B vs. ρ_0 for published (\bullet) and unpublished (\circ) data of Koshnevisan et al. 10 , 11 for Ag and Cu and published data (\blacktriangle) of Barnard and Caplin for Ag	•	110

Figure		Page
3.5	ρ_0 vs. % strain for Cu 11 (\bullet), CuAg 2 (\blacksquare) and CuAg 1 (\blacktriangledown)	. 112
3.6	$\frac{1}{\rho} \frac{d\rho}{dT}$ vs. T for Ag ₂₀ , run 1 (°) and run 2 (•). Dashed line is $\rho(T)(\rho)$ times integral of solid curve through data). Other solid line is the derivative of Eq.(3.9) with parameters from fit to AgC ₃ divided by ρ_0 from Ag ₂₀	. 128
3.7	$\frac{1}{\rho} \frac{d\rho}{dT}$ vs. T for Cu_{13} run 2	. 130
3.8	$\frac{1}{\rho} \frac{d\rho}{dT}$ vs. T for Cu_{13} run 1	. 136
A.1	G vs. T for Cu II $_{\rm u}$ -Cu II $_{\rm u}$. Percent strain given with each line	. 138
A.2	G vs. T for $\underline{Cu}Ag2_a - \underline{Cu}Ag2_w$. Percent strain given with each line	. 139
A.3	G vs. T for CuAgl -CuAgl . Percent strain given with each line	. 140
A.4	A Nordheium Gorter type of plot of ρ_0^{-1} vs. G(T=0). The horizontal axis has reciprocal ruling (note the zero on the right)	. 141

CHAPTER I

BACKGROUND AND THEORY

The resistivity of the noble metals, copper, silver and gold, continues to be of interest to theoretical and experimental physicists who study electron transport properties in metals. The earliest work was partly due to the fact that as a group they are the best electrical conductors known at ordinary temperatures. More recently they have been of interest because their band structures and Fermi surfaces are now well known allowing realistic calculations of the contribution to the resistivity due to various scattering mechanisms.

The major goal of the work presented in this dissertation was the direct observation of the minuscule T^2 contribution of electron-electron scattering to the resistivity of the noble metals. The magnitude of this term has been calculated by several authors 1,2 and its observation was felt to be within reach of our highly sensitive techniques. In the process, interesting new results were obtained. A resistivity which varied quite strictly as T^4 over a significant temperature range (roughly 2-7 K) was observed for all three metals. The constant of proportionality showed a high degree of variation between different samples of the same metal leading to a systematic study of the effects of impurities and dislocations. Extensive computer analysis of these results was stimulated by recent theoretical work 3 which attempts to show the T^4

behavior is due to the combination of electron-electron and electronphonon scattering with dislocation scattering having a crucial role in their relative magnitudes.

A. Some General Aspects

In this section we will try to touch all of the key aspects of the theory which bear on understanding our results. While it is not within the scope of this dissertation to consider the problem of electrical resistivity in general, we will try to set forth the framework of assumptions and basic concepts underlying the theory. It is assumed that the reader is already familiar with such fundamental concepts as the reciprocal lattice and k-space, the Fermi surface, and basic quantum mechanics including the Born approximation in scattering theory. The validity of the Boltzmann equation and the so called relaxation time approximation will be assumed without further discussion.

At the simplest level one can state that electrical conductivity arises from the freedom of electrons or other charged carriers to move in response to an applied field. In metals this freedom is due to the availability of states, almost infinitesimally separated in energy, into which an electron can move allowing it to gain kinetic energy from the field. These states may be available because the electrons do not entirely fill a band of energy states or, if there are enough electrons to fill a single band, there may be overlapping bands such that the electrons are distributed among several partially filled bands. In any case, at absolute zero the electrons fill all the lowest energy states and the Fermi surface is the surface in k-space which defines the boundary between occupied and unoccupied states. At any temperature where

the metal remains a solid and particularly at the low temperatures of concern here, the slight fuzziness at the boundary between the occupied and unoccupied states due to thermal excitations above the Fermi surface does not detract from the validity of the concept. This is because the Fermi energy, E_f , is roughly ten-thousand times greater than the thermal energy, k_BT , at room temperature. At thermal equilibrium the probability that a state of energy E is occupied is given by the Fermi-Dirac distribution function:

$$f_0 = \frac{1}{\exp[(E - E_f/k_B T] + 1}$$
 (1.1)

which rapidly approaches one for E-E $_{\rm f}$ < - $k_{\rm B}$ T and zero for E-E $_{\rm f}$ > $k_{\rm B}$ T. In simple free electron models where the k dependence of an

electron's energy is given by

$$E = \frac{\pi^2 k^2}{2m} \tag{1.2}$$

the Fermi surface is obviously a sphere. Electron velocities are normal to the Fermi surface and are given by

$$\vec{V} = \frac{1}{10} \nabla_{\mathbf{k}} E \tag{1.3}$$

In the case of a spherical Fermi surface the velocities are in the same direction as the wave vectors. Although this simple geometry is often used to simplify calculations and may even be quite correct for the alkali metals, it is, in general, a rather gross simplification. Real Fermi surfaces, especially in polyvalent metals, may be extremely complex and $\vec{v}(\vec{k})$ will not generally be in the direction of \vec{k} . However,

٧ 0f all Fermi surfaces have the basic symmetry of the reciprocal lattice. Thus, at the very least, they have inversion symmetry. So, the fact that Eq.(1.1) depends only on energy implies that at equilibrium every electron moving in one direction has a counterpart moving in the opposite direction, so the net current is zero.

Figure 1.1 shows the Fermi surface of the noble metals. While the largest fraction of the surface, comprising the so called belly regions, is nearly spherical, the regions in the <111> directions, called the necks, protrude from the sphere to intersect the Brillouin zone boundaries. As we shall see, the different character of these two regions is crucial in understanding the details of their conductivity.

Now we must consider the effect of applying an electric field $\dot{\epsilon}$ to a metal. Momentarily neglecting the effect of collisions, the electrons' wavevectors will increase with time according to the law of motion:

$$\frac{d\vec{k}}{dt} = \frac{1}{\hbar} e \dot{\epsilon}$$
 (1.4)

Thus all the occupied states are uniformly displaced in a direction parallel to the applied field. In a time δt the amount of displacement will be given by

$$\delta \vec{k} = \frac{1}{4} e \vec{\epsilon} \delta t \tag{1.5}$$

The net effect on the full electron distribution function is a shift of origin

$$f = f_0(\vec{k} - \delta \vec{k}) \tag{1.6}$$

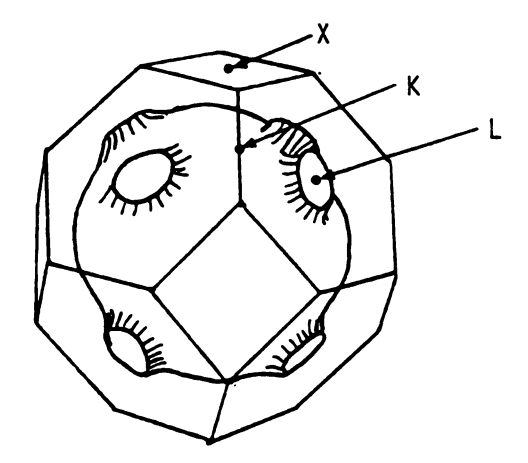


Fig. 1.1(a) A noble metal Fermi surface within the first Brillouin zone.

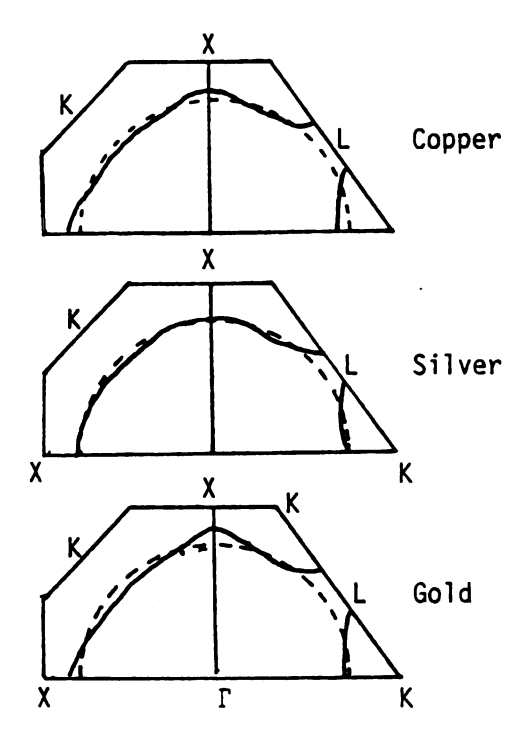


Fig. 1.1(b) Cross section of the individual Fermi surface of each ${\rm metal.}^{4}$

For small displacements we can expand this to first order

$$f = f_0 - \nabla_k f_0 \cdot \frac{e \dot{\epsilon}}{4 \hbar} \delta t \qquad (1.7)$$

Using Eq.(1.3) we then obtain

$$\frac{df}{dt}\Big|_{\text{field}} = -\frac{df_0}{dE} e \vec{v} \cdot \vec{\epsilon}$$
 (1.8)

The amount of displacement that occurs is limited by scattering processes which restore the equilibrium distribution when the field is removed. Clearly, the greater the rate of scattering the smaller will be the displacement from equilibrium for a given field and the more rapidly the distribution function will relax when the field is removed. Thus we are lead to the concept of a relaxation time, τ , which is inversely proportional to the scattering rate. For the moment assume that a scattering event completely randomizes the electron's wavevector and velocity and that the distribution function, $f(\vec{k})$, will return exponentially, with a characteristic time $\tau(\vec{k})$ to the equilibrium distribution $f(\vec{k})$ when the perturbing field is removed. This implies the rate of change of f due to collisions is

$$\frac{df(\vec{k})}{df}\Big|_{\text{collisions}} = -\frac{f(\vec{k}) - f_0(\vec{k})}{\tau(\vec{k})}$$
 (1.9)

We assume a unique value of τ can be defined at each point in k-space. Under steady state conditions the rate of change of f due to collisions must be equal and opposite to that due to the electric field. Thus,

$$\frac{df}{dt}\Big|_{collisions} = -\frac{df}{dt}\Big|_{fields}$$
 (1.10)

This is simply a statement of the steady state Boltzmann equation which is much more general than implied here, where we are only considering electric fields. The right hand term may generally be due to the simultaneous action of several generalized fields; electric, magnetic, thermal gradients etc. While f may be a function of \vec{r} as well as \vec{k} , we will assume that the material is homogeneous and that no other fields are present. Substituting into Eq.(1.10) we obtain:

$$-e \frac{df_0}{dE} \vec{v} \cdot \vec{\epsilon} = \frac{f(\vec{k}) - f_0(\vec{k})}{\tau(\vec{k})}$$
 (1.11)

Because f_0 contributes no current we are only interested in the distribution difference

$$g(\vec{k}) = -e \frac{df_0}{dE} \tau(\vec{k}) \vec{v}(\vec{k}) \cdot \vec{\epsilon}$$
 (1.12)

From now on we will call this the electron distribution function or e.d.f. We will call f the full e.d.f. To calculate the current we must evaluate the integral

$$\vec{j} = -\frac{e}{4\pi^3} \int d^3k \ \vec{v}(\vec{k})g(\vec{k}) \qquad (1.13)$$

where the $(4\pi^3)^{-1}$ comes from the electron density of states in k-space. The -df_o/dE term in g is essentially a delta function, $\delta(E-E_f)$, especially at low temperatures. This reduces the integral to a surface integral over the Fermi surface, if we make the following change of variables:

$$d^{3}k + dS \frac{dE}{|\nabla_{\nu}E|} = \frac{dSdE}{\hbar |\nu(k)|}$$
 (1.14)

resulting in

$$\vec{j} = \left[\frac{e^2}{4\pi^3 n} \int_{\text{F.S.}} dS \ \tau(k) \ \frac{\vec{v}(\vec{k})\vec{v}(\vec{k})}{|v(k)|} \right] \cdot \vec{\epsilon}$$
 (1.15)

The quantity in brackets is just the conductivity tensor $\overset{\longleftrightarrow}{\sigma}$ which appears in Ohm's law

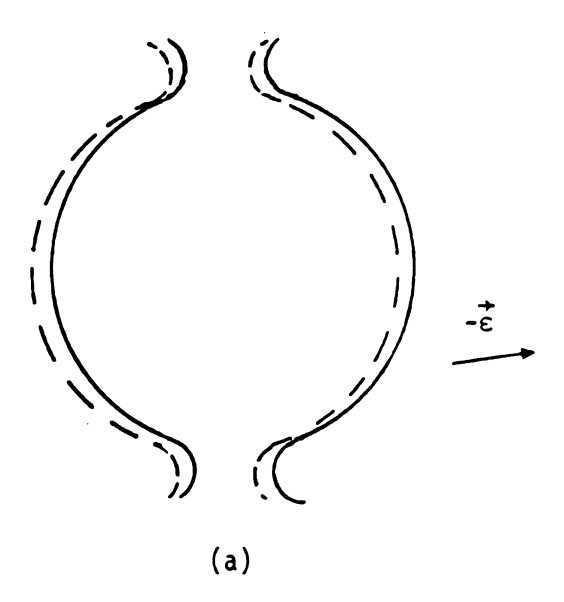
$$\overrightarrow{j} = \overrightarrow{\sigma} \cdot \overrightarrow{\varepsilon} \tag{1.16}$$

In isotropic or cubic crystalline materials such as the face-centeredcubic noble metals the conductivity is just a scalar and we have

$$\sigma = \frac{e^2}{4\pi^3 \text{fi}} \left\{ F.S. \quad dS \ \tau(\vec{k}) \nu(\vec{k}) = \frac{e^2}{4\pi^3 \text{fi}} \right\} F.S. \quad dS \ \lambda(\vec{k})$$
 (1.17)

where $\lambda(\vec{k})$ is the electron mean free path.

The meaning of Eq.(1.13) is easily visualized in Fig. 1.2 which shows the response of the electrons on a simplified noble metal Fermi surface to an electric field. Part (a) shows the simplest case where τ is a constant over the Fermi surface. As we shall see, this approximation may be quite realistic for many types of impurity scattering. Part (b) shows the e.d.f. for an anisotropic $\tau(k)$. In the case shown the relaxation time on the necks is much less than on the bellies $(\tau_n << \tau_b)$. We shall see that this case is appropriate to scattering by dislocations or low temperature phonons. We shall also find that the differences in relaxation time anisotropy between two scattering mechanisms play a crucial role when both mechanisms are operating concurrently.



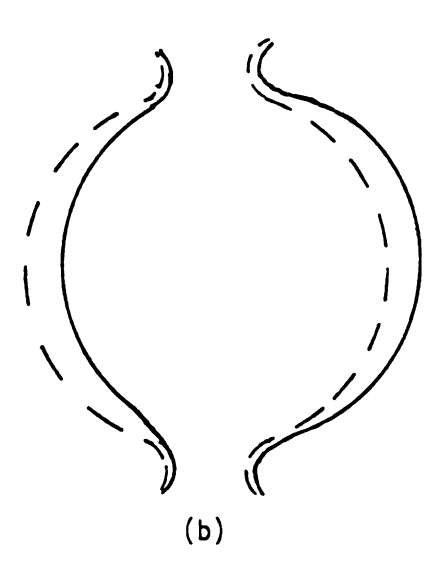


Fig. 1.2 A simplified noble metal Fermi surface (solid line) displaced from its equilibrium position (dotted line) by an electric field. The region between the dotted and dashed lines is the schematic form of the electron distribution function for (a) an isotropic relaxation time and (b) an anisotropic relaxation time.

The magnitude of the e.d.f. in the direction of the field is very small being only about 10^{-10} of the Fermi radius at typical current densities of 100 Acm^{-2} . This helps explain why Ohm's law, which requires an expansion of q which is linear in the electric field, works so well.

It is obvious that $\tau(\vec{k})$ plays a crucial role in any real calculations of electrical conductivity. Thus, we must be able to determine $\tau(\vec{k})$ from a knowledge of the fundamental scattering processes. Let us assume that we can calculate the transition probability $P(\vec{k},\vec{k}')$ from state \vec{k} in the range dk'. Then the conductivity relaxation time is defined as

$$\frac{1}{\tau(\vec{k})} = \begin{cases} P(\vec{k}, \vec{k}')(1 - \cos \Lambda_{V}^{V'}) dk' \end{cases}$$
 (1.18)

where $\Lambda_{\mathbf{v}}^{\mathbf{v}'}$ of the angle between the velocities \mathbf{v} and \mathbf{v}' of the two states. Without the $(1-\cos\Lambda)$ weighting factor this integral would just yield the total inverse scattering rate. The $(1-\cos\Lambda)$ term is included to properly weight the scattering events since small angles are much less effective than large angles in reducing an electron's contribution to the current. The origin of this term can only be rigorously shown on a spherical Fermi surface for elastic scattering with a probability depending only on energy and the angle between k and k'. However, something like this term must be included to properly weight the angular changes in an electron's velocity on any Fermi surface.

Not only is an electron's velocity randomized by scattering but, on the average, it also loses the kinetic energy it gained from the field. This lost energy exhibits itself as Joule heat. However, one can still treat some types of scattering events as elastic because this energy loss per electron is extremely small, being on the order of 10^{-10} of the Fermi energy. Yet it must be emphasized that it is the randomization of the electron's momentum that produces the resistivity.

To summarize these fundamental ideas: conductivity arises when electrons are able to coherently acquire momentum in the direction of an applied electric field. Resistivity is due to the random redistribution of these momenta by incoherent scattering. It is the mechanism by which these two processes are held in dynamic balance that is the subject of the rest of this dissertation.

B. Specific Scattering Mechanisms

1) Impurity Scattering

Scattering by impurities and lattice defects produces the major part of the electrical resistivity in a metal at low temperatures. This resistivity is generally independent of temperature and at low temperatures contributes a constant background resistivity usually called the residual resistivity ρ_0 . (One important exception to be briefly considered later is the so called Kondo effect due to magnetic impurities.)

If a lattice were perfect with no impurities or defects, then the resistivity would go to zero as the temperature approaches zero. The introduction of impurities in a random way produces perturbations in the periodic lattice potential which cause electrons to scatter. The probability $P(\vec{k},\vec{k}')$ of scattering between states \vec{k} and \vec{k}' depends on the exact form of the scattering potential, and the initial and final states. In the simple case of a spherical Fermi surface, which implies single plane-wave states, the scattering probability is only a function of scattering angle θ for any spherically symmetric potential.

Scattering calculations yield a relaxation time independent of \vec{k} , i.e. isotropic, given by

$$\frac{1}{\tau} = v_f \left[\frac{d\sigma(\theta)}{d\Omega} (1 - \cos\theta) d\Omega \right]$$
 (1.19)

where $d\Omega$ is the differential element of solid angle and $d\sigma(\theta)/d\Omega$ is the differential scattering cross section related to the scattering probability by $P(\theta)$ = v $\frac{d\sigma}{d\Omega}$. Note again the presence of (1 - cos θ) weighting factor.

Although treating tas a constant is a fair approximation for many impurities, it may be important to consider the effect of differences in character of states at different points on the Fermi surface of real metals to get a more realistic picture of how τ , and thereby, $g(\vec{k})$, depends on \vec{k} . In the noble metals, the nearly spherical belly portions of the Fermi surface (see Fig. 1.1) can be treated very well by single plane wave states. These states are said to be s-like, that is, they exhibit essentially no angular momentum with respect to the ion cores. Hence, there is no centrifugal potential to reduce their wave functions at the core of an impurity ion. The highly non-spherical neck states, on the other hand, must be represented by at least two OPWs. These states have an angular momentum character that is essentially p-like. 7 Hence, they are prevented from significant overlap with the ion cores and remain largely in the interstitial regions. This implies that neck electrons would be much less scattered by short range potentials largely restricted to the core regions. Homovalent impurities such as Ag in Cu are not charged and therefore, have such a short range potential . Such **impurities** would be expected to exhibit an anisotropy in τ such that

$$\tau_n > \tau_b$$
.

Now we will briefly consider the temperature dependent resistivity due to magnetic impurities, the so called Kondo effect. But it is well known that free magnetic ions such as iron can produce temperature dependent effects at low temperatures resulting in a minimum in the resistivity versus temperature curve. One of the most common examples is gold with dilute iron impurities; another is manganese in copper. It would take us too far afield to consider the theory of the Kondo effect. The essential point here is that extreme care is necessary to avoid any magnetic contaminants when doing measurements on the low temperature resistivity in the noble metals. If such contamination exists it may be difficult or impossible to subtract its effects from the data. What is worse, the effect may not produce an obvious minimum making it virtually undetectable by resistivity measurements alone. However, one can use thermoelectric data to help detect its presence.

For our purposes the important facts about impurity scattering are: First, it is ordinarily dominant at low temperatures. Second, it can produce large angle scattering. Third, it is characterized by an essentially isotropic (constant) relaxation time over the Fermi surface except as mentioned.

2) Phonon Scattering

In a perfect crystal the electron states of definite \vec{k} are stationary states of the system. However, at finite temperatures, the vibrations of the crystal lattice produce density fluctuations and thus disturb the lattice periodicity so that transitions occur among the \vec{k} states. Although not stationary, these \vec{k} states are still relatively long lived and thus still provide an appropriate and particularly

convenient basis for describing the electrons. This convenience is in no small part due to the fact that the lattice vibrations themselves occur as quanta, called phonons, which are also states of definite \vec{k} . Any interaction between electrons and phonons must conserve the total crystal momentum to within a reciprocal lattice vector \vec{G} so that

$$\vec{k}_1 - \vec{k}_2 = \pm \vec{q} + \vec{G}$$
 (1.20)

where \vec{k}_1 and \vec{k}_2 are the initial and final electron wave vector and \vec{q} is a phonon wave vector (we use q's to distinguish phonon from electron wave vectors). The plus sign represents emission and the minus sign absorption of a phonon. Events in which \vec{G} is zero are called normal or N processes while nonzero \vec{G} 's are called Umklapp or U processes. With a multiply connected Fermi surface, as in the noble metals, the distinction is somewhat academic especially at low temperatures since a U process can usually be represented as N process in an extended zone scheme.

Electron-phonon scattering also involves the gain or loss of the phonon's energy by the electron and is thus inelastic which means, in the context of transport theory, that electron energy changes are of order $k_B T.^9$ These energy changes are so small ($k_B T << E_f$) especially at low temperatures that the electron remains essentially on the Fermi surface. (This is just restating what was said in Section A about df_0/dE being essentially a delta function.)

At low temperatures the only phonon modes which can be excited are those of low frequency (i.e. long wavelength). In the Debye model, which is usually appropriate at low temperatures, the number of phonons in the range of frequencies $d\omega$ is proportional to

$$\frac{\omega^2 d\omega}{\exp(\hbar\omega/k_B T) - 1}$$
 (1.21)

This has a maximum when

$$πω = πωT ≈ 1.6 kBT$$
(1.22)

Thus we can define a dominant wavevector at a given temperature

$$q_T = \frac{\omega_T}{v_s} = \frac{1.6 k_B T}{v_s \pi}$$
 (1.23)

where ${\bf v}_{\bf S}$ is the speed of sound which we assume is isotropic but may depend on polarization. This is roughly a maximum value of q because the Bose Einstein function rapidly cuts off phonons of higher energy. Thus at low temperatures where q's are small compared with the Fermi radius, the maximum scattering angle $\theta_{\rm T} \simeq q_{\rm T}/k_{\rm F}$ increases as T. This is illustrated on the spherical portion of Fig. 1.3. We have seen that small angle scattering is not effective in producing electrical resistance. This was taken into account by using the $(1-\cos \Lambda)$ weighting factor in the relaxation time formula (1.18). Thus for small angle scattering the inverse relaxation time for phonon scattering must acquire a ${\sf T}^2$ factor.

$$\frac{1}{\tau} \propto (1 - \cos\theta_{T}) = 2 \sin^{2} \frac{\theta_{T}}{2} = \frac{1}{2} \left(\frac{q_{T}}{k_{f}}\right)^{2} = \frac{1}{2} \left(\frac{1.6 \, k_{B}}{\hbar v_{s} k_{f}}\right)^{2} T^{2}$$
 (1.24)

It also seems clear that the inverse scattering time, the scattering rate, must increase as the number of phonons increases. In isotropic media the number of phonon modes is essentially the volume of a sphere

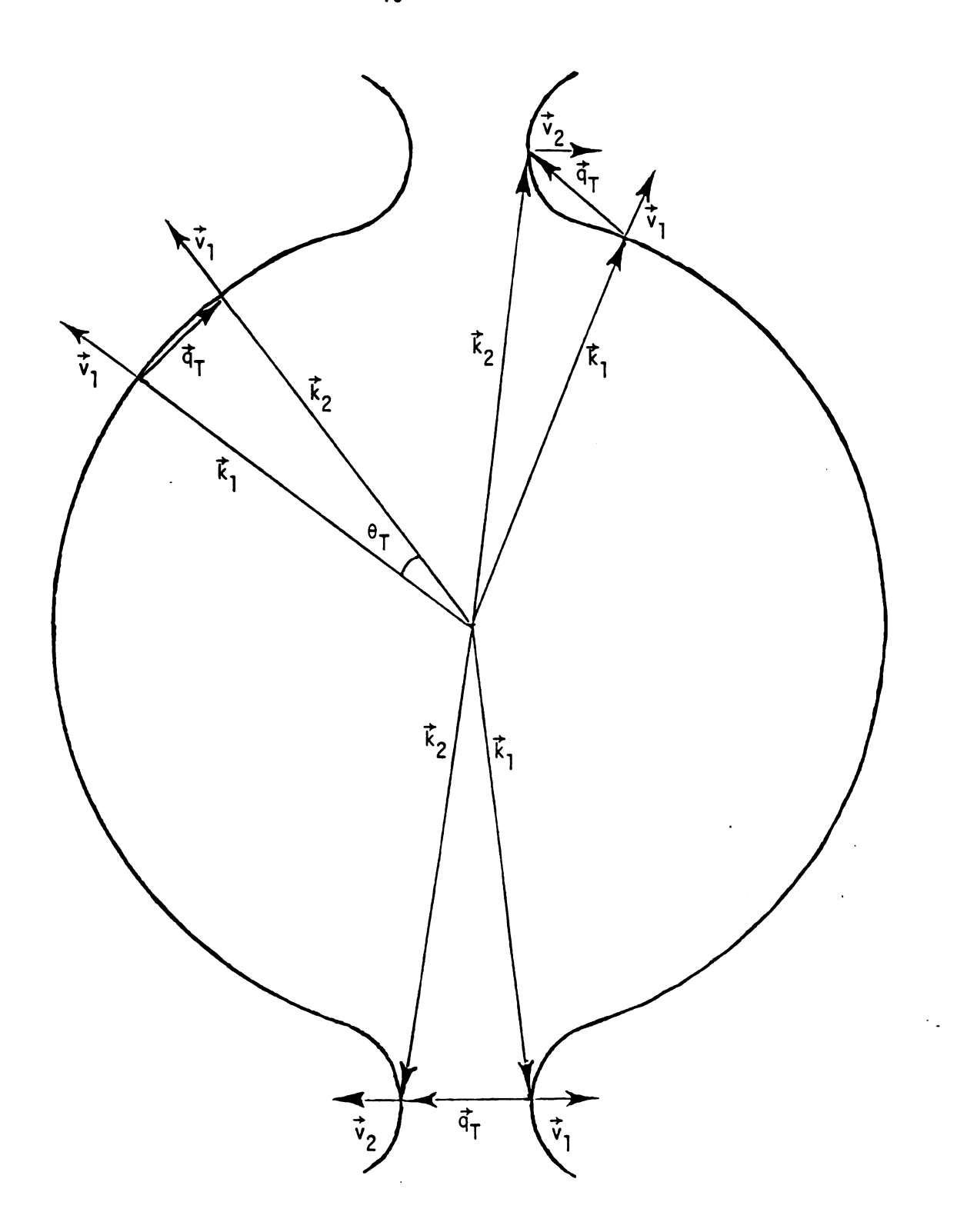


Fig. 1.3 A simplified Fermi surface showing variation of angular change in velocity for a fixed $|\vec{q}_T|$.

of radius q_T . Thus the number of phonons increases roughly as T^3 . However, the constraints of momentum and energy conservation require that the initial and final electron states remain essentially on the Fermi surface. Thus a given state may only be scattered into states which lie on the surface of intersection of the Fermi surface with this phonon sphere with its origin at the original electron k vector (see Fig. 1.4). Hence, the number of phonons available for scattering increases as q_T^2 i.e. as T^2 . This means that $1/\tau_{\rm phonon}$ has another factor of T^2 .

Now, as Dugdale 10 points out, the actual calculation of the magnitude of phonon resistivity is a very difficult problem. However, it can be shown that the square of the scattering matrix element which goes into the scattering probability is proportional to q and hence to T. (A very nice demonstration of this can be found in Ashcroft and Mermin. 6) Thus we have deduced that in the case of low temperature small angle scattering the phonon resistivity should vary as T^{5} . One factor of T^{2} is from the small angle weighting factor, another T^{2} factor is from the number of phonons available and a factor or T from the square of the scattering matrix element. This behavior, first described by Bloch is often called the Bloch T^{5} law. While there are reports of such behavior at low temperatures, 11,12 the basis for this law is rather idealized and the many reported deviations from it should not be unexpected. $^{13-18}$

One source of trouble for the T⁵ law may be seen by considering the neck regions in Fig. 1.3 and 1.4. These regions may violate the small angle scattering criterion due to their high curvatures. Thus, electrons on the neck would experience a resistivity going as some lower and probably temperature dependent power of T while the belly electrons are

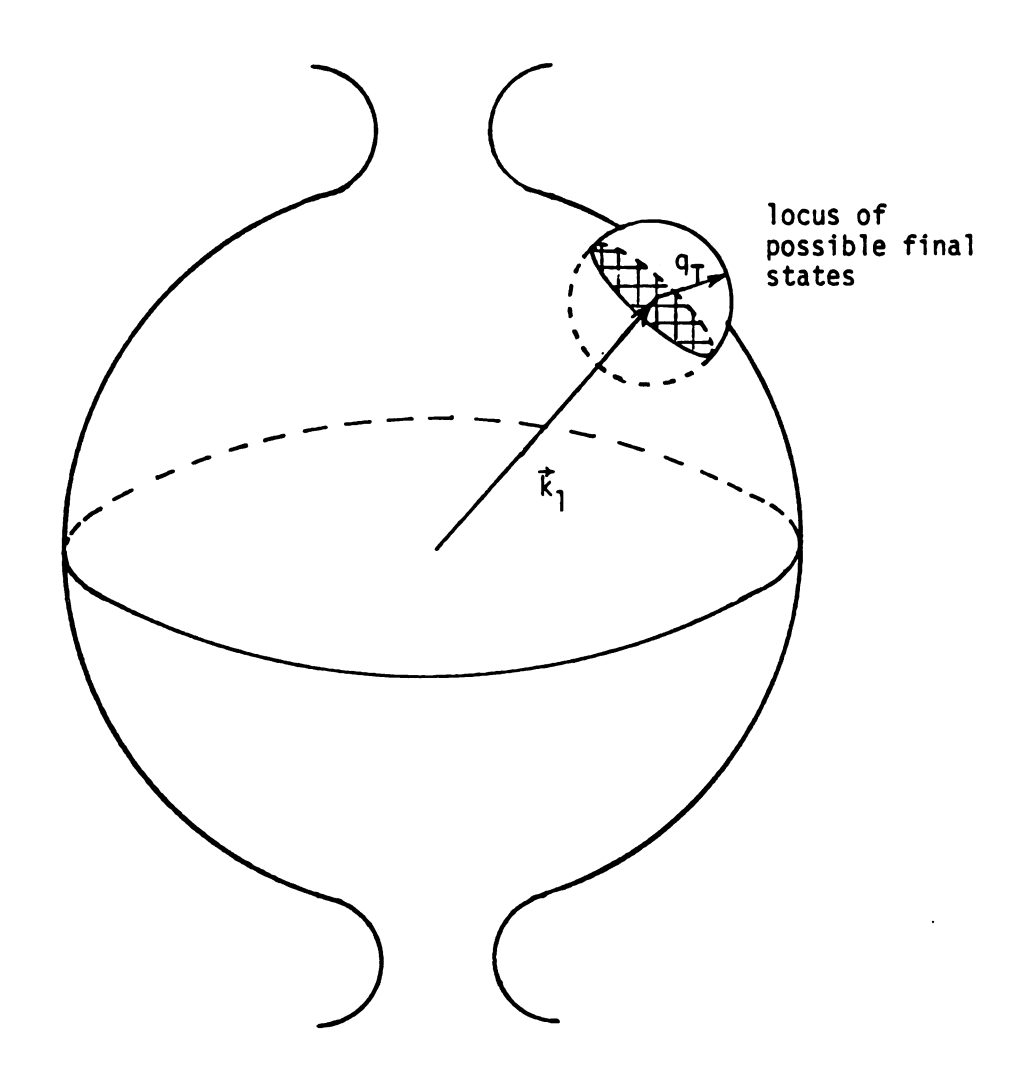


Fig. 1.4 Intersection of Debye phonon sphere with Fermi surface showing locus of possible final states which grows as T^2 .

in the T^{5} regime. Figure 1.3 shows that the same value of \textbf{q}_{T} which produces small angle scattering on the belly can produce large angle scattering, including complete velocity reversal, on the necks. $Rumbo^{15}$ points out that in Cu near 4 K the <111> transverse acoustic mode has a q_T of about 0.3 \mathring{A}^{-1} which is comparable to the neck radius of 0.26 \mathring{A}^{-1} . Thus large angle scattering would surely occur at this temperature. Presumably at low enough temperatures q_{τ} will become small even on the scale of the neck radius in which case the T^5 law would again apply. Another assumption behind the T^5 law is that the phonon population is in thermal equilibrium. This assumption may be invalid at low temperatures. The electron current may drag the phonon distribution out of equilibrium because the equilibrium restoring mechanisms are quite weak--long wavelength phonons are not strongly scattered by impurities. In any case, it is clear that significant anisotropy of the electron relaxation time due to phonons $\boldsymbol{\tau}_{\boldsymbol{n}}$ should exist at low temperatures due to the high degree of curvature at the necks.

This is not the only source of anisotropy, however. Ziman⁵ points out that neck electrons should be much more sensitive than belly electrons to transverse phonons. He also notes that the density-of-states factor in the scattering probability is larger on the necks. Thus, since the scattering produces transitions to nearby states on the Fermi surface, there are more states available into which an electron can scatter, enhancing the scattering rate. Finally he notes that the two-OPW states necessary to describe the neck wave functions can also lead to an enhanced scattering rate.

So, we have four sources which can produce a shortened relaxation time on the necks: high curvature, greater sensitivity to transverse phonons, higher density of states, and differing character of the wave functions. It is this type of anisotropy which we shall see also applies to dislocation scattering.

3) Scattering by Dislocations

Dislocations are extended crystal defects of which an edge dislocation is shown in Fig. 1.5. One can imagine that an initially perfect crystal has a half plane of atoms displaced, as shown, leaving a half plane on the end and effectively inserting a half plane in the center. The idealized defect shown here extends along an infinite line perpendicular to the paper. Actual dislocations often do extend almost to infinity on an atomic length scale and thus they are essentially two-dimensional as far as their scattering properties are concerned.

The theory of the electrical resistivity of dislocations is still not complete. Many attempts to explain the experimental data have been made with varying degrees of success. At present, the two most successful are the theories of Basinski et al. ¹⁹ and of Brown. ²⁰ The emphasis of Basinski et al. is on the strain field of the dislocation. They argue that one can use the ideal resistivity to the thermal energy ratio, which is roughly constant, to relate the dislocation strain field energy to the dislocation resistivity. Because the core has only about one-fifth of the total strain energy, they suggest the strain field rather than the core is the main contributor to the resistivity. The theory of Brown assumes a resonance in the s-wave scattering of Fermi electrons from the dislocation core. The existence of this resonance is fundamentally connected with the extended line nature of the dislocation.

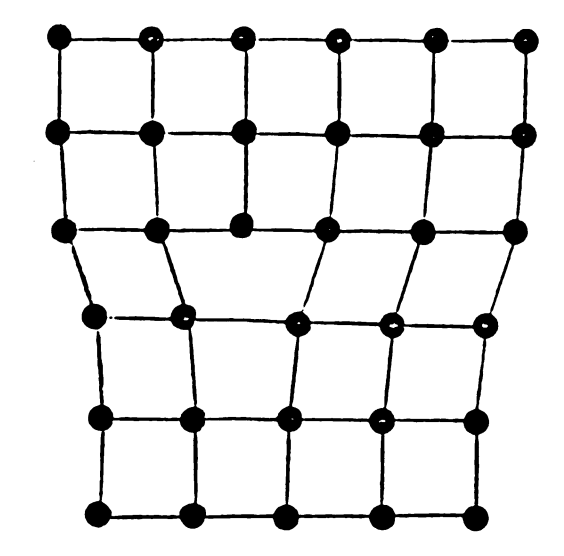


Fig. 1.5 Cross section of an edge dislocation with dislocation line normal to the page.

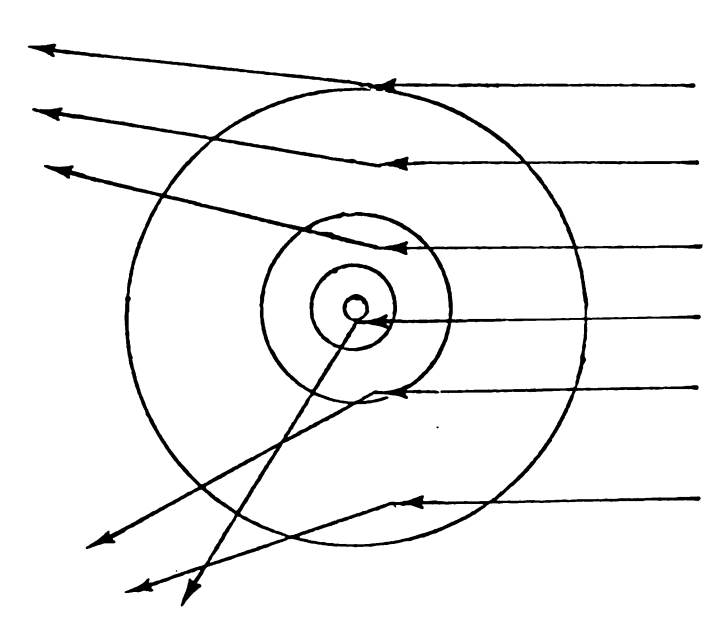


Fig. 1.6 Scattering from extended strain field around dislocation core showing predominance of small angle events.

We shall not enter the debate here but simply point out that both approaches have more or less equal success in explaining experimental data although the physical models are quite different. Especially important in the present context is that both are compatible with observed large scattering cross sections for small angle scattering and both attribute this to the strained regions away from the core. These large, small angle cross sections are seen in investigations of the radio frequency size effect²¹ and the deHaas-van Alphen effect.²² The importance of this fact here is that small angle scattering is characteristic of phonons at low temperatures. Thus, we might expect a relaxation time anisotropy over the Fermi surface similar to that for phonons. Intuitively this propensity for small angle scattering seems reasonable because, while the highly localized core of the dislocation is severely distorted and capable of large angle scattering, the broad strain field axially surrounding the core is much larger in volume and would intercept the paths of many more electrons. However, the distortions in this strain field, which fall off rather slowly away from the core, are not so severe. Therefore, the electrons are deflected only through small angles (see Fig. 1.6). In fact, this portion of the dislocation problem has been modeled by using superpositions of frozen phonons of long wavelength to build up the strain field. 23 This phonon like behavior will have important consequences when we consider the temperature dependent resistivity of strained copper.

4) Electron-Electron Scattering

Electron-electron scattering in simple metals such as the noble and alkali metals is expected to be an extremely small contribution to

the total resistivity at low temperatures. This may at first be surprising when one considers the large electron densities and velocities in a metal. However, a moment's consideration will show why.

First, the electrons screen one another so that the potential of an electron extends for only about an interatomic distance. Second, we shall see shortly the Pauli exclusion principle allows only those electrons within ${}^{\sim}k_{R}T$ of the Fermi surface to interact and even those are limited by the constraints of energy and momentum conservation. Third, large portions of the Fermi surface for the noble metals are essentially spherical with plane-wave-like functions. Thus their velocities are parallel to the wavevectors of these states. Any collision, which must conserve the total crystal momentum, will also conserve the center of mass velocity provided the initial and final states are on the spherical portions of the Fermi surface. It is clear that most scattering events will have little effect on the current carried by the Now it also becomes clear that the neck portions of the Fermi surface are essential for producing significant changes in the velocity of the center of mass while still satisfying k-vector conservation. This is because in these regions the velocity is not parallel to the k-vector nor does it have the same magnitude as the velocity of belly electrons.

In transition metals the electron-electron contribution to the resistivity is greatly enhanced due to the presence of the sluggish d electrons of large effective mass. The highly conducting s electrons can scatter off the heavy d electrons and undergo large changes of direction. The d bands of the noble metals are filled and not available for such processes.

The temperature dependence of such scattering is expected to go as T^2 quite independent of the exact mechanism by which it is able to contribute to the resistivity. The reason for this dependence is quite simple.

The Fermi distribution ensures that state below about $2k_{\text{R}}T$ of the Fermi surface are filled and states above $2k_{\mbox{\scriptsize B}}T$ are virtually devoid of electrons which could engage in scattering (see Fig. 1.7). This defines a shell of thickness $\sim 4k_RT$ about the Fermi surface which we will call the thermal shell. Figure 1.8 shows an electron well below the thermal shell at point A. It is prevented from scattering with an electron in the thermal shell, say at point B, because one or both of the final states allowed by energy conservation, points C and D, for example, are those below the thermal shell which, the Pauli principle will not allow. It is clear from Fig. 1.7 that the number of occupied and unoccupied states (which are respectively proportional to the areas below and above the curve) are linear in T. Thus the number of electrons with which a given electron can scatter increases as T. The number of final states available for one of the electrons also increases as T. The final state of the second electron is then fixed by energy and wavevector conservation. Thus the scattering rate of the original electron goes as T^2 . Because there are no restrictions on scattering angle, the resistivity is proportional to the scattering rate and thus shows a T^2 variation. The smallness of the effect is due to a dominant factor of $(k_{R}T/\epsilon_{F})^{2}$ as shown by Ziman. 24 However, this term is 100 times larger in the transition metals where $\epsilon_{\mbox{\scriptsize F}}$ is measured from the top of the d band. This is the reason that only recently has evidence for its existence been obtained in metals such as Cu, 14 in the present work, and A1. 25,26

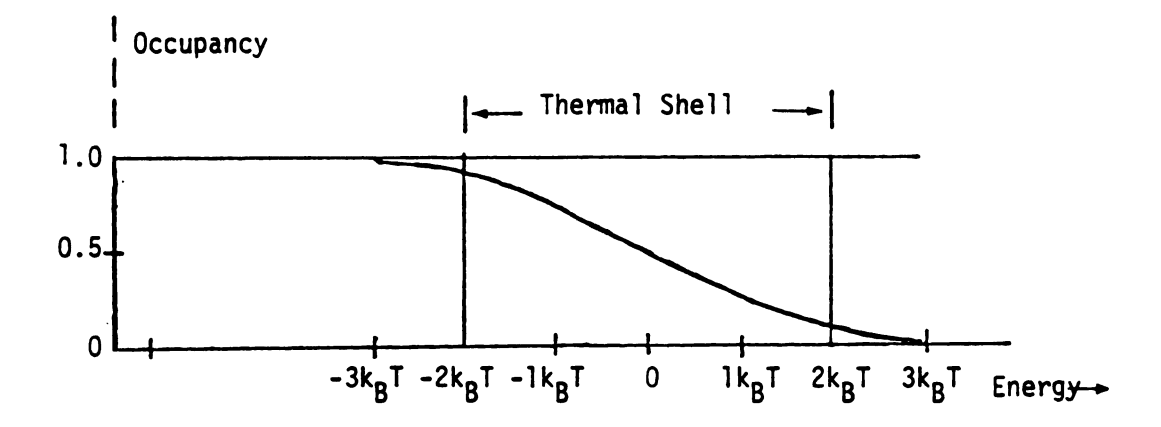


Fig. 1.7 Fermi distribution function with $\boldsymbol{E}_{\boldsymbol{F}}$ set to zero.

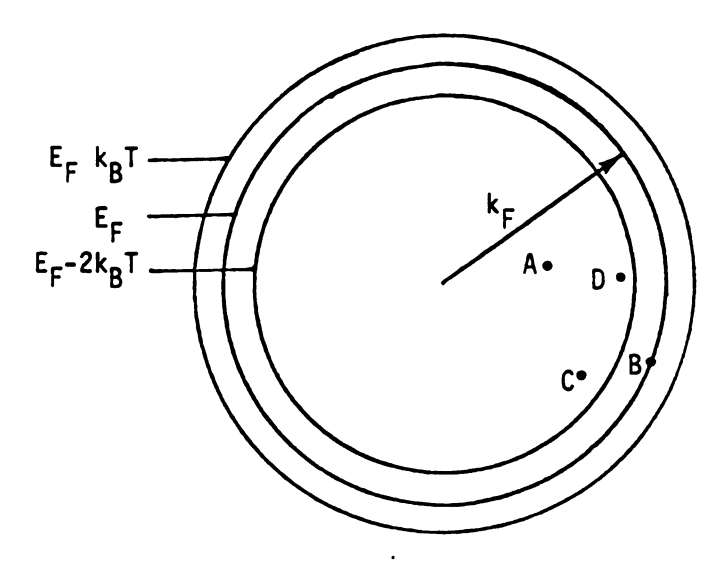


Fig. 1.8 Schematic representation of the thermal shell about a spherical Fermi surface (see text for discussion).

There is also evidence for potassium but the matter is not entirely settled. $^{27-30}$

C) Concurrent Scattering Mechanisms

When several mechanisms are scattering electrons simultaneously, the assumption that their contributions to the total resistivity are independent can be quite incorrect. This is the assumption that underlies Matthiessan's Rule which can be stated as follows:

$$\rho_{\text{total}} = \rho_0 + \rho(T) \tag{1.25}$$

where ρ_{total} is the resistivity of a dilute alloy, ρ_{O} is the residual resistivity of the alloy measured at a temperature low enough to neglect the phonon contribution, $\rho(T)$ is the temperature dependent part of the host resistivity of the pure host metal. While Eq.(1.25) does fit a lot of experimental data quite well, deviations from Matthiessan's Rule (DMR) are well known and have been given extensive reviews by Bass³¹ and Cimberle et al.³² While the DMR have many possible causes such as shifts in the phonon spectrum and shifts in the band structure to name two, the most likely cause with the temperatures and metals of our concern is that due to differences in relaxation time anisotropy among various scattering mechanisms. Our chief concern will be with concurrent impurity, phonon and dislocation scattering. We shall also consider concurrent impurity, electron-electron and dislocation scattering.

To understand the competition and interference between scattering mechanisms due to anisotropy we must consider the influence of each on $g(\vec{k})$ (the electron distribution function) and in return the effect $g(\vec{k})$

has on the resistivity due to each mechanism. No matter what juxta-position of mechanisms is present, there exists a unique $g(\vec{k})$ which satisfies the Boltzmann equation (1.10). (g(k) and f(k) are interchangeable in this equation because f_0 is independent of time by definition.)

It can be shown 33 that the correct solution to the Boltzmann equation is the one which minimizes the total resistivity. This is known as the variational principle for resistivity and is often used in theoretical calculations. Herein lies the heart of the matter. Although the correct $g(\vec{k})$ may minimize the total resistivity, the individual contributions of different mechanisms may not be minimized. In fact, one or another may be significantly enhanced.

Let us call $g_i(\vec{k})$ the characteristic e.d.f. for impurity scattering and compare it to $g_p(\vec{k})$, characteristic e.d.f. for phonon scattering. In this discussion we are not concerned with the absolute magnitude of $g(\vec{k})$ because that depends on the strength of the applied field (Eq.(1.12)). We are interested in the relative shape of the distribution around the Fermi surface. If the relaxation times for two different scattering mechanisms are such that their ratio is independent of \vec{k} , then we say their characteristic e.d.f.'s are of the same form.

 $g_i(\vec{k})$ and $g_p(\vec{k})$ can be qualitatively compared in Fig. 1.2. Part (a) shows the uniform nature of $g_i(k)$ over the Fermi surface. Part (b) shows the form of $g_p(k)$. The small value of $g_p(k)$ on the necks relative to the bellies is due to the shorter electron-phonon relaxation time, τ_p , on the necks for the reasons previously discussed. Any form of $g(\vec{k})$ other than $g_p(\vec{k})$ will increase the resistivity due to phonons. Now, in real samples, impurities are always present. If they dominate the scattering,

which must be true at low enough temperatures, then the actual form of g will be closer to \mathbf{g}_i than to \mathbf{g}_p causing an increase in the resistivity due to phonons. The main contribution to this increase is due to the fact that the population of current carrying electrons is enhanced at the necks relative to the bellies. But, τ_p is much smaller on the necks. Thus the relative importance of the necks in determining the phonon resistivity is enhanced. The temperature dependent resistivity (often called the ideal resistivity) of a pure metal is usually determined by subtracting the residual resistivity from the total resistivity

$$\rho(T,i) = \rho_{Total} - \rho_{o}$$
 (1.26)

where the i reminds us that it was measured in the presence of some impurities. This is called the ideal resistivity because it is supposed to be the resistivity of a perfectly pure metal in which phonons are the only scattering mechanism. This so called ideal resisitivity may in reality be rather far from the true $\rho(T)$ because at low enough temperatures we get into the so called dirty limit where impurity scattering is dominant, even for nominally pure metals. However, $\rho(T,i)$ is often ideal used to determine the DMR, $\Delta\rho(T)$, of dilute alloys by

$$\Delta \rho(T) = \rho(\text{alloy}) - \rho_0(\text{alloy}) - \rho(T,i)$$
Total ideal (1.27)

In the dirty limit the addition of more impurities may have little effect on $\rho(T)$ since $g(\vec{k})$ is already dominated by impurity scattering. Thus Matthiesan's rule may work quite well in this regime. At somewhat higher temperatures, where the scattering may no longer be dominated by

residual impurities in the "pure" metal, $g(\vec{k})$ may have a form intermediate between $g_p(\vec{k})$ and $g_i(\vec{k})$. The addition of more impurities may then cause a significant shift of g(k) toward the impurity dominated form. At still higher temperatures, when phonons can scatter through large angles, the intrinsic differences between $g_i(\vec{k})$ and $g_p(\vec{k})$ may not be very great and so again, the addition of more impurities would not strongly affect the form of $g(\vec{k})$. These facts are one reason why the observed DMR are often greatest between the high and low temperature regions we have described.

Another consequence of the fact $g(\vec{k})$ is not the "ideal" $g_p(\vec{k})$ at low temperatures is the possibility of apparent negative DMR if some type of scattering mechanism is introduced which can shift $g(\vec{k})$ in the direction of $g_p(\vec{k})$. Such effects have been observed 34,35 and were the object of much of the work to be reported in Chapter 3. We shall later see that dislocations can produce just such effects.

A highly simplified model of these ideas is the so called two-band model. In this model, the electrons are divided into two groups ("bands") composed of the neck electrons and the belly electrons. The properties of all electrons within a group are assumed to be the same. To organize our notation, we will use labels (n) or (b) to specify a particular group (necks or bellies). We will use subscripts p, i, and d to denote phonon, impurity or dislocation scattering. The absence of labels and/or subscripts implies that the quantity applies to the combination of all groups and/or mechanisms respectively. For example ρ is the total resistivity, ρ_p is the total phonon resistivity, $\rho_p(n)$ is the phonon resistivity of the neck. What follows is essentially along the lines of Dugdale's treatment. We assume these two groups are conducting in parallel. Thus, for pure phonon scattering we have

$$\sigma_{p} = \sigma_{p}(n) + \sigma_{p}(b) \tag{1.28}$$

or

$$\frac{1}{\rho_p} = \frac{1}{\rho_p(n)} + \frac{1}{\rho_p(b)} \tag{1.29}$$

In this simple picture we can relate the conductivities to the relaxation times by

$$\sigma_p(n) = N\tau_p(n)$$
 and $\sigma_p(b) = B\tau_p(b)$ (1.30)

where the factors N and B involve the areas and Fermi velocities of their respective parts of the Fermi surface (see Eq.(1.17)). We saw earlier that $\tau_p(n) << \tau_p(b)$. Because the area of the necks is much less than the bellies, N << B. Thus $\sigma_p(n) << \sigma_p(b)$ and $\rho(n) >> \rho(b)$. Therefore

$$\rho(T) = \rho_{p} = \frac{\rho_{p}(n)\rho_{p}(b)}{\rho_{p}(n)+\rho_{p}(b)} \simeq \rho_{p}(b) = \frac{1}{B\tau_{p}(b)}$$
(1.31)

So it is the bellies which determine the temperature dependent resistivity. For impurity scattering we will assume a single relaxation time $\tau_{\bf i} = \tau_{\bf i}({\bf n}) = \tau_{\bf i}({\bf b}), \text{ for both the necks and the bellies.} \text{ Thus for only impurity scattering}$

$$\sigma_{i} = \sigma_{i}(n) + \sigma_{i}(b) = (N+B)\tau_{i}$$
 (1.32)

and

$$\rho_{i} = \frac{\rho_{i}(n)\rho_{i}(b)}{\rho_{i}(n)+\rho_{i}(b)} = \frac{1}{(N+B)\tau_{i}}$$
 (1.33)

Within a group we assume the scattering probabilities of separate mechanisms add. Hence, if we combine phonon and impurity scattering

$$\frac{1}{\tau(n)} = \frac{1}{\tau_p(n)} + \frac{1}{\tau_i}$$
 (1.34)

and

$$\frac{1}{\tau(b)} = \frac{1}{\tau_{p}(n)} + \frac{1}{\tau_{i}}$$
 (1.35)

Thus, within a group the mechanisms add like resistances in series. The equivalent circuit is shown in Fig. 1.9.

For now, we assume impurity scattering strongly dominates on the bellies but is comparable on the necks to phonon scattering. That is

$$\tau_{i} \sim \tau_{p}(n) << \tau_{p}(b)$$
 . (1.36)

The total conductivity is

$$\sigma = B\tau(b) + N\tau(n) \tag{1.37}$$

or

$$\sigma = \frac{B}{1/\tau_{p}(b) + 1/\tau_{i}} + \frac{N}{1/\tau_{p}(n) + 1/\tau_{i}}$$
 (1.38)

But we can neglect $1/\tau_p(b)$ compared with $1/\tau_i$ so that

$$\sigma = B\tau_i + \frac{N\tau_i\tau_p(n)}{\tau_i+\tau_p(n)}$$
 (1.39)

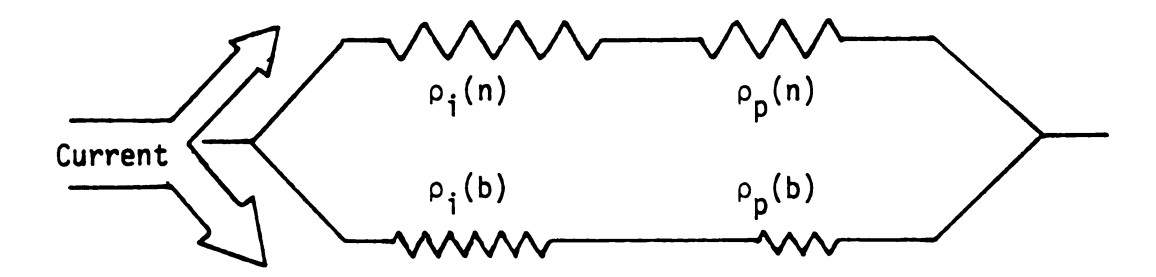


Fig. 1.9 Schematic representation of the two-band model for impurity and phonon scattering. The height of resistors in a branch is inversely related to the Fermi surface area times Fermi velocity for that band. The length of a resistor is inversely related to the relaxation time for the represented mechanism.

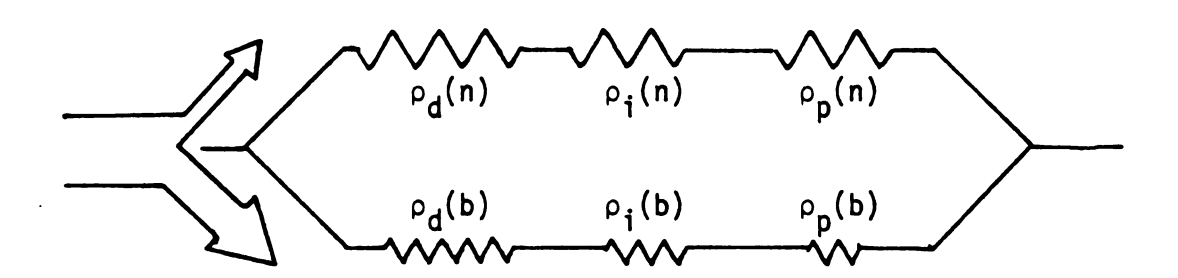


Fig. 1.10 Schematic representation of two-band model including dislocation scattering. Conventions are the same as for Fig. 1.9.

we can write this as

$$\sigma = (B+N)\tau_i - N\tau_i \left(\frac{\tau_i}{\tau_i + \tau_p(n)}\right)$$
 (1.40)

By Eq.(1.32) this becomes

$$\sigma = \sigma_{i} \left[1 - \frac{N}{B+N} \frac{\tau_{i}}{\tau_{i} + \tau_{p}(n)} \right]$$
 (1.41)

But N/B+N is small thus

$$\rho \simeq \rho_{i} \left[1 + \frac{N}{B+N} \frac{\tau_{i}}{\tau_{i} + \tau_{p}(n)} \right] = \rho_{i} + \frac{N}{(B+N)^{2}} \frac{1}{\tau_{i} + \tau_{p}(n)}$$
 (1.42)

We see this is just the residual resistance ρ_i plus a temperature dependent part. Comparison with the result for a perfectly pure metal (Eq.(1.31)) shows that the effect of adding impurities is to shift the temperature dependent resistivity from dependence on the belly relaxation time to the neck relaxation time.

Let us define the effective phonon conductivity in the presence of impurities as though the neck phonon relaxation time $\tau_p(n)$ were applicable to the bellies as well.

$$\sigma_{\mathbf{p}}' = (\mathbf{B} + \mathbf{N}) \tau_{\mathbf{p}}(\mathbf{n}) \tag{1.43}$$

Then we can write Eq.(1.42) as

$$\rho = \rho_{i} + \frac{N}{B+N} \frac{1}{\sigma_{i} + \sigma_{p}^{i}} = \rho_{i} + \frac{N}{B+N} \frac{\rho_{i} \rho_{p}^{i}}{\rho_{i} + \rho_{p}^{i}}$$
(1.44)

This equation represents the parallel combination of ρ_i and ρ_p' in series with ρ_i . If the impurity concentration is large enough to dominate the scattering even on the necks, i.e. $\tau_i \ll \tau_p(n)$ then $\rho_i \gg \rho_p'$. In that case, Eq.(1.43) becomes

$$\rho = \rho_{i} + \frac{N}{B+N} \rho_{p}' = \rho_{i} + \rho'(T)$$
 (1.45)

Although $\rho_p' >> \rho_p$ the weighting factor N/(B+N) tends to offset this effect. In fact, if N/(B+N) is small enough one may wonder if $\rho'(T)$ could be less than $\rho_{ideal}(T)$. Such a result would invalidate this model since it would violate the variational principle. However, one can use the equivalent circuit of Fig. 1.9 to calculate exactly the total resistance in terms of $\rho_{ideal}(T)$ and ρ_i as defined in Eqs.(1.31) and (1.33). After a bit of algebra one obtains

$$\rho = \rho_i + \rho_{ideal}(T)$$

$$+ \frac{(\rho_{i}(n)\rho_{p}(b) - \rho_{i}(b)\rho_{p}(n))^{2}}{(\rho_{p}(n)+\rho_{p}(b))(\rho_{i}(n)+\rho_{i}(b))(\rho_{i}(n)+\rho_{i}(b)+\rho_{p}(n)+\rho_{p}(b))}$$
(1.46)

The first two terms on the right are just the terms from Matthiessan's rule and the last term is the DMR which is seen to be greater or equal to zero. It is zero only if

$$\frac{\rho_{\mathbf{p}}(\mathbf{n})}{\rho_{\mathbf{p}}(\mathbf{b})} = \frac{\rho_{\mathbf{j}}(\mathbf{n})}{\rho_{\mathbf{j}}(\mathbf{b})} \tag{1.47}$$

which means the ratio of the conductivities of the necks and bellies is the same for each mechanism. This would require the ratio of the neck and belly relaxation times to be the same for each mechanism. Since this is certainly not the case for phonons and impurities the DMR is non-zero. Hence, $\rho'(T) > \rho(T)$.

We have seen that dislocations have certain similarities to low temperature phonons and hence produce much more small than large angle scattering. Because of this, one might expect the characteristic e.d.f. due to pure dislocation scattering, $g_d(\vec{k})$, to have a form similar to g_p . If this is so, introducing dislocations into a sample where the impurities are dominant would tend to drive g back toward the low temperature form of g_p . This would result in a lower $\rho_p(T)$ because the variational principle for pure phonon scattering would be more nearly satisfied. The mechanisms of this process are again revealed in the anisotropy of the relaxation time. The value of g is reduced in the necks because of the small relaxation time for dislocation scattering in this region.

Finally, let us consider whether this picture has implications for the functional form of the temperature dependence. In the ideal case of no impurities where $g_p(\vec{k})$ obtains, the belly regions would carry the bulk of the current since they have a much higher conductivity than the highly scattered necks. Another way to view this is that the volume of $g_p(\vec{k})$ over the bellies is much greater than over the necks. Thus, with the bellies shorting out the necks, the overall temperature dependent behavior would be dominated by the bellies. So, we would expect a T^5 behavior. The enhancement of the necks' contribution to $\rho_p(T)$ by impurity scattering should cause the temperature exponent to be less than five due to the larger angle character of the velocity changes on the necks as discussed earlier. However, the re-emphasis of the bellies over the necks when dislocations are introduced might cause the temperature dependence to again follow the Bloch T^5 law.

Let us briefly examine the influence of dislocations in the same two band model. We assume dislocations scatter much more strongly on the necks than on the bellies and that we have added enough dislocations to dominate the neck scattering while being roughly equivalent to the impurities on the bellies. Symbolically this means

$$\tau_{\mathbf{p}}(\mathbf{n}) \sim \tau_{\mathbf{i}} >> \tau_{\mathbf{d}}(\mathbf{n}) \tag{1.48}$$

$$\tau_{\mathbf{p}}(\mathbf{b}) >> \tau_{\mathbf{i}} \sim \tau_{\mathbf{d}}(\mathbf{b}) \tag{1.49}$$

Adding the scattering probabilities within each group we have

$$\frac{1}{\tau(n)} = \frac{1}{\tau_{p}(n)} + \frac{1}{\tau_{1}} + \frac{1}{\tau_{d}(n)} \simeq \frac{1}{\tau_{d}(n)}$$
 (1.50)

$$\frac{1}{\tau(b)} = \frac{1}{\tau_{p}(b)} + \frac{1}{\tau_{i}} + \frac{1}{\tau_{d}(b)} \simeq \frac{1}{\tau_{i}} + \frac{1}{\tau_{d}(b)}$$
(1.51)

Hence

$$\rho(n) \simeq \rho_{\mathbf{d}}(n) = \frac{1}{N\tau_{\mathbf{d}}(n)}$$
 (1.52)

$$\rho(b) \simeq \rho_{i}(b) + \rho_{d}(b) = \frac{1}{B\tau_{i}} + \frac{1}{B\tau_{d}(b)}$$
 (1.53)

Adding the two groups in parallel we get

$$\frac{1}{\rho} = N\tau_{\mathbf{d}}(\mathbf{n}) + \frac{B\tau_{\mathbf{i}}\tau_{\mathbf{d}}(\mathbf{b})}{\tau_{\mathbf{i}}+\tau_{\mathbf{d}}(\mathbf{b})}$$
 (1.54)

Since N << B and Eq.(1.48) applies, we can neglect $N\tau_{d}(n)$ yielding

$$\rho = \frac{\tau_i + \tau_d(b)}{B\tau_i \tau_d(b)}$$
 (1.55)

Thus, the belly regions again dominate the resistivity. In terms of the equivalent circuit of Fig. 1.10, the neck branch is being shorted out by the belly branch. The temperature dependence of the belly branch is thereby emphasized.

We will now briefly consider the interplay of electron-electron scattering with impurity and dislocation scattering. As mentioned previously, a perfectly spherical Fermi surface with no anisotropy in $\tau(\vec{k})$ would exhibit no resistivity ρ_{ee} due to e-e scattering. Since zero resistivity is certainly the minimum possible resistivity, an isotropic $\tau(\vec{k})$ must give the form of the e.d.f. which satisfies the variational principle. Thus $g_{ee}(\vec{k}) \propto g_{i}(\vec{k})$ since $\tau_{i}(\vec{k})$ is isotropic. Here $g_{ee}(\vec{k})$ represents the form of $g(\vec{k})$ characteristic of e-e scattering alone. The introduction of any scattering mechanism which introduces anisotropy into $\tau(\vec{k})$ would therefore cause an increase of ρ_{ee} from its zero value.

Dislocations, being line defects, are anisotropic scatterers in real space. The question is, how can we produce an anisotropic $\tau(\vec{k})$ on a spherical Fermi surface by introducing an array of randomly oriented dislocations. Kaveh and Wiser 36 state that the anisotropic scattering by dislocations can produce the necessary k-space anisotropy of $\tau(\vec{k})$ to yield a non-zero ρ_{ee} for a spherical Fermi surface. However, they do not make clear the distinction between anisotropy in real space and in k-space.

If we suppose that we can define a local Fermi surface in the vicinity of a dislocation (which seems justified due to its great length and long range strain field) then this local Fermi surface will reflect the non-spherical symmetry introduced by the dislocation. In addition, since the k-vectors are still essentially parallel with the velocities, the fact that dislocations only alter velocity components perpendicular to the dislocation line will introduce a corresponding anisotropy in $\tau(\vec{k}).$ This will then be sufficient to produce a non-zero $\rho_{\mbox{\footnotesize{ee}}}$ even for an ideal spherical Fermi surface. For the noble metals we saw that even if e-e scattering were the only mechanism operating, $\rho_{\mbox{\footnotesize{ee}}}$ would be nonzero because of the non-sphericity of the Fermi surface. Since both electrons and charged impurities engaged in large angle scattering via a screened coulomb potential it is still reasonable to assume that $g_{ee}(\vec{k})$ is more or less proportional to $g_i(\vec{k})$. Thus, in the presence of impurities, $\rho_{\mbox{\footnotesize ee}}$ should be near its minimum value. The introduction of dislocations with their associated anisotropic relaxation time should therefore cause an increase in ρ_{ee} .

While most of the foregoing has been qualitative, we shall see that it is consistent with the experimental and theoretical literature.

Reference to the latter will provide the interested reader with a considerably more rigorous development of these concepts.

D. A Review of Experimental and Theoretical Literature

Any attempt to bring order to the experimental data of low temperature resistivity measurements of the noble metals must confront the problem that each author tends to analyze his data with respect to the prevailing theory. Conversely, a single experiment often generates one

or more new theories to explain it. This procedure often makes comparison with other theories difficult or impossible. In addition, we must sometimes make guesses about information not included in the original article in order to reconcile conflicting results. Nevertheless, we shall try to give a coherent account of experimental results obtained since 1966 and theoretical developments since 1960. Of course, our own bias in reinterpreting these past results is obvious, namely, that we believe the data can be accounted for primarily on the basis of the scattering mechanisms and the anisotropy model discussed heretofore. In particular, we will be looking for evidence that: 1) Phonon resistivity is increased by impurities and will have a temperature dependence substantially different than the simple Bloch T^5 law. 2) Dislocations should decrease the phonon resistivity. 3) Electron-electron scattering should contribute a characteristic T² term which may be observable at low enough temperature in sufficiently precise measurements. 4) This e-e term will probably exhibit an increase when dislocations are introduced.

1) Some Experimental Results

The Bloch T⁵ law is broken by so many metals at low temperatures. that the high esteem it is given in the literature hardly seems warranted. In fact Kaveh and Wiser³⁷ state flatly "The Bloch T⁵ does not describe the low-temperature electrical resistivity of any metal." We shall see that, generally, the noble metal data supports this conclusion. Before considering the individual publications, some of the results of their analyses are presented as a group to facilitate intercomparisons and provide some numerical values not included in the discussion. These results are summarized in Tables 1.1, 1.2, and 1.3. These tables are

for Ag, Au and Cu respectively. In order to understand the information in the table, the following explanation and code-key is necessary.

Guide to Interpretation of Table 1.1, 1.2, and 1.3

The general data fitting equation used can be expressed as

$$\rho = \rho_0 + AT^M + BT^N \tag{1.56}$$

For a given case, some of the five parameters on the right side were fixed while the other were allowed to vary to produce the best fit. Any parameters which were held constant have their values <u>underlined</u> in the tables. If a single power fit was used, the coefficient of the remaining term is set to zero. Each quantity is expressed with the error in parenthesis if known. The least significant digit of the error is to be ascribed to the last (rightmost) digit of the expressed quantity. For example, .73291(12) means .73291±.00012 (note that to save space nonsignificant zeros left of the decimal point are suppressed). The following is a column by column explanation:

Author (Ref): Only the surname of the first author is given along

with the reference number.

Samp: Author's sample identification label.

 $\rho_{\alpha}(n\Omega cm)$: The residual resistivity which is a fitting para-

meter unless underlined.

A($f\Omega$ cm): The coefficient A of the lower power of T given in

 10^{-15} ohm cm. Normally goes with power of three or

less.

M: The lower of the two powers, M, generally three or

less.

 $B(f\Omega cm)$: The coefficient B of the larger power of T given in

10⁻¹⁵ ohm cm. Normally goes with powers greater

than three.

N: The larger exponent, N, generally greater than three.

Range(K): The temperature range over which the fit was made

in degrees Kelvin.

 $RRR(10^3)$: The residual resistance ratio, RRR = R(room tempera-

ture/R(4.2 K), expressed in units of 1,000.

Crystalline state s = single crystal, p = poly-Cry:

crystalline.

Imp: The added impurity in a dilute alloy.

Str: If a sample is known to have been strained either by

> choice or accident, it will be marked with an X. If a set of samples can be sequenced by the amount of strain each has suffered, they will be marked in increasing order of strain by Roman numerals. If a sample has probably been strained, it will be marked with a P. A sample known to be relatively

strain free will be marked with a 0 (zero).

 $\Delta_{\mathtt{dat}}(\mathtt{f}\Omega\mathtt{cm})$: The estimated error of measurement in $f\Omega$ cm.

 $\Delta_{\text{fit}}(f\Omega\text{cm})$: The estimated error of the fit. Should be of the same

order as $\Delta_{\mbox{\scriptsize dat}}$ for a good fit. If too small, indicates overfit or mistake in published error.

Comments: This is a catch-all for other bits of information

with the following code: BE = best equation of several; NBE = not best equation; d = diameter or thickness in the smallest dimension in mm. For example, d = .50. VA = vacuum annealed; NA = not annealed; OA = oxygen annealed; Gen = generated from

results given in different form.

Before we consider the violations of the Bloch T^5 law we will first mention two claims in support of it. Recall from Eq.(1.17) that the conductivity can be expressed as an integral of the mean free path over the Fermi surface. A T^{-5} temperature dependence of electron mean free paths is deduced from high-field and open orbit ultrasonic attenuation data in Cu by Cox and Gavenda. 38 However, they assumed the mean free paths, ℓ , could be expressed according to Matthiessen's rule

$$\ell^{-1} = \ell_1^{-1} + \ell_p^{-1} \tag{1.57}$$

Table 1.1 Some published experimental results for Ag (see text for interpretation)

		Po nsscm	A (focnik ^{-M})	I	B (focnk ^{-N})	E	ox.	Range (K)	RRR (10 ³)	Cry Imp	좥	Stra	Stra A _{dat} A _{fit} (focm) (focm)	^A fit (facm)	Comments
Kos ⁽³⁹⁾	Ag3	.718609	14.9 (1.6)		2.34 (17)	v	1.4	- 4.2	2.1	٩		-	9-	2.5	BE d=.25, VA,G
		.718570	38.5 (3.7)	2	2.71 (10)	8								7.2	NBE
	Ag2	173191	16.0 (1.0)	٣	2.14 (1)	2	1.4	- 4.2	2.0	٩		=	-10	9.	BE d=.50,VA,G
		.773158	37.5 (1.8)	2	2.60 (5)	S								3.8	NBE
	Agl	.873620	17.5 (7)	e	1.47 (7)	S	1.4	- 4.2	1.7	۵		=	-10	-	BE d=1.0,VA,G
		.873576	42.3 (9)	2	1.96 (2)	S								8.	NBE
Barber ⁽¹⁷⁾	61	2.20	0		21.5 (1)	•	ĸ	- 12	69.	٥					0A,G
	19	4.62	0		22.5 (1)	•	ď	- 20	.33	۵					0A,G
	29	1.71	0		17.5 (1)	4	4	- 15	68 .	٩					0 A ,G
	99	1.46	0		17.5 (1)	•	М	- 15	1.0	۵					0A, G
	11	1.54	0		(1) 61	4	4	- 16	1.0	۵					0 4 ,G
	68	1.22	0		16 (1)	4	S	- 15	1.2	۵					0A,G
	38	123	0		(2)	•	4	- 10		۵	₹				0A,G
	37	65	0		58 (2)	4	4	0.		۵	₹				0A,G
	35	15.6	0		4 3 (2)	•	4	œ •		۵	¥				0A,G
	45	14.4	0		28 (2)	•	4	- 20		٩	2				0A,G
	6	6.07	0		24 (2)	4	7	- 20		۵	В				0 4 ,6
	45	290	0		43 (2)	4	•	<u> </u>		۵	2				0A,G
	43	472	0		48 (2)	•	4	- 20		۵	2				0A,G

Table 1.1 continued.

Author (Ref.)	Samp	Po nisca	A (fixmK ^{-M})	I	B (focmK ^{-N})	*	Range (K)	RRR (10 ³)		ap St	Cry Imp Stra A _{dat} A _{fit} (focm)	Adat Afit (fucm)	Comments
Barnard ⁽¹⁶⁾	38	0.75	0		25.5 (5)	-	1.7 - 4	2.0	5				0A, BE
	36	0.77	0		20.1 (2)	•	2 - 5	2.0	ø		•		OA, BE
	4	0.70	0		30.2 (3)	•	1.2 - 4	2.2	•				Ø, 8€
	2	1.1	0		51.3 (2)	~	1.2 - 5			Ą			OA, BE
Koshnevis an⁽¹³⁾	AgA	.36267			11.9	3.97	3.9 - 7.6	4.7	۵				OM, d=2
	AgB	. 18126	0		13.4	3.94	2.0 - 4.33	3 8.0	۵		7		0A, d=2
		. 18118	47.4	2.46	0	-	0.14 - 1.11	=					
	A ₉ C2	.16846	•		13.0	3.94	2.0 - 6.0	=	۵		.3		0A, d=2
	AgC3	.29871	0		13.4	4.03	1.7 - 4.2	9.6	۵		Ģ		0A, d=2
		.29862	47.2	2.62	0		0.03 - 1.65	Ş.					
		. 29862	52.6	2.44	0		0.03 - 1.04	¥					
	AgD	.21941	0		13.0	3.89	1.5 - 6.17	1.7 7.1	۵		7		0A, d=2
		.21935	46.1	2.39	0		0.03 - 1.54						
		.21935	46.7	2.19	0		0.03 - 1.28	8.					

Table 1.2 Some published experimental results for Au (see text for interpretation)

						ואב ובצו ו	(see text for interpretation)	(E)				
Author	Samp	°	⋖	E	•	z	Range	RRR	Cry Si	tr Adat	Afit	RRR Cry Str Adat Afit Comments
		(nocm)	(focmK ^{-M})		(focmK ^{-N})		ı	(10 ³)		(facm)	(focm) (focm)	
Koshnevisan ⁽¹⁴⁾ Aul	Au J	.389840 (9)	0		43.3 (2)	3.975 (2)	43.3 (2) 3.975 (2) 1.48 - 6.40 5.6	5.6		α,		
		(6) 662688.	0		44.5 (5)	3.959 (6)	44.5 (5) 3.959 (6) 1.48 - 6.80	!		•		C. 1-B . 50
		.389886	0		65.2(3.0)	3.28 (41)	65.2(3.0) 3.28 (41) 0.5 - 1.0					
	Au3	.775220 (28)	0		51.0 (3)	3.987 (3)	51.0 (3) 3.987 (3) 2 - 7.1	2.8	·	31.		
		(2) 901577:	0		63.7(3.0)	63.7(3.0) 3.47 (15) 0.5 - 1.3	0.5 - 1.3	}	,	2		e

Table 1.3
Some published experimental results for Cu (see text for interpretation)

Author	Samp	P ₀	A M (focmk ^{-H})	B (focmK ^{-N})	z	Range	RRR (10 ³)	RRR Cry Str ådat åfit 10 ³) (focm) (focm)	dat (focm)	dat Arit (focm) (focm)	Comments
Rumbo ^(4,7)		ונוו ס	16.45	0.0679	vo v	1 - 8.5 8.5	13.5	v	٠,	8 9	OA, BE
Koshnevisan (14)	[3]	0.653902 (4)	0 40.3 (1.3) 2.38(4)	5.10 (5)		3.930 (5) 3.06 - 7.00	2.6	٩	. £	8	0A, d-2
			41.9 (1.3) 2.32(9)	0 (6)		0.6 - 1.85					
	Cu5	0.312961 (8)	0	2.55 (7)		4.020(15) 3.47 - 7.00	5.4	•	9		0A, d-2
	gno	0.404212 (5)	0	3.00 (5)	3.994 (7)	2.57 - 7.53	4.2	٩			OA, d-2
,			34.8 (1.7)2.03 (7)	0 (2)		0.064 - 2.15			80		
Koshnevisan	R-Cu)	R-Cul 0.11314 (10)	0	10.6 (2.	10.6 (2.5) 3.32 (10) 3.3 - 7.21	3.3 - 7.21	13.7	ø	-50		8
(analysis of	R-Cu3	R-Cu3 0.17612 (2)	0	4.56(.3	4.56(.30) 3.69 (3)	3.08 - 7.28	8.8	v	-35		ĕ
Rumbo's	R-Cu4	R-Cu4 0.20991 (20)	0	15.4 (8.	15.4 (8.0) 3.0 (2)	3.03 - 7.27	7.4	•	07-		8
data)											

where i and p again represent impurity and phonon scattering. They further assume

$$\ell_{\rm p}^{-1} \propto (T/\theta_{\rm D})^{\rm N} \tag{1.58}$$

where N is a constant. In this case the best fit is for N = 5. We have seen that these assumptions may be very poor for an anisotropic Fermi surface. It should be noted, however, that the copper sample used was extremely pure (RRR = 35,000) and consequently may well have been dominated by scattering from dislocations which are always present at some concentration. We have seen that dislocations may bring out the presumably T^5 behavior of the belly electrons. Of course, these are not resistivity measurements per se and they are made in a magnetic field. The validity of making a direct transfer of this temperature dependence to the electrical resistivity of a metal with a complicated Fermi surface is not obvious.

Ehrlich and Schriempf¹¹ measured very high purity single crystal silver (RRR = 10,000) between 2 and 20 K. They find an approximate T⁵ temperature dependence below 10.5 K and a slightly higher exponent above this temperature. These exponents were determined by the slopes of loglog plots of $\rho(T)$ vs. T and hence, are not very precise. 10.5 K is the temperature at which $\rho(T) = \rho_0$, the residual resistivity. A close look at their log-log graph reveals that between 5 and 10 K many of the points lie above the line drawn through the data and the total number of points, especially at the lower temperatures, is rather small with appreciable scatter. Thus, the exact power dependence is somewhat uncertain particularly at the lower temperatures. However, in light of the anisotropy model, a nearly T⁵ behavior at temperatures where $\rho(T) \sim \rho_0$ is not too

surprising since the neck conductivity should be dominated by phonon scattering and thus be quite low relative to the bellies. The now dominant bellies might be expected to give a T^5 dependence.

We now turn to results which show definite departures from the Bloch T^5 law.

J. F. Kos³⁹ measured the electrical resistivity of long silver wires (0.25-1.0 mm diameter) from 1.4-4.2 K using a nanovolt potentiometer and galvoamplifier obtaining a precision of about 4 in 10^5 . The silver was rather pure having an RRR (residual resistivity ratio) value of about 2,000. Still, this data is well within the dirty limit and therefore it should not exhibit a simple T^5 temperature dependence. This is indeed the case. Kos could best fit the data with the following equation

$$\rho = \rho_0 + A_1 T^{m} + B_1 T^{5}$$
 (1.59)

with m = 3. He interpreted this as support for a since discredited theory invoking phonon drag. However he got nearly as good a fit with a T^2 rather than a T^3 term in Eq.(1.59). In fact, if the published fitting errors are correct, both equations would seem to over-fit his data since the fitting errors claimed are on the order of 2 in 10^6 . This may be due to the fact that only nine points were fit with three parameters, ρ_0 being adjustable. In that case, it is hardly justified to say that the one fit is really better than the other. The coefficients of the T^2 term are included in Table 1.1 for comparison. He notes that the larger diameter samples probably had more strain introduced by winding them on the sample holder causing larger residual resistivities. However, he notes that the more strained samples had lower $\rho(T)$ values (where $\rho(T)$, as

before, refers to just the temperature dependent part of the resistivity). This is indicated by a systematic downward shift of the T^5 coefficient and is consistent with our expectations. In a second paper 40 dealing with similar samples from 1.4-295 K, Kos claims to have determined the true ideal resistivity $\rho(\mathsf{T})$ by extrapolating data to zero residual ideal resistivity from samples of differing purity at a set of fixed temperatures. The procedure used is of dubious validity at the lowest temperatures since it involved a linear extrapolation from various samples which were all in the dirty limit. The value of ρ_{ideal} so determined is likely to be simply proportional to the $\rho(\mathsf{T})$ of his actual samples. Thus, the 4.56 temperature exponent of ρ_{ideal} which he finds between 2 and 9 K still corresponds to the dirty limit.

Barber and Caplin ¹⁷ measured the resistivity of pure Ag and its dilute alloys with Au, Pd and Pt from 2-20 K. Using a galvanometer amplifier of nanovolt sensitivity with sufficiently large geometrical factors (length/cross section) they could make meaningful measurements down to 4.2 K and even below in a few cases. While there was appreciable uncertainty in the temperature determination, the resistivity of most samples could be fit well between 4 and 10 K by

$$\rho = \rho_0 + BT^4$$

where ρ_0 was quite well known from the lowest temperature measurement. Other fitting equations appreciably different than this did not fit as well. Significantly, the equation used by Kos (Eq.(1.59)) did not fit well. While at the lower temperatures these results are not precise enough to provide a very meaningful appraisal of a possible T^2 contribution, the higher temperature deviation from the T^4 behavior is quite interesting. In the nominally pure silver samples,

the purest of which had an RRR \approx 1,400, the resistivity began to increase more rapidly than T^4 at temperatures above 10 K. This is consistent with the T⁵ behavior of the much purer sample of Ehrlich and Schriempf because at the higher temperatures the phonon scattering is becoming strong enough to influence the form of the distribution function; shifting it toward the ideal $g_{\mathbf{p}}(\mathbf{k})$. Again, the corresponding increase in the bellies' contributions to the conductivity causes a trend toward T^5 behavior. Conversely, they found the samples alloyed with Au and Pt to deviate downward from the T⁴ behavior above 10 K. In fact, given the scatter of the data, the graphs for these alloys do not really appear to favor T⁴ over any part of the temperature range from 4 to 20 K with the possible exception of the most dilute AgPt alloy. It would appear that a power somewhat less than four would produce a better fit. Unfortunately, they did not try this possibility. The AgPd alloys, on the other hand, did not show any systematic deviations from the T^4 behavior over the entire temperature range. While a detailed calculation using appropriate scattering potentials for each type of impurity might reveal the origin of these differences and actually determine the temperature exponent in a particular temperature range, there is little we can say. on the qualitative level of the present analysis. We can only suppose that each type of impurity contributes a characteristic anisotropy of its own to the relaxation time and this may in turn have an effect on the temperature exponent. However, these data show no systematic differences between the homovalent impurity Au and the impurities Pt and Pd which both lie in the same column of the periodic table just to the left of Ag. Measurements and calculations of such impurity relaxation time anisotropies are reviewed by Bass. 31

One final note of interest is that whatever the temperature exponent, the values of $\rho(T)$ all show monotonic increase with impurity content. increasing roughly as log $\rho_{\text{\tiny O}}$ and showing no clear signs of saturation for large impurity concentrations. If we define these increases in $\rho(T)$ in terms of the usual equation for DMR (Eq.(1.27)) we find these DMR can be very large. For example, if we obtain $\rho(i,T)$ from the purest sample of Ehrlich and Schriempf we find the DMR to be about 40 ρ_{ideal} for the most concentrated alloy at 4.2 K. These authors indicate that the fact that the DMR do not saturate over three orders of magnitude of ρ_{O} may be more than the anisotropy model can handle and other mechanisms may be necessary. While other mechanisms may indeed be necessary, only realistic calculations of the DMR based on the anisotropy of neck and belly relaxation times can determine at what point it fails if at all. Bergman et al.41 performed such calculations to explain the DMR observed in Al by Caplin and Rizzuto. 42,43 These calculations fit the DMR at 14 K very well showing that, using the more realistic 2-OPW electron wave functions rather than 1-OPW functions, the anisotropy model can account for the two orders of magnitude change in ρ_{Ω} required to produce saturation of the DMR in Al. The anisotropy of phonon scattering in the noble metals is such that even though the belly electrons may be well within the dirty limit at a given temperature, the neck electrons may require much higher impurity concentrations before they are completely dominated by impurity scattering at the same temperature. Thus, three orders of magnitude change in $\boldsymbol{\rho}_{0}$ may not be entirely unreasonable before DMR saturation occurs. 44 In any case, even if the anisotropy model fails to entirely account for the DMR of metals with rather large impurity content (~lat%) it should be applicable to the rather pure metals.

Rumbo 15 achieved much greater sensitivity than the aforementioned authors at temperatures below 8.5 K by using a type of Josephson junction device called a SLUG. This allowed use of shorter and thicker samples whose purity is more easily controlled and which can be grown as single crystals. The mechanical strength of such thicker samples makes it less likely they will be strained during handling. Four samples were prepared. Two were single crystal and two were polycrystalline. They had RRR values from 1,100 to 3,300 with the highest values belonging to the single crystals. They all exhibited a region of approximately $T^{3.5}$ dependence above 3.5 K. From 1 to 3 K their resistivities were preportional to about $T^{2.5-2.8}$.

The effect of strain on the temperature dependent resistivity $\rho(T)$ in Ag as well as Pd and Al was measured by Rowlands and Woods 35 at a series of fixed temperatures starting at 10 K for the Ag sample and going up to 49 K. They observed a decrease in $\rho(T=10 \text{ K})$ with strain for deformations which were not too severe. This decrease was still apparent within their resolution at 13 K but at 20 K and above it could no longer be resolved. However, at these higher temperatures $\rho(T)$ remained constant which is not what is observed with the addition of chemical impurities. They interpreted this behavior, as well as the more marked decrease of $\rho(T)$ in Al and Pd in terms of the anisotropy model as presented here. Because of their limited resolution the effect is just resolvable at 10 K and its detailed behavior cannot be determined. Unfortunately, they did not possess sufficient sensitivity to make useful measurements at lower temperatures.

Now we turn to work in Ag more directly relevant to this dissertation, i.e. high precision measurements at liquid helium temperatures. Barnard

and Caplan¹⁶ performed very high precision measurements (up to 1 ppm) on large single crystals of Ag and on Ag 0.02% Au alloy from 1.2 to 9 K. They achieved the necessary sensitivity by using a SQUID null detector circuit similar to that described in Chapter 2. These measurements could be fit with great fidelity in the temperature range of 1.2-4.2 K using the equation

$$\rho = \rho_0 + BT^4 \tag{1.60}$$

However, above this temperature the points of all the pure Ag samples drop below this line. When they plot $\rho(T)/T^4$ vs. T on a log-log plot they get a level line which remains very constant at the value of B in Eq.(1.60) to about 4 K. Above this temperature the curves bend downward with increasingly negative slopes, up to their highest temperatures, ~9 K, with no clear sign of stopping. Since the slope of this log-log plot is proportional to the effective temperature exponent N(T), it is clear that N(T) is decreasing with increasing temperature. If one calculates the effective temperature exponents from these plots they are found to range downward from the constant value of 4 to values in the vicinity of 3.45 to 3.25 at the highest temperatures measured. The data would seem to indicate that they will drop still lower although one would hardly expect them to drop below 3, the value obtained from phonon scattering at low temperatures if the small angle restriction is dropped. These values are significantly lower than the temperature exponent of 3.5 found by Rumbo. This downward trend has been rather well reproduced in calculations by Bergman et al. 45 Unfortunately, they do not include specific details of the calculation for Ag although they show a similar calculation for aluminum. The calculation includes the effects of dislocations within

the anisotropy model. It is interesting to note that the pure polycrystalline samples of Barbar and Caplin went to values of N larger than 4 for T > 10 K. However, the values of N for two of the dilute Ag alloy systems deviated below the value 4.

Similar high precision measurements on Ag by Koshnevisan et al. 13 in which this author was involved also observed a rather strict T^4 dependence between 2 K and 8 K. These samples, although polycrystalline, were of higher purity, having RRR values between 4,700 and 11,000. The coefficient of the T^4 term was as much as a factor of four lower than the values obtained by Barnard and Caplin. Again, this variation is consistent with the enhancement of $\rho(T)$ by impurities and the fact that these purer samples may have had a larger fraction of their residual resistivity attributable to dislocations which would further reduce $\rho(T)$. This comparison will be made in greater detail in Chapter 3.

These measurements were done on a dilution refrigerator where the high precision of about 1-2 parts in 10^5 along with the low temperatures allowed meaningful fits to be made to data below 1.5 K. Details of these results are also given in Chapter 3.

There were no high precision measurements of the resistivity of gold at liquid helium temperatures prior to the work of Koshnevisan et al. 14 in which this author was also a participant. The work of Damon et al. 46 on DMR in gold alloys are not precise enough at liquid helium temperatures to say anything about the details of their temperature dependence. Above 10 K, they show increasing DMR with impurity concentration. They attribute part of the the effect to the anisotropy model and part to "phonon-assisted impurity scattering," or "inelastic impurity scattering as it is more commonly designated. Koshnevisan et al. observed the same rigorous T4

dependence in Au as seen by Barnard and Caplin and Koshnevisan et al. in Ag between ~ 1.5 and ~ 7 K. The two samples measured were pure single crystals with RRR values of 5600 and 2800. Again, the sample of lower purity had a larger coefficient of T^4 . Neither sample showed any clear T^2 dependence at lower temperatures. When fit by a single power, T^N , the exponents were 3.28 and 3.47. Further analysis is included in Chapter 3.

In the same paper, Koshnevisan et al. gave the results of similar high precision measurements on copper between 0.06 K and 7.5 K. Again between ~ 3 and ~ 7 K a very strict T^4 dependence is observed in these polycrystalline samples with RRR values of 2,600 and 5,420. The largest deviation from a perfect power of four was an exponent of 3.93 for the sample of lowest purity. Again, the coefficients increased with increasing impurity content. The magnitude of the T^4 coefficient was on the order of ten times less than in gold and about four times smaller than in silver.

Because Cu of the three noble metals was the highest Debye temperature (θ_D = 315 K) and thus, has the smallest phonon contribution at a given T, there may be a better chance of seeing the T² term from electron-electron scattering. In only one run were the experimental problems sufficiently subdued, including the elimination of the Kondo effect due to magnetic impurities, that the low temperature data could be fit with a high degree of confidence. In this case, the fit produced an exponent of 2.03 providing the best evidence published to date for e-e scattering in one of the noble metals. The coefficient was in excellent agreement with theoretical predictions which will be considered shortly.

These results are somewhat at odds with those of Rumbo 15,47 which preceded them. In the earlier of these publications he fit data from

a extremely pure (RRR = 13,500) single crystal of Cu to an equation of the form used for Ag by Kos (Eq.(1.59)) which he found to give the best fit over the full temperature range from 1-8.5 K. Like Kos, he found the next best fit when substituting T^2 for the T^3 term. However, while other variants of this term were tried, the T⁵ term was never varied, again showing the faith which most experimentors had that low temperature results should contain a additive T⁵ term in keeping with the Bloch T^{5} law. He found a single power fit from 5 to 8.5 K to work quite well with an exponent of 3.5. In the later publication he expanded his studies to more Cu single crystals, with resistance ratios between 13,690 and 5,850, as well as the Ag samples already discussed. While using Eq.(1.59) to extrapolate to ρ_0 , he then plotted $\log(\rho-\rho_0)$ vs. log T to obtain single temperature exponents. He found an exponent of 3.5 above 4 K and about 2.8 below. However, with the SLUG type null-detector circuit his precision was 1 or 2 parts in 10^4 on his best runs. Thus his low temperature data cannot be pushed for much detail.

While the values of $\rho(T)$ systematically increased with ρ_0 for his Ag samples, his Cu camples showed the lowest $\rho(T)$ for the <u>second</u> most pure specimen. He guessed that it might be due to size effect. However, in the light of what has already been said, it is more likely that the residual resistivity of this sample contained a larger ratio of dislocations to impurities than the purer sample, thus producing a lower $\rho(T)$. We shall see there is strong evidence for this view in Chapter 3.

2) Theoretical Developments

Having already discussed the general theory, in which several references were given, we now will consider some specific calculations

for phonon and electron-electron contributions to $\rho(T)$ and the effects of dislocations and impurities.

Dosdale and Morgan 18 have calculated the dirty limit resistivity of Cu between 5 and 30 K. This calculation used a pseudopotential which gave reasonable values for the band gap at $\frac{1}{2}\frac{1}{2}\frac{1}{2}$. By using two plane wave states the neck and belly radii were given reasonable values. They performed the calculation in a manner similar to that used for A1. 48 The calculation incorporated the electron-phonon relaxation time anisotropy but assumed isotropic impurity scattering. Although the calculated $\rho(T)$ was too large by about a factor of 2.5, the temperature dependence agreed quite well on a log-log graph with experimental results showing an average exponent of about 4.7 from 5 to 10 K and 3.8 from 10 to 30 K. We shall see that this behavior is in good agreement with our own experimental results.

Brett and Black 44 performed variational calculations of the phonon electrical resistivity in copper below 20 K. They used 2-0PW electron states to determine the electron-phonon scattering matrix element where the phonon frequencies and eigenvectors were determined by the Born-Karman method. A rather realistic analytical representation of the Fermi surface was used--the so called "eight cone model" of Ziman. In this model the Fermi surface is approximated by eight identical surfaces, each bounded by a cone whose axis lies in one of the eight [1,1,1] direction. The shape of the surface is determined in the model by specifying a neck radius and the Fourier component of the lattice pseudo-potential in the [1,1,1] direction. The variational trial function was proportional to $\vec{v}(\vec{k}) \cdot \vec{\epsilon}$, where $\vec{v}(\vec{k})$ is the group velocity, rather than the simpler $\vec{k} \cdot \vec{\epsilon}$ which is correct for 1-0PW states. The anisotropy of the

phonon relaxation time was also explored and used to calculate the resistivity using a <u>total</u> relaxation time which is constant, i.e. an impurity dominated distribution function $g(\vec{k})$. The ratio of these relaxation times is included in Table 1.5.

They claim to find a T^5 behavior of the resistivity below 20 K. although examination of their published figures shows the exponent to actually be about 4.9. A value so close to 5 is a little surprising for a dirty limit calculation and is at variance with Dosdale and Morgan's calculation. They state that it is unlikely that the precise temperature dependence will be revealed by any of the OPW calculations to date. However, they believe that the lower powers of T seen by Rumbo and Kos may be due to a change from dirty limit behavior at low temperatures to clean limit behavior at higher temperatures, say 20 K. The magnitude of their calculated $\rho(T)$ is too large compared with experimental values at most temperatures but the experimental results tend toward their calculated values as impurity content increases and come to within a factor of 2 at 20 K. At 3.5 K the experimental results for the less pure samples agree quite well with the calculation although at 2 K the experimental values are actually larger. The better agreement at 3.5 K may be due to the fact that the true dirty limit has been reached while the larger experimental values at 2 K may be due to a significant electron-electron contribution which was not included in the calculation.

They also performed a rough calculation for the clean limit phonon resistivity and find values which are slightly lower than the purest published values between 5 and 10 K. The experimental values are seen to approach their calculated ones as purity increases. They also calculated the phonon-electron relaxation times in the clean limit for various

points on the Fermi surface at various temperatures. These results are listed with others in Table 1.5.

We now turn to calculations of the electron-electron term in the noble metals. W. E. Lawrence l used a 2-OPW model which is somewhat similar to the eight-cone noble metal Fermi surface of Ziman mentioned above. He starts by factoring ρ_{e-e} into a term due to the characteristics of the translationally invariant electron gas and a term he calls the "fractional umklapp scattering" Δ . This term represents the essential effect of the ionic medium and is a measure of the effectiveness of scattering events $(\vec{k}_1, \vec{k}_2) \rightarrow (\vec{k}_3, \vec{k}_4)$ in degrading the current.

$$\rho_{e-e} = \frac{m}{ne^2} = \{ [\pi^3 (k_B T)^2 / 12 \pi E_F] \Gamma \} \Delta$$
 (1.61)

$$\Delta = \langle |\vec{v}_1 + \vec{v}_2 - \vec{v}_3 - \vec{v}_4|^2 W \rangle \langle |\vec{z}_V|^2 W \rangle^{-1}$$
 (1.62)

where \vec{v}_i is the velocity of the state \vec{k}_i . The angular brackets denote the Fermi surface integrals over all quartets of crystal-momentum-conserving states with scattering probability W. The values of \vec{v}_i and W are determined from the 2-OPW model. He estimates Δ to be ~3/4 for the noble metals with the value for Cu slightly greater and Ag slightly less. The quantity in curly brackets is the basic e-e scattering rate; Γ is a dimensionless number representing the Fermi surface average of the scattering probability. The calculated values $\rho_{e-e}T^{-2}$ are included in Table 1.4.

Lawrence also determined "crossover" temperatures below which his values of ρ_{e-e} exceed ρ_p values which he also calculated. These crossover temperatures are 2.4 K, 2.2 K, and 3.6 K for Ag, Au, and Cu

Table 1.4. Theoretical estimates of the e-e contribution to the resistivity.

	Δ±30%	$(10^{-15} \Omega \text{cm/K}^2)$ $\rho_{ee} T^{-2} \text{ (Lawrence)}$	Δ±30%	ρ _{ee} T ⁻² (Black)
Ag	0.73	140		
Au	0.77	140		
Cu	0.79	76	0.28-0.41	27-39

respectively. Lawrence attributes the T^3 term in the fit to Rumbo's data as the result of being in this crossover temperature regime. In light of the success of including a ρ_{e-e} term in fitting our results which will be demonstrated in Chapter 3 it seems Lawrence may be correct.

J.E. Black² attempted to improve the calculation of Lawrence by removing some of the approximations. The improvements were applied to the calculation of the fractional umklapp parameter Δ for Cu. One improvement was the explicit use of the eight-cone model of the Fermi surface. A second was the inclusion of a number of neglected terms. The third improvement was the inclusion of exchange effects. Because, by and large, these improvements caused an increase in the denominator of Eq.(1.62) their calculated values were lower than those of Lawrence by 30-50%. The range of values results from uncertainties of the effects of the Fermi surface. Their values are also included in Table 1.4 They point out that their use of the Born approximation (also used by Lawrence) may produce values as much as two to five times larger than a proper phase shift calculation would yield. This could make e-e scattering very difficult to detect in silver and gold. However, the low temperature data of Koshnevisan et al. show a $T^{2.2-2.6}$ dependence below 1.5 K in Aq suggesting the term is not as small as the worst case estimate and the factor of two reduction 49 seems about right.

Recent theoretical work by Berman, Kaveh and Wiser ³ specifically addresses the experimental findings of Barnard and Caplin and Koshnevisan et al. regarding the T⁴ behavior of the resistivity in Ag. Their explanation of the origin of the T⁴ dependence and the sample dependence of its coefficient is based on the concurrent interaction of all four scattering mechanisms under discussion; impurity, dislocation, phonon, and

electron-electron scattering. The basis of the interaction is via the anisotropy model we have set forth. They show graphically that despite its apparent rigor, the T^4 term can be represented within experimental error by a fortuitous juxtaposition of a T^2 electron-electron term and a $T^{4.5}$ electron phonon term between about 2 and 5 K. That is

$$\rho = \rho_0 + AT^2 + CT^{4.5} \tag{1.63}$$

Since the samples in question can be regarded as being in the dirty limit below 5 K they refer to previous parameter free calculations 50,51 of ρ_n to obtain the 4.5 exponent for $2 \le T \le 5$. Below 2 K the exponent is ~5. To fit a typical case where the T⁴ coefficient B was experimentally determined to be about 30 f Ω cm K⁻⁴, they find a T² coefficient A of 30 f $\Omega cm\ K^{-2}$ is required. This value is a factor of ~4 lower than the value predicted by Lawrence. This factor of 4 is easily accounted for if one assumes that the 30-50% reduction Black found for his refined calculations for Cu can be applied to Ag and the remaining reduction is attributed to phase shift corrections. To account for the variation of B they invoked dislocation scattering and the anisotropy of $\tau_d(\vec{k})$. In the dirty limit, if only impurities are contributing to the residual resistivity (i.e. $\rho_0 = \rho_i$), the value of $\rho_0(T)$ should be independent of ρ_0 . Bergmann et al. argue that the observed sample dependence of $\rho_0(T)$ exhibited by the reported variations of B are due to the fact that in any high purity sample the residual resistivity is actually composed of contributions from impurities and dislocations so that

$$\rho_0 = \rho_1 + \rho_d \tag{1.64}$$

The variations of the ratio of ρ_i/ρ_d between samples of the same ρ_o can then account for the sample dependence. In Chapter 3 we shall provide ample experimental justification for this conjecture.

In an earlier paper 45 these same authors have performed calculations of $\rho(T)$ which indeed account for the discrepancy in B between two different samples of Barnard and Caplin by assuming different relative amounts of ρ_i and ρ_d .

To demonstrate the strong dominance of the dislocation scattering in the neck regions they schematically express the phonon resistivity as

$$\rho_{p}(T) \sim \iint ds(\vec{k}_{1})ds(\vec{k}_{2})[g(\vec{k}_{1})-g(\vec{k}_{2})]^{2} P_{p}(k_{1}k_{2};T)$$
 (1.65)

where $P_p(\vec{k}_1\vec{k}_2;T)$ is the phonon scattering probability between states \vec{k}_1 and \vec{k}_2 . This double Fermi surface integral contains the electron distribution functions $g(\vec{k})$ which are solutions to the Boltzmann equation in the presence of a unit electric field $\hat{\epsilon}$.

$$g(\vec{k}) = -e\tau(\vec{k})\vec{v}(\vec{k}) \cdot \hat{\epsilon}$$
 (1.66)

By assuming a constant, impurity dominated $\tau=\tau_0$ they domonstrate that scattering through angles such that both initial and final states remain in the neck region can enhance the factor in square brackets in (1.65) by as much as two orders of magnitude. This is due to the fact that both states require a 2-OPW description. The neck region is large enough so that both states can be within an angle of ~2°-5°. Thus, both dislocation scattering, dominated by angles <1°, and small angle phonon scattering at low temperatures would be strongly enhanced in the neck regions for an isotropic $\tau(\vec{k})$. They also show that the anisotropic relaxation time

which would result if a small but significant dislocation density were present say 0.01 $\stackrel{<}{_{\sim}} \rho_d/\rho_i \stackrel{<}{_{\sim}}$ 0.10 would be sufficient to account for the observed 35% variations in B. This is because even a small value of $\boldsymbol{\rho}_{\boldsymbol{d}}$ can imply complete domination of the total relaxation time in the neck regions. They note that the phonon anisotropy is even greater than the dislocation anisotropy at the temperatures under consideration. (We might speculate therefore, that even a dislocation dominated e.d.f. might not result in the true $\rho_{ideal}(T)$). They stress however that if even one of the electron states involved in the scattering is in a belly region so that it can be described by a single OPW state this enhancement does not occur. Small angle scattering mechanisms produce, therefore, precisely the type of scattering which is least resistive in the belly regions but strongly resistive in the necks because it satisfies the necessary condition that both initial and final states remain in the neck region. This leads to the high degree of anisotropy in the electronphonon and electron- dislocation transport relaxation times.

3) Determinations of Relaxation Time Anisotrophy

We have based our arguments on the anisotropy of the conductivity relaxation times over the Fermi surface for phonon and dislocation scattering. In this section we shall show experimental and theoretical evidence obtained by other methods to substantiate the anisotropy and to show that it is of similar character for phonons and dislocations. These values can then be compared with estimates obtained from resistivity measurements. We shall use the ratio of belly to neck relaxation times $\tau(b)/\tau(n)$ as a measure of the anisotropy.

There are a number of methods which can be used to probe the relaxation time for scattering by impurities dislocations and phonons at various points on the Fermi surface. These methods all involve the use of magnetic fields at low temperatures and all rely on the fact that an electron follows a cyclic trajectory in real space and k-space if allowed by the geometry of the Fermi surface in planes normal to field direction. It is not within our scope to describe the details and theory of each experimental procedure. We shall merely give the relevant results and refer to the references for more details. The importance of these techniques is that they allow one to obtain direct measurements for the rate of scattering or, its inverse, the relaxation time unweighted by the $(1-\cos\theta)$ factor. Indeed, $\tau(T)$ is observed to vary as $\sim T^{-3}$ rather than $\sim T^{-5}$. The only requirement is that the scattering be through an angle sufficient to destroy the phase coherence of the electron orbits to which a given technique is sensitive. The deHaas van Alphen effect (dHvA), for example is sensitive to scattering through angles as small as ~0.01° while the radio frequency size effect (RFSE) can only detect scattering by roughly 1° or more.

Tables 1.5 and 1.6 give $\tau(b)/\tau(n)$ for phonon and dislocation scattering respectively. Because many results exhibited a range of relaxation times on the bellies, we have chosen the maximum ratios in such cases. We have included ratios determined from conductivities for comparison but one must remember these are weighted according to scattering angle by roughly $(1-\cos\theta)$. Because of the different temperatures, measuring techniques and calculating methods, the discrepancies in the table should not be of great concern. The essential point is that there is definite anisotropy even at 63 K and it is of similar form for

phonons and dislocations. One interesting point not shown in the tables is that the magnitude of τ determined by de Haas-van Alphen techniques is on the order of 100 times smaller than τ determined by the radio-frequency size effect indicating 100 times more scattering at angles less than about 1°. Comparison with actual dislocation resistivities shows that the conductivity relaxation time is on the order of 100 times longer still. While the anisotropies of the non-transport relaxation times in Tables 1.5, 1.6 are not as great as the anisotropy implied by Bergman et al. it must be remembered that their relaxation times are conductivity relaxation times whose anisotropy is greatly enhanced for small angle scattering.

Relaxation time ratio for scattering by phonons in Cu. Table 1.5.

Reference	Haussler and Wells ⁵²	Koch and Doezema	Gantmakker et al.	Nowack and Lee ⁵⁴	Schmidt and Mann ⁵⁵	Ziman ⁷	Lengeler et al. ⁵⁶	Dugdale and Basinski ⁵⁷	Brett and Black ⁴⁴	Brett and Black ⁴⁴	Brett and Black 44	Brett and Black 47
Method	CR	MFISQS	RFSE	Theory	Theory	C Theory	2BR	2BR	C Theory (dirty limit)	C Theory (dirty limit)	C Theory (clean limit)	C Theory (clean limit)
Temp (K)		2-20			(max)	63	20	~25	20	2	20	5
$\tau_{\rm p}(b)/\tau_{\rm p}(n)$	5-20	6 (max)	~10	30 (max)	20 (max) and 80 (i	2.2*	3.6*	2.5*	63* (max)	4000* (max)	8.6 (max)	260*

*These are conductivity relaxation times and contain (1-cos0) weighting 2BR----2-band model analysis of resistivity data

CR----cyclotron resonance

C Theory----conductivity calculations dHvA----deHaas-van Alphen measurements

MFISQS----Magnetic field induced surface quantum states

RFSE----radio frequency size effect

Theory---direct calculations of the scattering rate not weighted with (1-cos0)

Table 1.6. Relaxation time ratio for dislocation scattering in Cu. †

$\tau_{\mathbf{d}}(\mathbf{b})/\tau_{\mathbf{d}}(\mathbf{n})$	Method	Reference
~2	RFSE	Gantmakker et al. ²¹
~4	dHvA	Chang and Higgins ²² Terwilliger and Higgins ⁵⁸
5*	2BR	Dugdale and Basinski ⁵⁷
8.3*	2BR	Lengeler et al. ⁵⁶

 $^{^{\}dagger}$ Interpret with the key for Table 1.5.

CHAPTER II

EXPERIMENTAL METHOD AND APPARATUS

All of the measurements described herein were performed using either a liquid He⁴ cryostat or a He³-He⁴ dilution refrigerator. The He⁴ cryostat, designed by the author, was used for measurements in the temperature range of 1 to 9 K. It has the advantage of being relatively quick and inexpensive to operate. Details of its design are given later. For lower temperatures, the dilution refrigerator, designed by professor William P. Pratt, Jr., was used. Details of its design and construction can be found in references 59 and 60. Also see Lounasmaa⁶¹ for more general discussion.

A. The SQUID Null Detector System

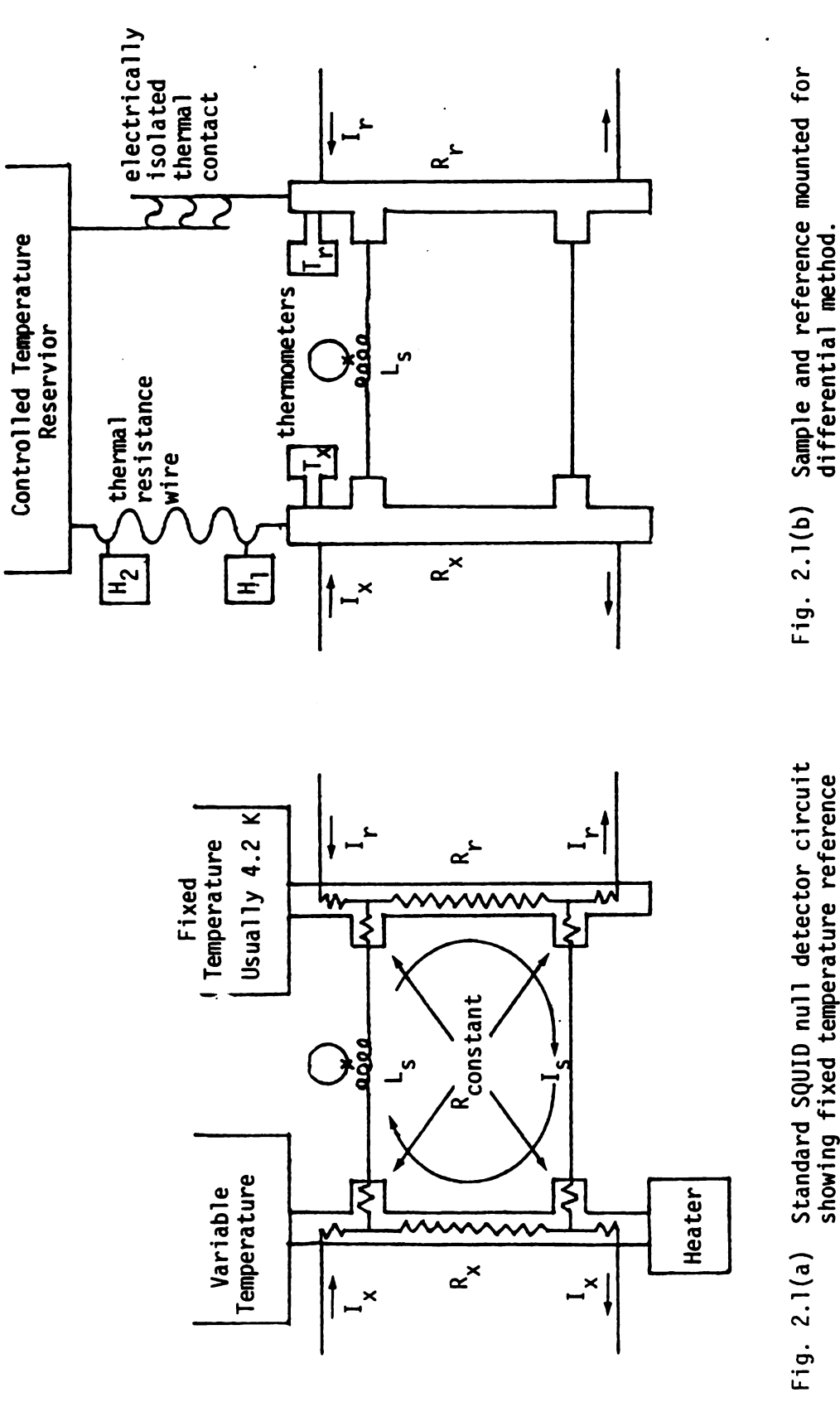
The real heart of the measuring system is the SQUID (Superconducting Quantum Interference Device) used as an ultra sensitive null detector in a potentiometric voltmeter circuit similar to those described in references 60 and 62. Because of its essential role in obtaining the precision and sensitivity necessary for these measurements, we shall review the basic circuit and consider some modifications used for some of the experiments.

Figure 2.1a[†] shows the basic experimental arrangement used in all the measurements on strained copper samples done in the He⁴ cryostat and the earlier runs on silver, copper and gold using the dilution refrigerator. 13,14 While the sample geometry shown is close to the actual shape used, the reference resistor generally had a geometry substantially different, being closer to a thin disk for the lowest values of resistance. The basic method of measuring resistance is very simple in principle. The rf SQUID electronics at room temperature (not shown) puts out a voltage proportional to the current $\boldsymbol{I}_{\boldsymbol{S}}$ through the SQUID coil, L_s (which produces a magnetic flux to which the SQUID itself is sensitive). When no current is present in either $\mathbf{R}_{\mathbf{X}}$ or $\mathbf{R}_{\mathbf{r}}$ the SQUID output voltage registers null. When a current $\boldsymbol{I}_{\boldsymbol{x}}$ is passed through the unknown resistance, $R_{_{\mbox{\scriptsize V}}}$, the SQUID output deviates from null. It can be balanced back to its null value by passing an appropriate current I, through the known reference resistor $R_{\rm p}$. The value of the unknown resistance is then simply

$$R_{x} = \frac{I_{r}}{I_{x}} R_{r}$$
 (2.1)

The earlier dilution refrigerator measurements 13,14 were made by measuring I_r and I_x separately with precision digital voltmeters which looked at the voltages these currents generated across General Radio standard resistors. The maximum precision obtainable was about 2 parts in 10^5 . Most other measurements were made using a modified and locally adapted commercial d.c. current comparator from Guildline

^{*}Note, although the figure schematically shows a large loop area for the circuit, in practice one must minimize this area to avoid noise pickup. Hence, all wires are varnished together in pairs.



Standard SQUID null detector circuit showing fixed temperature reference resistor R_r. Fig. 2.1(a)

Instruments, Ltd. † This device is capable of providing two electrically isolated currents up to about 50 mA, whose ratio can be set to a precision of 1 part in 10^7 . Details of this device can be found in Edmunds et al. 63

Now that the necessary precision in the current ratio was available, the stage was set to try to measure the resistivity of even purer samples than heretofore and to make meaningful measurements well below 1 K where the temperature dependence is extremely small. To do this requires minimizing any noise in the system. The main source of noise is Johnson noise, which expressed as a voltage, is given by

$$\langle V_n \rangle_{RMS} = \sqrt{4k_B TBR} = \sqrt{\frac{k_B TR}{\tau}}$$
 (2.2)

where B is the noise bandwidth and τ is the averaging time employed in detection. To make use of the full precision of the current comparator, we require $R_r \approx R_\chi$. To ensure that the Johnson noise from the reference does not dominate the total noise, we require $T_r \gtrsim T_\chi$.

One approach is to maintain R_r at the lowest temperature at which measurements are to be made, say 50 mK, subsequently raising the sample, R_x , to higher temperatures. This is done by mounting the sample on the end of a thermal resistance such as a length of nonsuperconducting wire (Fig. 2.1b). The heater, H_1 , can then raise the sample temperature by any desired amount. The resistance should be low enough to allow sufficient thermal anchoring to the temperature reservoir (in this case the mixing chamber of the dilution refrigerator) and yet allow the

[†]Guildline Instruments, Ltd., Smith Falls, Ontario, Canada K7A 459.

temperature of the sample to be raised to any desired temperature without changing the temperature of the mixing chamber and $R_{\rm m}$. This last condition is quite difficult to meet if very large temperature gradients are required across the thermal resistance. A rather ingenious solution, which has been used successfully on the latest dilution refrigerator runs, was proposed by Dr. John Rowlands[†] while at MSU as a research associate. Although the details can be found in Edmunds et al., 63 the method will be reviewed here. The essence of this set-up is also shown in Fig. 2.1b. One of the two heaters H_1 or H_2 is always on during a measurement so that the heat load to the mixing chamber is constant. The use of H_2 is probably not required if an automatic temperature controller is used to maintain the mixing chamber at a constant temperature. The procedure is as follows: The current comparator setting C which balances the SQUID when ${\rm H}_{1}$ is off is determined. If the sample is connected to the primary (or master) and the reference to the secondary (or slave) side of the comparator, then

$$C = \frac{I_r}{I_x} = \frac{R_x}{R_r}$$
 (2.3)

 H_1 is turned on to raise the sample temperature by roughly 10% at lowest temperatures, somewhat less at higher temperatures. An uncalibrated resistance thermometer, T_r , may be used to monitor the reference resistor's temperature to be sure it hasn't changed. The change in the sample's resistance, ΔR_{χ} , due to this temperature increment, ΔT_r , requires a change, ΔC_r , in the value of C needed to balance the SQUID. The change

[†]Present address: Radiological Research Laboratories, Room 5267, Medical Sciences Building, University of Toronto, Toronto M5S.1A8, Canada.

in C gives the change in R_{χ} relative to R_{r} . Definition (2.3) then leads to the result

$$\frac{1}{\rho} \frac{d\rho}{dT} \bigg|_{T=\overline{T}} = \frac{1}{R_{X}} \frac{dR_{X}}{dT} \bigg|_{T=\overline{T}} \simeq \frac{1}{C} \frac{\Delta C}{\Delta T}$$
 (2.4)

where \bar{T} is the average temperature of the sample. †

Because the total resistivity will vary by less than 1% over the entire temperature range of interest, one will introduce less than 1% error in the temperature dependence of the resistivity if the $1/\rho$ factor in Eq.(2.4) is treated as a constant $1/\rho_0$ (the same holds for 1/C).

The advantages of this method are: The elimination of the exact value of the residual resistance from consideration and elimination of the need for a calibrated standard resistor because the reference drops out of the equation. A bonus is that one can actually use a second sample for the reference and measure it in the same run by interchanging the roles of sample and reference. This sort of double run was actually done in the last two dilution refrigerator runs using copper and silver as the pair of samples.

The error introduced by approximating the temperature derivative at $\overline{1}$ with finite differences is rather small, in general, for the type of smoothly varying resistivities usually encountered at ultra low temperatures. The error has a leading term second order in ΔT and given by

$$\frac{1}{4} \frac{(\Delta T)^2}{3!} \frac{d^3 \rho}{dT^3} \tag{2.5}$$

[†]If the current leads from the comparator to the sample and reference were switched so that $C = I_X/I_r$, then one must replace ΔC by $-\Delta C$ in Eq.(2.4).

For example, if the temperature dependent resistivity were given by the equation (which will be shown to be typical in Chapter III)

$$\frac{\rho(T)}{\rho_0} = 10^{-5} \text{ T}^2 + 10^{-6} \text{ T}^5 \tag{2.6}$$

Then the relative error, i.e., the ratio of Eq.(2.5) to the derivative of Eq.(2.6), for $\Delta T/T = 0.1$, is given by

$$\frac{1}{4} \left(\frac{\Delta T}{T} \right)^2 \frac{T^4}{2T + \frac{1}{2}T^4} \tag{2.7}$$

Thus at 1 K the relative error due to the finite difference approximation is only 0.1% and is completely negligible below 1 K. At higher temperatures the relative error approaches a limiting value of $\frac{1}{2}$ %, being 0.48% at 4 K, for example. At low temperatures other errors such as the error in ΔT certainly dominate. At higher temperatures one can always reduce ΔT a little if necessary.

Because of the thermal resistance between the sample and the mixing chamber this method of mounting the sample is not as well suited to measuring the thermo-electric ratio, G (= $I_{\chi}/\mathring{Q}_{\chi}$). \mathring{Q}_{χ} is a heat current which generates a thermal e.m.f. in the sample. I_{χ} is the electrical current necessary to cancel this thermal e.m.f. with an ordinary resistive voltage drop. The usual experimental arrangement is shown in Fig. 2.1a where the heater at the end of the sample generates the heat current. Some thermo-electric ratio measurements were done in the early dilution refrigerator runs. These results can be found in Koshenevisan et al. $^{13},^{14}$ G was also measured in the strained copper runs on the He 4 cryostat. These results are given in Appendix A.

B. Special Problems with Very Low Resistance Samples

1) Contact Resistance

The elimination of contact resistance at all junctions in the SQUID measuring circuits of Fig. 2.1 is paramount to successful measurements. Any contact resistance of greater magnitude than the series combination of the sample and reference would make the dominant contribution to the Johnson noise given by Eq.(2.2), thus reducing the signal to noise below its optimum. In addition any such resistance would reduce the current through the SQUID signal coil per unit voltage induced across the sample thus reducing the sensitivity of the SQUID.

Niobium titanium superconducting wire with copper-nickel cladding is very suitable for making junctions with ordinary lead tin solder (or Rose's or Wood's metal if lower melting point solders are desired).

Both single and multi-filament wires have been used successfully. The single filament variety has the advantage of being of smaller diameter and more flexible; it is also easy to etch off the copper-nickel cladding with nitric acid if one wishes to make pressure contact with a block of superconductor such as niobium. The disadvantage is that it seems to be somewhat more difficult to reproducibly achieve true superconducting contacts with critical currents greater than 50 mA. The multifilament typed used by the author is made by IMI Titanium[†] in two diameters,

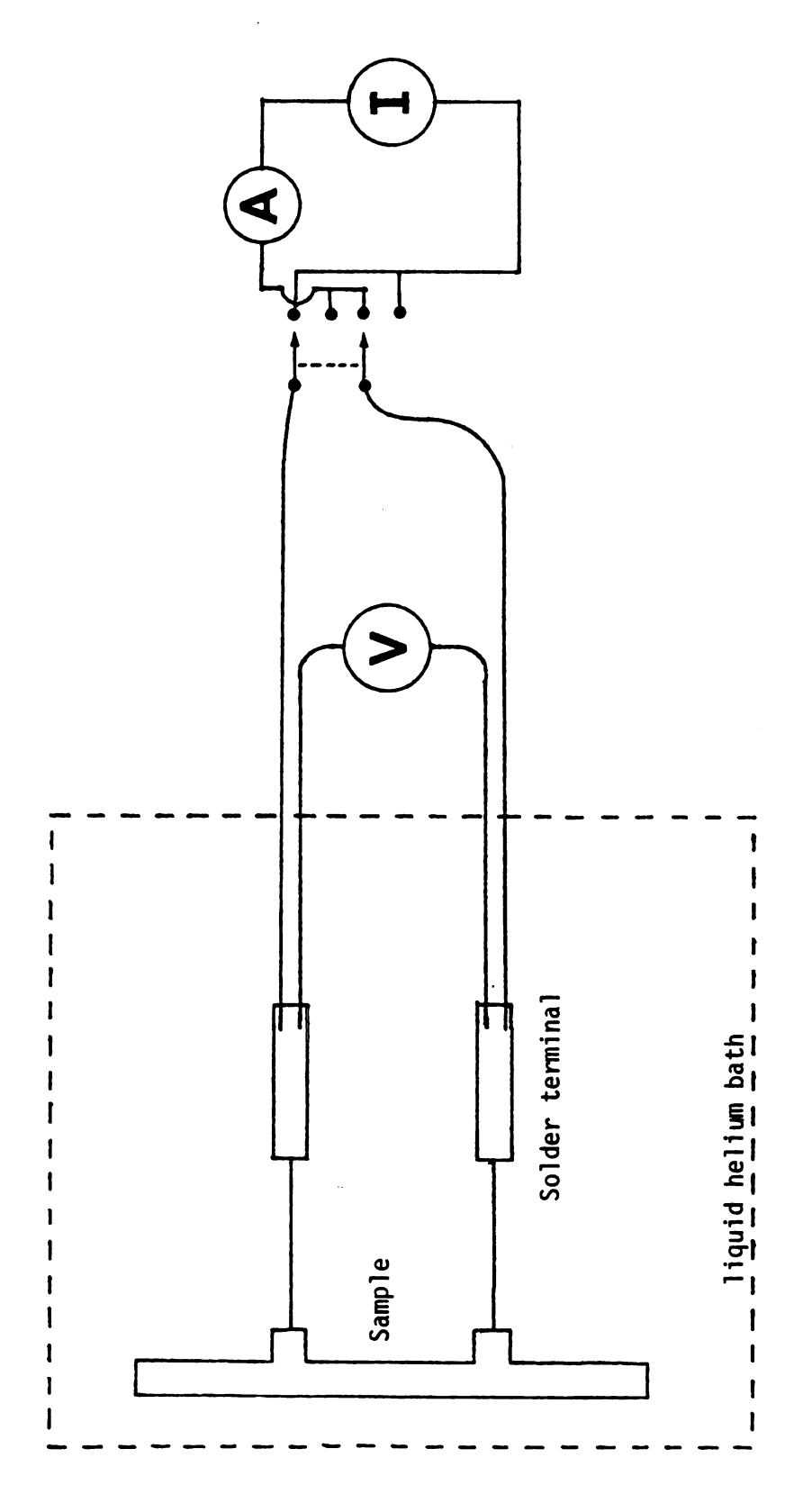
0.05 mm and 0.1 mm. The filaments are embedded in a Cu-Ni matrix which, when dissolved in acid, leaves a bundle of very fine superconducting wires which are difficult to use in making superconducting pressure contacts. For soldered contacts however this type of wire was found superior, reliably

[†]The wire is called Niomax-CN made by IMI Titanium, P.O. Box 216, Kynoch Works, Witton, Biringham, England B67BA.

producing junctions with critical currents in excess of 200 mA. The smaller of the two diameters seemed to produce the most reliable superconducting junctions.

To prepare both single and multifilament wires one should strip off the insulation either by abrasion or with a solvent such as x-var and immerse the end of the wire in molten lead-tin solder after treating it with soldering flux. The tip should be held in the molten solder for about a minute then withdrawn while the solder is cooling to the point that a heavy layer of solder will coat the wire. When subsequently soldering these wires to the sample or other places it is important that the very tip of the wire be fully embedded in solder.

Before actually mounting the sample in the cryostat it is generally worthwhile to measure the contact resistance of the potential leads in liquid helium (or at least set an upper limit on this resistance) by a four-wire technique as shown in Fig. 2.2. Of course one must use currents of the same magnitude as will be used in the actual measurements because larger currents may exceed the critical current of one of the junctions. This sets a lower limit of about 0.1 micro-ohm on the measurable contact resistance if one uses an instrument such as the Keithley 160 nanovoltmeter with 0.01 microvolt sensitivity using a 100 mA reversible measuring current. When extremely low contact resistances are needed, if no resistance is detectable by this method, one must either assume that the true resistance is essentially zero--not too bad an assumption from the author's experience--or use a more sophisticated measuring technique. One relatively simple way to make such a measurement which has been used on the lowest resistance copper and silver samples is to simply connect the potential leads to the signal coil of



Set up to measure contact resistance using constant current source \mathbf{I} , ammeter \mathbf{A} , and sensitive voltmeter \mathbf{V} . Fig. 2.2

a SQUID in a simple cryostat. Then by sending a constant current through the sample and measuring the time constant of the SQUID system output voltage, one can obtain the total resistance by dividing the self inductance of the SQUID coil by the time constant.

2) Response Time Control with Superconducting Transformers and Chokes

Another problem associated with measuring resistances below 10^{-8} ohms is the response time of the SQUID measuring circuit of Fig. 2.1. This time constant is given by

$$\tau = L_{s}/R_{T} \tag{2.8}$$

where R_T is the total circuit resistance due to sample, reference and contact resistances and L_S is the inductance of the SQUID signal coil in place within the SQUID body. In the measuring systems used the value of L_S is about 2 μ H. The response time for R_T = 10^{-8} ohms would be about 200 seconds if no special measures were taken.

During the measuring process one typically sweeps the currents I_{χ} and I_{r} from positive to negative at a rate sufficiently slow that the SQUID feedback voltage does not exceed its maximum value of 10 volts. This in itself would require many minutes. Then one would have to wait another 9 time constants, about 30 min., before the value of the SQUID feedback voltage had reached its zero to within the noise level of roughly 1 mV. Since a single measurement generally requires several current reversals it is clear that several hours would be required for a single point. During this time the zero of the SQUID would have

to undergo no flux jumps. These requirements along with the nearly geological times necessary to complete an entire run clearly make such measurements impossible. The obvious solution of increasing the sample resistance by making longer and thinner samples does not work because boundary scattering would become a problem—the electron mean free paths are on the order of 1 mm. The introduction of additional resistance in the circuit is ruled out because it would increase Johnson noise and lower sensitivity. The only answer is to reduce the effective inductance.

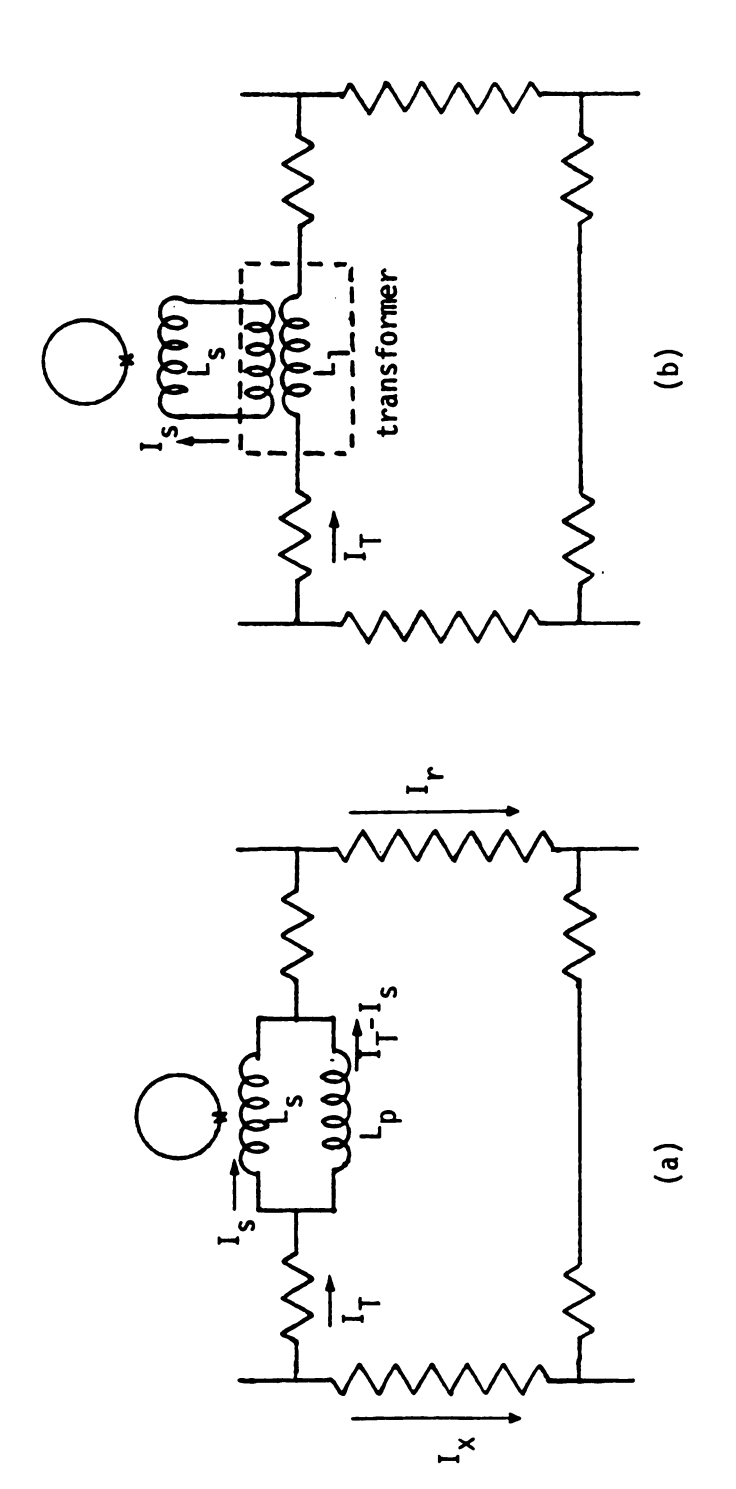
The ideal way to lower the inductance is the SQUID circuit would be to reduce the number of turns on the sensing coil of the SQUID. Although this would lower the current sensitivity it would lower the inductance even more because the former goes as N while the latter goes as N^2 . However, this is not very practical in a multipurpose cryostat such as the dilution refrigerator because once a SQUID is in operating condition it is very risky to tamper with it. There remain two methods of lowering the inductance: either put a superconducting choke, L_p , in parallel with the SQUID sensing coil (Fig. 2.3a) or use a superconducting transformer (Fig. 2.3b).

The effective inductance of the two parallel inductors in Fig. 2.3a is simply

$$L_{e} = \frac{L_{s}L_{p}}{L_{s} + L_{p}}$$
 (2.9)

It is easy to show (see Appendix B) the effective inductance of the superconducting transformer (Fig. 2.1d) is given by

$$L_{e} = L_{1} \left(1 - \frac{k^{2}L_{2}^{2}}{L_{s} + L_{2}} \right)$$
 (2.10)



Two ways to lower the effective inductance. (a) Use of an inductance L_p in parallel with the SQUID coil L_{ς} . (b) Use of a superconducting D.C. transformer. Fig. 2.3

where k is the coefficient of coupling for the transformer and is given by

$$k = \frac{M}{\sqrt{L_1 L_2}} \tag{2.11}$$

where L_1 and L_2 are the primary and secondary self inductances and M is their mutual inductance.

We now consider what effect these changes will have on the sensitivity and precision of the measurements. First let us define the true signal current, I_T , as the loop current which would flow if no balancing potential were being supplied by $R_{\rm m}$. This should not be confused with the net loop current, I_n , which actually flows when balancing the SQUID. $\boldsymbol{I}_{\boldsymbol{n}}$ is zero at balance. Although for both methods only a fraction of the true signal current, I_{T} , passes through the SQUID coil, this alone does not affect the signal to noise ratio because both signal and noise are reduced by the same fraction, provided we are well within the regime where the primary noise is Johnson noise. In the regime where intrinsic device noise is important or if the additional superconducting current loop picks up noise, there will be a reduction of the signal to noise ratio. The real problem is due to requiring the time constant to remain fixed. Previously no one had been forced to fix the time constant. In such cases the maximum precision, i.e. the inverse of the signal to noise ratio, is independent of sample resistance. This is easily seen as follows: In the absence of a choke or transformer, the mean square Johnson noise current is given by

$$I_n^2 = \frac{k_B T}{L_c} \tag{2.12}$$

This is seen to be independent of the source resistance. The true signal current is given by

$$I_{\mathsf{T}} = I_{\mathsf{X}} \, \frac{\mathsf{R}_{\mathsf{X}}}{\mathsf{R}_{\mathsf{T}}} \tag{2.13}$$

where R_{χ} and I_{χ} are respectively the resistance of the sample and the current through it and R_{T} is the total circuit resistance, i.e. the sum of the sample, reference and contact resistances. Keeping in mind the fact that in these measurements the sample, reference and contact resistance are roughly equivalent, we can write

$$R_{T} = aR_{x}$$
 2 < a < 10 (2.14)

The signal to noise current ratio, which defines the absolute limit of precision, is then given by

$$\frac{I_T}{\langle I_n \rangle_{RMS}} = \sqrt{\frac{L_S}{k_B T}} \frac{I_X}{a}$$
 (2.15)

Thus the ultimate precision, independent of the sample resistance, is limited only by the available measuring current which is about 50 mA for the current comparator. This gives a signal to noise of about 4×10^6 at 1 K for $L_s = 2 \mu H$ and a = 5. In terms of voltages this result can be viewed as a consequence of the fact that although the signal voltage decreases linearly with R_x , the Johnson noise voltage does also because it goes as

$$\langle V_n \rangle_{RMS} = \sqrt{\frac{k_B T a R_X}{\tau}} = \sqrt{\frac{k_B T}{L_S}} a R_X$$
 (2.16)

In other words, the decrease in the noise bandwidth, $(4\tau)^{-1}$, provides the necessary compensation to allow the signal to noise ratio to remain independent of R_{χ} . This is no longer the case when we fix the value of τ to some value τ_0 , say 10 sec. To fix τ we must change the effective inductance of the circuit with each experiment on a sample of different resistance. Now, we must replace L_{χ} by $L_{\chi} = aR_{\chi} \tau_0$ in Eq.(2.12) yielding

$$\frac{I_{\mathsf{T}}}{\langle I_{\mathsf{n}} \rangle_{\mathsf{RMS}}} = \sqrt{\frac{\tau_{\mathsf{o}}^{\mathsf{R}_{\mathsf{X}}}}{ak_{\mathsf{B}}^{\mathsf{T}}}} I_{\mathsf{X}}$$
 (2.17)

This has a value of 1.3×10^6 for τ = 10 sec., R_{χ} = 5×10^{-9} ohms, I_{χ} = 50 mA and a = 5 at 1 K. Compared with the results of Eq.(2.15) we find the signal to noise ratio has been reduced by about a factor of 3. Because of the simultaneous reduction of signal and noise current through the sensing coil it would not seem that there is any advantage to using a superconducting transformer rather than a simple shunting inductor in an attempt to tailor the effective inductance. However, if noise were being coupled in to the SQUID due to pick-up in the superconducting loop formed by the two inductors or from the room temperature SQUID electronics there might be reason to try to maximize the amount of signal passing through the SQUID coil. While in the simple parallel inductance circuit of Fig. 2.3a the current, I_s , through the SQUID branch is fixed, the circuit of Fig. 2.3b can be optimized within the limits of practical transformer design to perform better than the simple parallel inductance. However, as outlined below, significant advantage may be rather difficult to achieve because it may require very strong coupling between the primary and secondary coils.

The following expression (whose derivation can be found in Appendix B) gives the ratio of the current through the squid coil using a transformer to that using a superconducting choke, assuming that the two would yield the same effective inductance and that the transformer design maximizes its output current for a given coefficient of coupling k. The minimum criterion for choosing a transformer would be

$$\frac{I_s(\text{transformer})}{I_s(\text{choke})} = \sqrt{\frac{L_s}{L_e}} \frac{k}{1 + \sqrt{1 - k^2}} > 1$$
 (2.18)

where L_e is the desired effective inductance. At this stage it might appear that for any sizable ratio of L_s to L_e the requirements on k are not too severe. For example Eq.(2.18) can be satisfied by k > 0.6 for $L_s/L_e = 10$. However, the degradation factor $k/1+\sqrt{1-k^2}$ increases rather slowly for k < 0.9 being only 0.63 at k = 0.9. Hence, to actually make the extra effort of winding and using the transformer worthwhile may require large values of k in turn increasing the effort required. In our example even if k were 0.9 we would only gain a factor of two and in the limit of perfect coupling only a factor of three. Hence we conclude that, unless the need is very great or the ratio of L_s/L_e is very large, the simpler choke circuit of Fig. 2.3a is to be preferred.

3) Enhanced Noise Pickup

Finally, a somewhat unexpected problem we had in trying to measure such low resistance was a greatly enhanced susceptibility to noise pulses from any equipment, particularly current comparator. These pulses would cause the SQUID zero to shift by an integer number of flux quanta despite the heavy filtering used on the all input lines. The

problem was solved by wrapping the samples and the terminal connections to the SQUID with superconducting foil to shield these regions of relatively large loop area from magnetic flux pulses. The reason for this enhanced sensitivity is probably due to the fact that as the resistance in the SQUID circuit goes down it becomes more and more effective in generating shielding currents to minimize the change in magnetic flux through the entire circuit from magnetic noise pulses, approaching the limit of perfect shielding in a loop of zero resistance. The shielding currents respond almost instantaneously and, passing through the SQUID coil, cause flux jumps in the SQUID because the slewing rate of the SQUID feedback circuit is too slow to compensate.

C. <u>Design and Construction of a He⁴ Cryostat</u>

A liquid He⁴ cryostat employing two SQUID measuring systems was designed and constructed. The basic objective of the design was to provide a versatile and efficient means to measure nonmagnetic transport properties in metals and alloys in the temperature range from 1-9 K. It was constructed to allow two samples to be mounted and measured in the same run.

1) Mechanical Construction

The room temperature end or head of the cryostat consists of a brass flange which mates with a brass collar on the top of the liquid helium dewar. All electrical connections to the SQUID's, samples, thermometers and heaters are made through various electrical connectors attached to this flange. The low temperature end or tail of the cryostat is suspended below this flange by a number of stainless steel

conduits and pumping tubes. The tail consists of a brass vacuum can which houses all of the paraphernalia necessary to make the measurements. Figure 2.4 shows the exterior appearance and dimensions of the cryostat and dewar. The lower portion of the brass can mates with a brass flange. These are held tightly together, with a lead 0-ring between them, by twelve brass screws. Steel screws were found unsatisfactory because they contract less than brass during cooling causing a loss of the vacuum seal. The inside of the can is tinned to provide a superconducting shield against external magnetic flux changes which would affect the SOUIDs. Within the brass can is a copper canister called the pot into which liquid helium can be admitted via a valve operated by a shaft from the cryostat head (see Fig. 2.5). The pot is suspended by a 1/2" stainless steel tube which acts as a vacuum pumping line and provides thermal isolation. The top surface of the pot has various holes and protrusions which allow one a variety of ways to attach samples and thermometers. A 1/2" copper stud has been attached to the bottom of the pot with cerrolow 117[†] low temperature solder to allow a low field superconducting magnet to be mounted in the eight inch space below the pot. There is therefore ample space both above and below the pot for mounting samples and auxillary apparatus.

The pot will hold about 80 cc of liquid helium. It is divided by a diaphragm into an upper region of about 30 cc and a lower region of about 50 cc. The diaphragm contains a special device which allows the insertion of a polished orifice to suppress the flow of superfluid ${\rm He}^4$ film below the λ transition. This provision was included to allow

[†]Cerro Copper and Brass Company, Stanford Works, Rolling Place, Stanford, Connecticut.

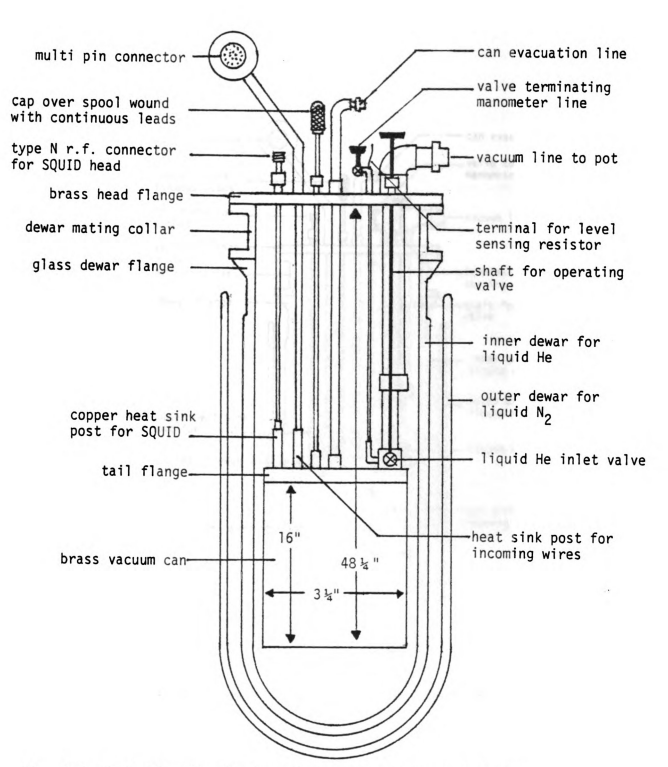


Fig. 2.4 Semi-schematic drawing of cryostat and dewar assembly.

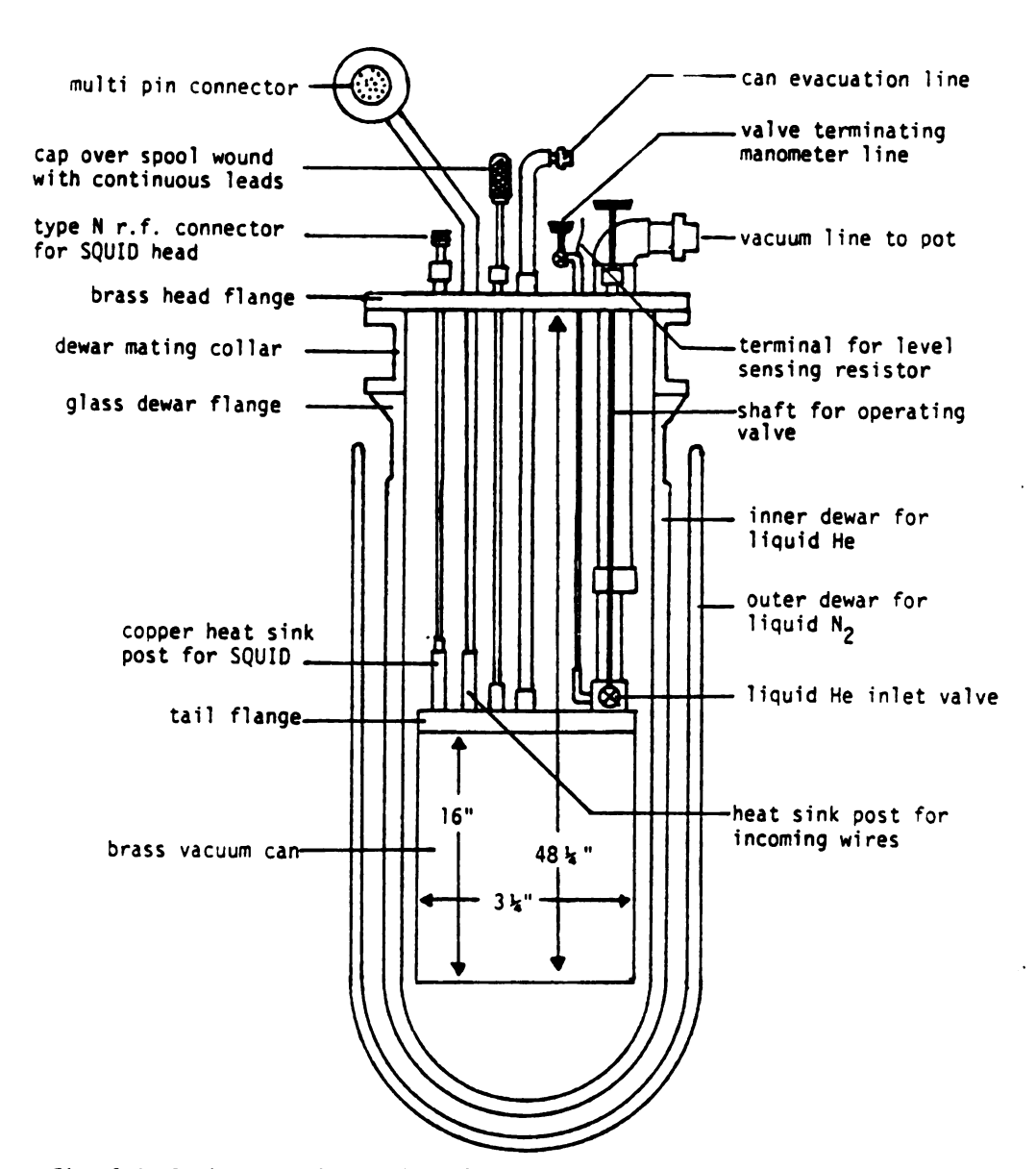


Fig. 2.4 Semi-schematic drawing of cryostat and dewar assembly.

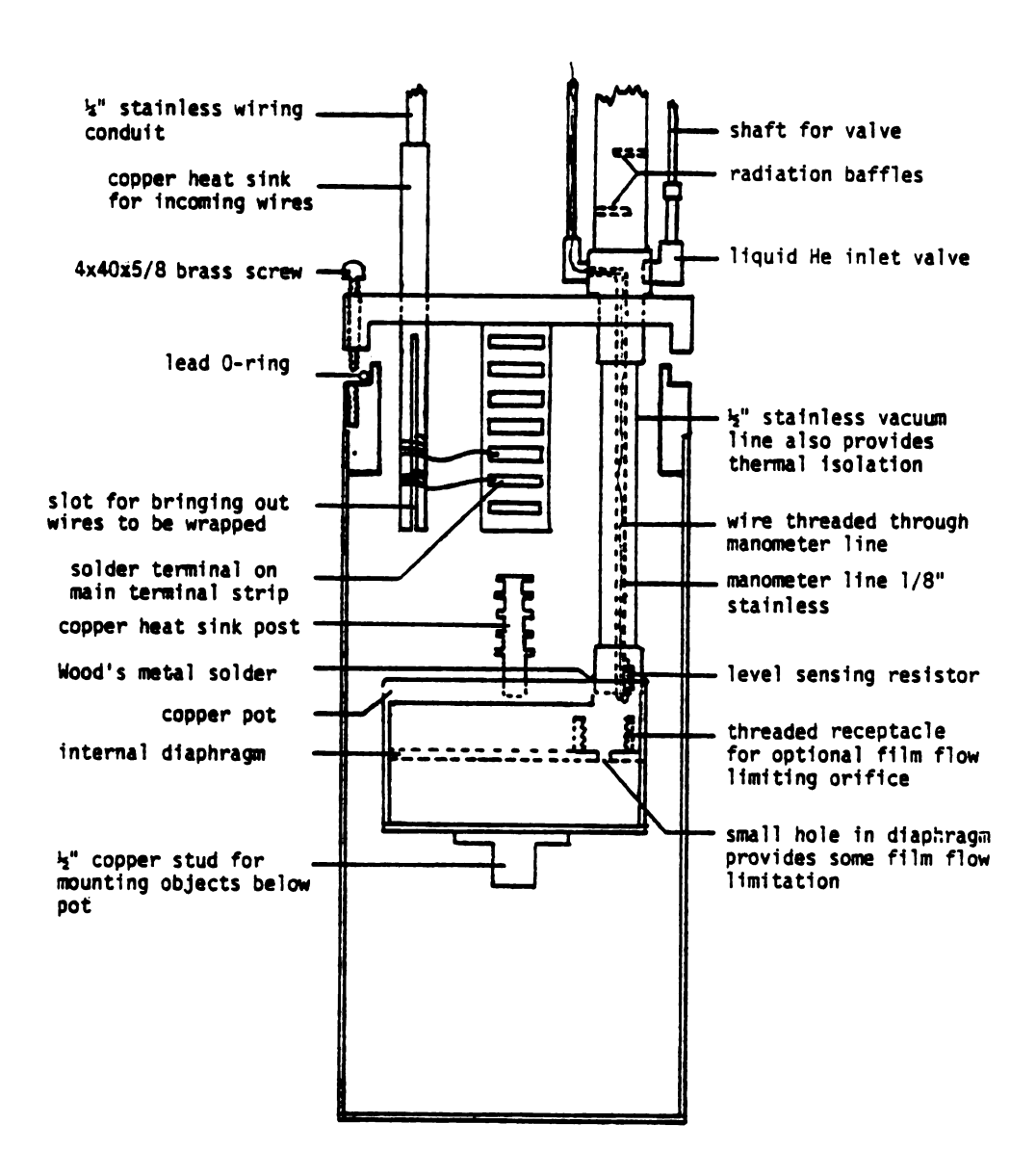


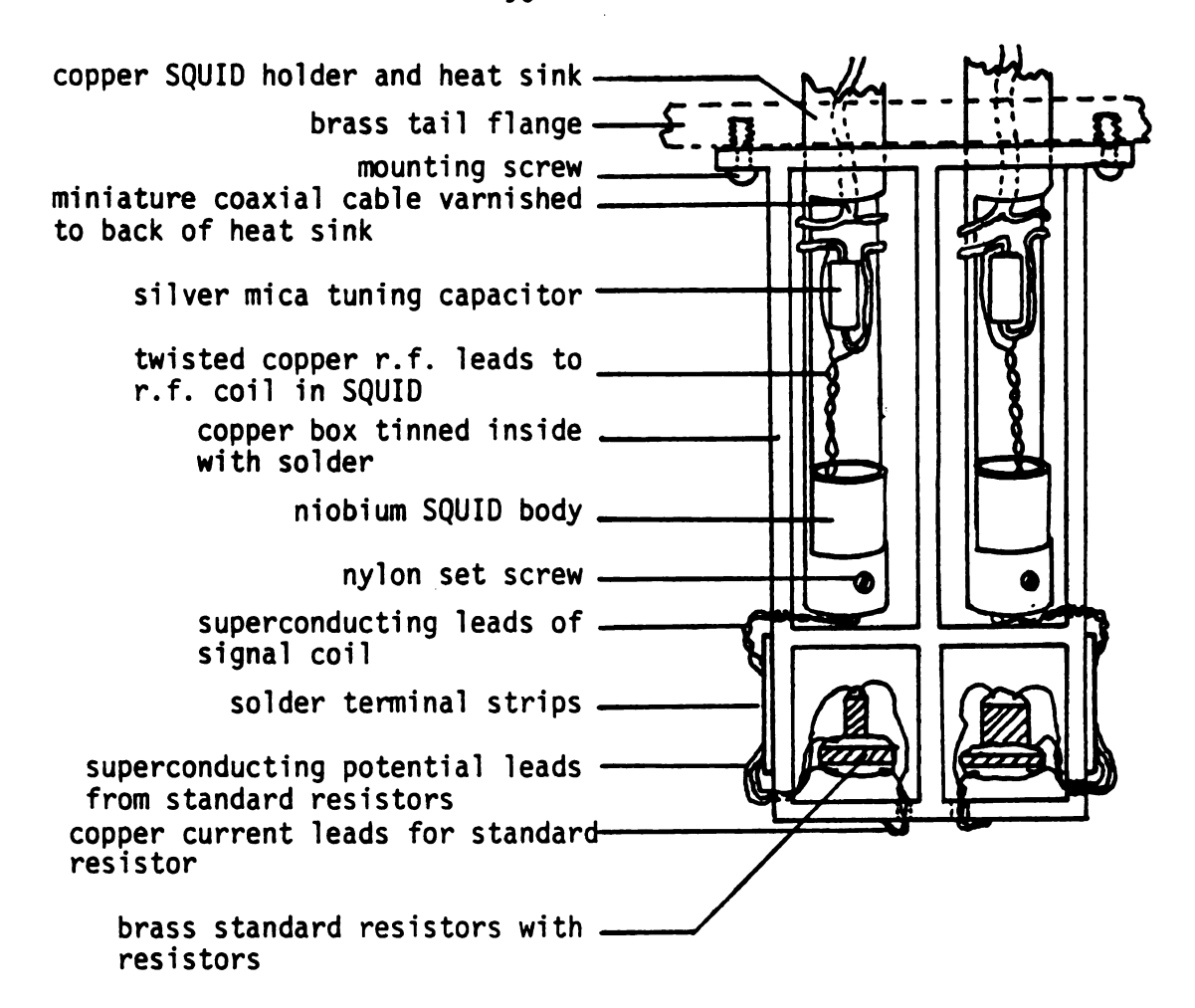
Fig. 2.5 Semi-schematic drawing of the tail section of the cryostat.

achieving the lowest possible temperatures, possibly slightly below 1 K. Although the polished orifice has not yet been installed, the small hole presently in the diaphragm probably helped achieve the 1.03 K already obtained in this cryostat. The pot is soldered with Wood's metal to a copper bushing on the pumping tube. Protruding from the top center is a copper post used to thermally lag various wires to the pot. This post can be pried out of the pot if one wishes to remove the pot.

To prevent the development of vacuum leaks from thermal cycling, all joints between dissimilar metals are made so that the material which contracts more during cooling surrounds the lesser contracting material. Such joints will be under compression when cooled. Thus brass always surrounds copper and either of these may surround stainless steel. Joints to stainless steel were made with hard silver solder whenever possible. Otherwise soft silver solder was used. All stainless tubes were soldered to bushings both at the head and tail of the cryostat to provide strength and facilitate repair. In particular, the 1/4" stainless tubes which house the miniature coaxial cable going to the SQUIDs were made to be easily changed because we thought the flexible coax might have to be replaced with rigid coaxial conductors.

2) SQUIDs and Standard Resistors

The SQUIDs themselves are mounted in copper holders which extend through the brass flange to become the bushings to which the 1/4" stainless tubes are soldered. These provide the heat sinking of the SQUIDs and the coaxial r.f. leads to the helium bath (see Fig. 2.6). The two SQUIDs are shielded from magnetic flux changes inside the vacuum can and from mutual interaction by a tinned copper box with a partition



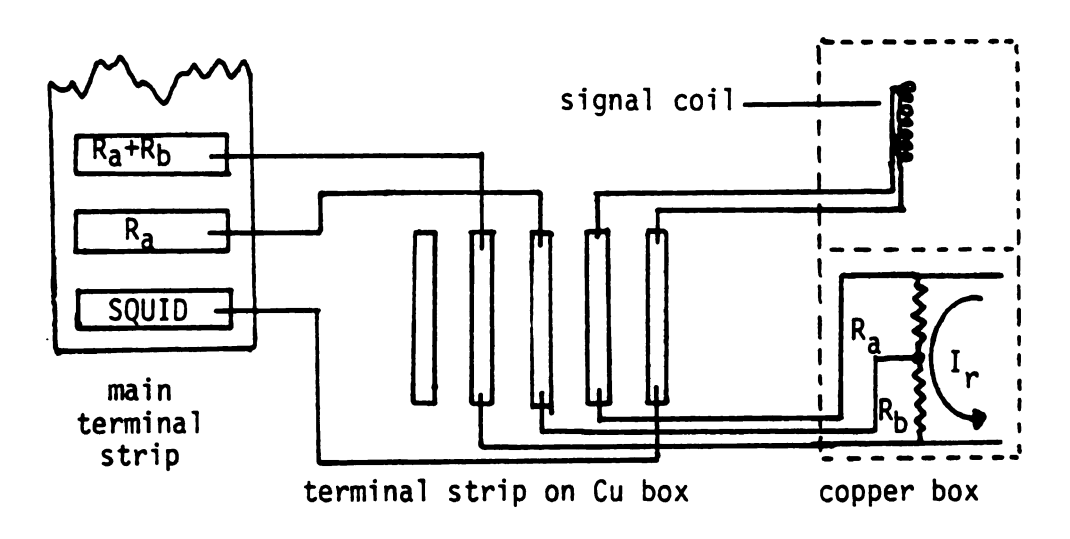


Fig. 2.6 Top: Mounting of SQUID's and standard resistors. Bottom: Terminal strip connections. Sample must be connected to appropriate terminals on main strip.

down the middle. The tinned copper lid to this box is attached with Cerrolow 117 solder. The box is attached to the underside of the brass flange with two screws. The standard resistors are also kept within separate partitions in this box.

There are two standard resistors made of brass associated with each SQUID. Those with the left SQUID have values of $8.75 \times 10^{-7} \pm 0.5\%$ and $1.79 \times 10^{-4} \pm 0.1\%$ ohms while those on the right side have values of $8.89 \times 10^{-8} \pm 1.5\%$ and $5.27 \times 10^{-6} \pm 0.2\%$. All were measured by a four probe technique in liquid helium with currents between 1 and 8 A. The exact ratio between these last two was measured with a SQUID to be 0.017240. While this is not exactly the ratio obtained from the original values it differs by only 2% which is consistant with the original error. By this ratio the lower resistance can be recalibrated against the higher one to obtain a value of $9.085 \times 10^{-8} \pm 0.3\%$ ohms.

Because of the way the standard resistors are wired to the SQUIDs and terminal strips, when the larger valued resistor is desired it is actually the series combination of the two which is used as the reference resistor in actual measurements.

The terminal strips just mentioned provide a convenient way to connect samples to the SQUID circuit. They are, in fact, used to make all connections between wires going to the cryostat head and anything inside the vacuum can with the exception of a set of four (more could be added) thermocouple grade chromel wires. These run continuously from the tail through a feed-through at the head. This allows one to make direct voltage measurements on high resistance samples with a digital voltmeter without large thermal e.m.f.s which might be caused by inhomogeneities in the leads.

All other electrical connections at the cryostat head are made through a pair of 17 pin hermetically sealed connectors, one for each "side." One of pins (pin A) is not used. There are filter boxes available to attach at the cryostat head to reduce electromagnetic pick-up above 3,000 Hz on all sixteen lines. However, these have generally not been necessary. The sixteen wires on each side are brought down to the tail through 1/4" stainless steel conduits which mate with copper bushings. These bushings protrude through the tail flange into the vacuum space to provide heat sink posts around which the wires are wrapped before being soldered to the terminal strip (see Fig. 2.5).

The temperature of the sample can be controlled in two ways. In the traditional method, for temperatures below 4.2 K, the vapor pressure of the liquid helium in the pot is regulated. While this method can be used it is much more cumbersome and less stable than the second method which involves an arrangement in which the sample is mounted at the end of a thermal resistance as depicted on the left side of Fig. 2.1b. A temperature gradient along the thermal resistor produced by a heater allows one to vary the sample temperature very easily by controlling the heater current. The pot can be at 4.2 K for temperatures above 4.2 and it can be pumped to the lowest temperatures by a vacuum pump for lower temperature measurements. The thermal resistors used were made from brass cut to about 3/4" long by 1/8" diameter. A heat flux of about 4 mW was sufficient to raise the temperature from 4.2 to 6.2.

3) Thermometry

The primary method of measuring temperatures is by the use of germanium resistance thermometers. There are four Cryocal † CR1000 thermometers, one of which (serial number 2844) was originally calibrated by Cryocal Inc. between 1.5 and 100 K. Unfortunately, although they provided some information about the accuracy of their calibrations, they did not indicate which sources of error are probably systematic and which are statistical. Treating all errors as though statistical and including our own errors in measuring the resistances with the prescibed currents (10 μ A above 3 K, 1 μ A below 3 K) using digital voltmeters with 1 μ V sensitivity the following formula gives a reasonable estimate of error:

$$\Delta_{T} = 0.002 \text{ T} + 0.001 \text{ K}$$
 (2.19)

where T is the measured temperature. It should be remembered that a large component of this error is systematic. Thus small temperature differences can probably be measured to about 0.005 T.

The Cryocal company provided a computer generated table of resistance versus temperature from the fitting equation

$$\log_{10} R = \sum_{i=0}^{N} A_i (\log_{10} T)^i$$
 (2.20)

where N is that which produces the best fit and the A_i are fitting parameters. Because the use of a table during the course of an experiment is a bit cumbersome, the author programmed an HP67 calculator to calculate the temperatures based on Eq.(2.20). Because the equation is in

[†]Cryo Cal, Inc., 1371 Avenue "E", Riveria Beach, Florida 33404.

the inverse form of what usually is desired, i.e. finding T given R, an iterative Newton Raphson procedure was used to find the solution. Appendix C contains further details including the actual calculator program.

The temperature of the pot can also be measured by helium vapor pressure thermometry. There is a 1/8" stainless steel tube which terminates inside the pot just below the opening to the pumping tube. The tube passes up the interior of the pumping tube until it reaches the vacuum can flange. From there it exits the pumping tube and passes through the helium bath. It is terminated with a valve atop the head which can be connected to a manometer. This manometer tube contains a wire connected to a sealed feedthrough at the head and to a carbon resistor mounted on the end of the manometer tube inside the pot. The other end of the resistor is grounded. The purpose of this resistor is to determine when the pot is full of liquid by registering a change in resistance caused by the greater rate of Joule heat dissipation due to liquid rather than gaseous helium. So far it has not been found necessary to use this level detector. Rather, the needle valve is simply opened for about a minute.

D. <u>Sample Preparation</u>

Our chief goal for much of this work was to prepare samples of noble metals with purities as high as possible. The reason was first to reduce the residual resistance $R_{\rm O}$ so that the small temperature dependent effects would constitute a larger fraction of the total resistance. Secondly, it was essential to eliminate magnetic impurities, iron being the most common, so that the Kondo effect would not

complicate our results. A handy if somewhat imprecise gauge of sample purity is given by the residual resistance ratio RRR defined to be the resistance at room temperature divided by the resistance at liquid helium temperatures. Our goal for silver and copper was an RRR greater than 10,000, preferably about 20,000. Although difficult, such ratios have been achieved by others. 15,65

The starting materials are listed in Table 2.1. These materials were then melted in various types of crucibles by an r.f. induction furnace and then cast into sample form, cut or otherwise formed directly from the inqut made in the crucible. The crucible material which gave the best results was made from pyrolytic graphite. Ordinary graphite never produced RRR values better than 5,000. Boron nitride was also disappointing although it was only tried once, on copper. Alumina was found unsuitable because the copper adhered to its surface. Both single crystal and large grained polycrystalline samples were prepared. The only exceptions were several silver samples which were prepared in quartz tubes. The procedure was to seal silver pellets under vacuum in a quartz tube of roughly 10 mm diameter which had previously been fused to a 2 mm ID quartz tube sealed on the opposite end. Then, the silver was melted by gas torch. When all the silver was melted, it was forced into the smaller tube with a single swift shake. The sample was removed by very carefully slicing the tubing lengthwise on opposite sides using a diamond saw being careful not to actually cut through to the silver. Then the tube could easily be split away from the sample. While this technique produced samples with RRR values of 10,000, the samples had a number of dimples on their surfaces as well as some internal voids revealed by careful density measurements.

Table 2.1
Source and purity of sample materials

Material	Source	Purity	Major impurities (in PPM)	Physical form
Copper	ASARCO	99.999+	Sb=1, Fe<0.5, Mg<1	extruded rod
			Si<1, Ag<0.1	or plate
			Se<1, S<1	
Gold	COMINCO	99.9999	Ca<01, Cu<0.5, Fe<0.1	pellets
			Mg<0.1, Si<0.1, Ag<0.3	
Silver	COMINCO	99.9999	Ca<0.1, Cu<0.1, Fe=0.4	pellets
			Pb=0.1, Mg<0.1, Si=0.1	

All samples were given an annealing treatment in oxygen or air at a pressure of from 1 to 8×10^{-4} torr at a temperature 50 to 100 C below their melting points. The purpose of this treatment was to improve the RRR value and eliminate the magnetic effects of iron impurity by forming iron oxide (see the review by Fickett ⁶⁶). There is evidence at least in copper that besides being oxidized the iron oxide tends to aggregate to form small precipitate particles which would contribute much less to the residual resistance than individual iron oxide molecules. ⁶⁷ Presumably due to this mechanism as well as the reduction of lattice defects and grain boundaries we found our RRR values to increase by factors of two to ten. It is not clear what effects this treatment might have on other magnetic impurities such as manganese although nickel and cobalt probably are oxidized like iron. Table 2.2 contains information on the preparation of various samples.

A way was needed to attach current and potential leads to avoid spurious temperature and current dependent effects. We found it necessary to attach our current and potential leads to arms of the sample material which protruded at least five times the arm thickness from the actual region to be measured. Sometimes these arms were spot welded on. In other cases the sample was cut or cast into a form having suitable arms. In the case of spot welded arms (only used for connection to potential leads) the arms were made from the same material as the sample rolled or drawn to a smaller size and annealed after spot welding. Because copper, silver and gold are easily soldered with lead tin solders it was then easy to solder the CuNi clad NbTi superconducting wires to the arms.

Table 2.2 Sample Information

C1-	Purity or	0	• · · · · • †	222	
Sample ————	Composition	Crucible	Anneal [†]	RRR	Geom.#
AgA	99.9999	quartz	0.5 _μ 0 ₂ 850C 3d.	4700	a
AgB	99.9999	quartz	0.5 ₄ 0 ₂ 850C 3d	8000	a
AgC ₂	99.9999	quartz	0.5 ₄ 0 ₂ 850C 3d	11000	a
AgC ₃	from AgC ₂	quartz	reannealed in 0 ₂	5600	a
AgD	from AgA	quartz	reannealed in 0 ₂	7100	a
^{Ag} 20	99.9999	pyrolytic graphite	0.5 ₄ 0 ₂ 900C 2d	20000	С
Au 1	99.9999	graphite	1 atm air 950C 2d	5600	a
Au3	99.9999	graphi te	-1 atm 0 ₂ 950C 2d	2800	a
Cul		none	0.5 _µ 0 ₂ 960C 3d	2600	a*
Cu 5		none	0.5 _µ 0 ₂ 960C 3d	54 20	a*
Cu 6		none	0.5 ₄ 0 ₂ 960C 3d	4190	a*
Cu10		none	0.5 _µ air 960C 3d	5300	b
Cull		graphite	l_{μ} air 950C, 1.5d	4300	a
Cu13		pyrolytic graphite	0.8 _u air 100 0C , 3d	13000	С
CuAg 1		0.1 at % Ag	lμ air 950C, 3d		a
CuAg2		0.025 at % Ag	6µ air 950C, 1d		a

 $^{^{+}\,}$ annealing treatment lists pressure in microns or atmospheres $^{++}\,$ see Figure 2.7

During the process of cutting and shaping the samples their surfaces would become contaminated. For example spark cutting, which is carried on in a kerosine bath, always left the surface dark with carbon and hydrocarbon deposits. Also one had to thoroughly clean the surface with acetone to remove the graphite impregnated plastic cement used to mount the sample to the spark cutter. Samples which were machined probably had iron contamination on the surface. Removal of these and other contaminants prior to annealing was accomplished by etching the surface.

Copper and silver can both be etched with nitric acid. Another excellent etch for silver is prepared by mixing 1:1 concentrated ammonium hydroxide with concentrated hydrogen peroxide. While many surface impurities may be removed from gold by nitric acid alone, aqua regia which actually dissolves some of the gold is probably a better choice. Before using acid etches, any oil residues were removed with detergent or solvent. After etching the samples were thoroughly washed in doubly distilled water after which they were usually rinsed in ethanol to speed drying.

The quartz tubes in which the samples were annealed were also thoroughly cleaned with nitric acid, doubly distilled water and occasionally with hydrofluoric acid to remove residues which seemed to be baked into the inner surface of the tube. Care was also taken to never use the same tube with different materials.

Figure 2.7 shows some of the sample geometries used and referred to in Table 2.2. The tuning fork geometry was used to reduce thermo-electric noise which might be generated by heat pulses passing along the length of the specimen due to small temperature fluctuations in the

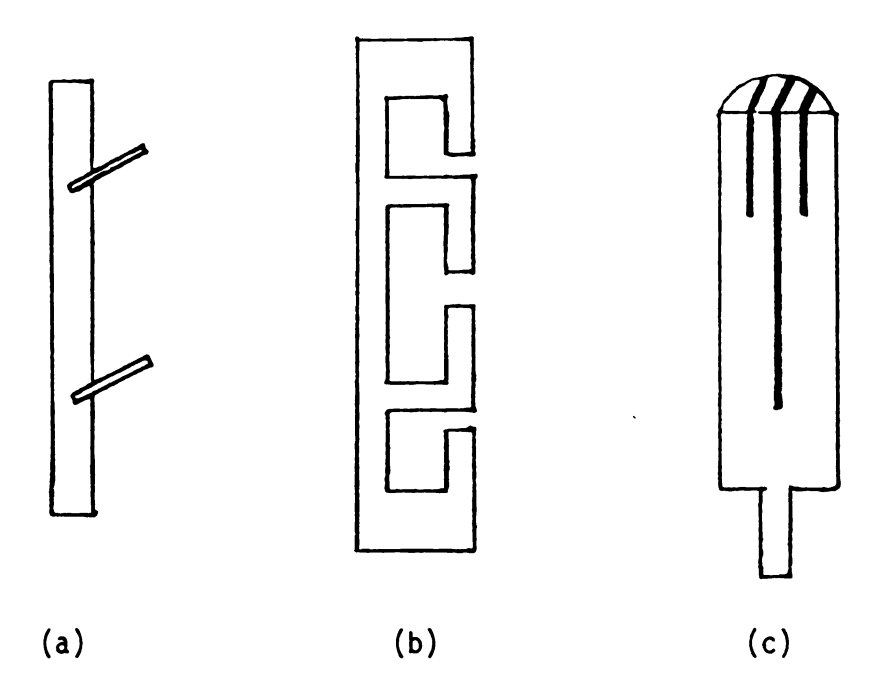


Fig. 2.7 Various sample geometries: (a) linear geometry, circular cross section with spot welded arms; (b) linear geometry, rectangular cross section with milled arms; (c) tuning fork geometry, semi-circular cross section cuts made with spark cutter from cylindrical ingot.

cryostat. In all geometries, but especially the tuning fork geometry, the easiest way to measure the effective geometrical factor was to measure the room temperature resistance and divide by published values of the room temperature resistivity. In samples of uniform cross section and simple linear geometry actual measurements were carried out and found to agree to within a few percent--consistent with the estimated error. Although the accuracy of our resistivity measurements was thus limited to several percent, this did not compromise the validity of our high precision results since we were concerned with the precise form of the temperature dependence and not with an absolute measure of the resistivity itself.

An attempt was made to purify copper by electrolytic techniques. Pure copper was dissolved in nitric acid. The solution was then used as an electrolyte in an electrochemical deposition of Cu from a very pure copper anode to a very pure, thin copper cathode. The deposited material was very dark and full of coral like modules and did not appear to be entirely metalic. A solution of copper sulphate with an excess of sulfuric acid was also tried. Though it produced much more uniform copper on the cathode, the results were disappointing in that after annealing in oxygen, samples produced from this copper had low RRR values. Further attempts at this technique were abandoned.

CHAPTER III

RESULTS

Our study of the noble metals' resistivity was originally motivated by a desire to unambiguously observe the electron-electron T² term at temperatures only accessible in the dilution refrigerator. However, the discovery of the strict T⁴ dependence over a significant temperature range for all three metals ^{13,14} and the initially puzzling behavior of its coefficient ¹³ lead to more detailed investigations of this behavior in Cu and Cu alloyed with small amounts of Ag. Believing this T⁴ behavior was due to phonon scattering, we set out to systematically study the effects of dislocations and impurities because we suspected they were influencing the magnitude of its coefficient B. Because ultra-low temperatures were not required, these measurements were carried out in a cryostat of the author's design as described in Chapter 2.

In what follows, we shall first describe the results of the purely empirical study of the sample dependence of B and then move on to an analysis of the data in terms of the theory of Bergman et al. (already discussed in Chapter 1) which appeared soon after the completion of our study. Because their theory includes a significant electron-electron contribution we shall be lead finally to a consideration of this term and our attempts to complete our original goal on the dilution refrigerator.

A) A Study of the Sample Dependence of BT⁴

In the original publications of Koshnevisan et al., 13,14 hereafter referred to collectively as K., we established to high precision the validity of the empirical fit

$$\rho = \rho_0 + BT^4 \tag{3.1}$$

where ρ_0 is also a variable parameter and thus not exactly the residual resistivity. This fit is valid for temperatures roughly within the following ranges: 2 < T < 7.5 for Ag; 1.5 < T < 7.1 K for Au; 2.5 < T < 7.5 K for Cu. The power of four was found to be correct to within +0.02 and -0.11 for all samples of all three metals when the best single power fits were obtained on the computer. Two examples from K. of the fidelity of such fits are shown in Fig. 3.1. Thus it is clear that one could obtain meaningful values of B for comparison if a series of samples were fit to Eq.(3.1). This comparison is motivated by considering the sample dependence of B for the same metal shown in Tables 1.1, 1.2 and 1.3 for samples of K. and Barnard and Caplin, hereafter known as B.C.

Copper was chosen to be the test material for the study of the B sample dependence. The preparation of the pure Cu, samples Cu 10 and Cu 11, and the dilute Cu 0.1 at.% Ag and 0.025 at.% Ag alloys, called CuAg 1 and CuAg 2 respectively, is detailed in Chapter 2. These samples were initially measured in the annealed state and then repeatedly in increasing states of strain. After each straining (which was done by simple stretching except in Cu 10) the geometrical factor was redetermined with an overall accuracy of better than 2%. Most runs were made using the current comparator described in Chapter 2 but several were done with less precise current sources. Due to this and other experimental

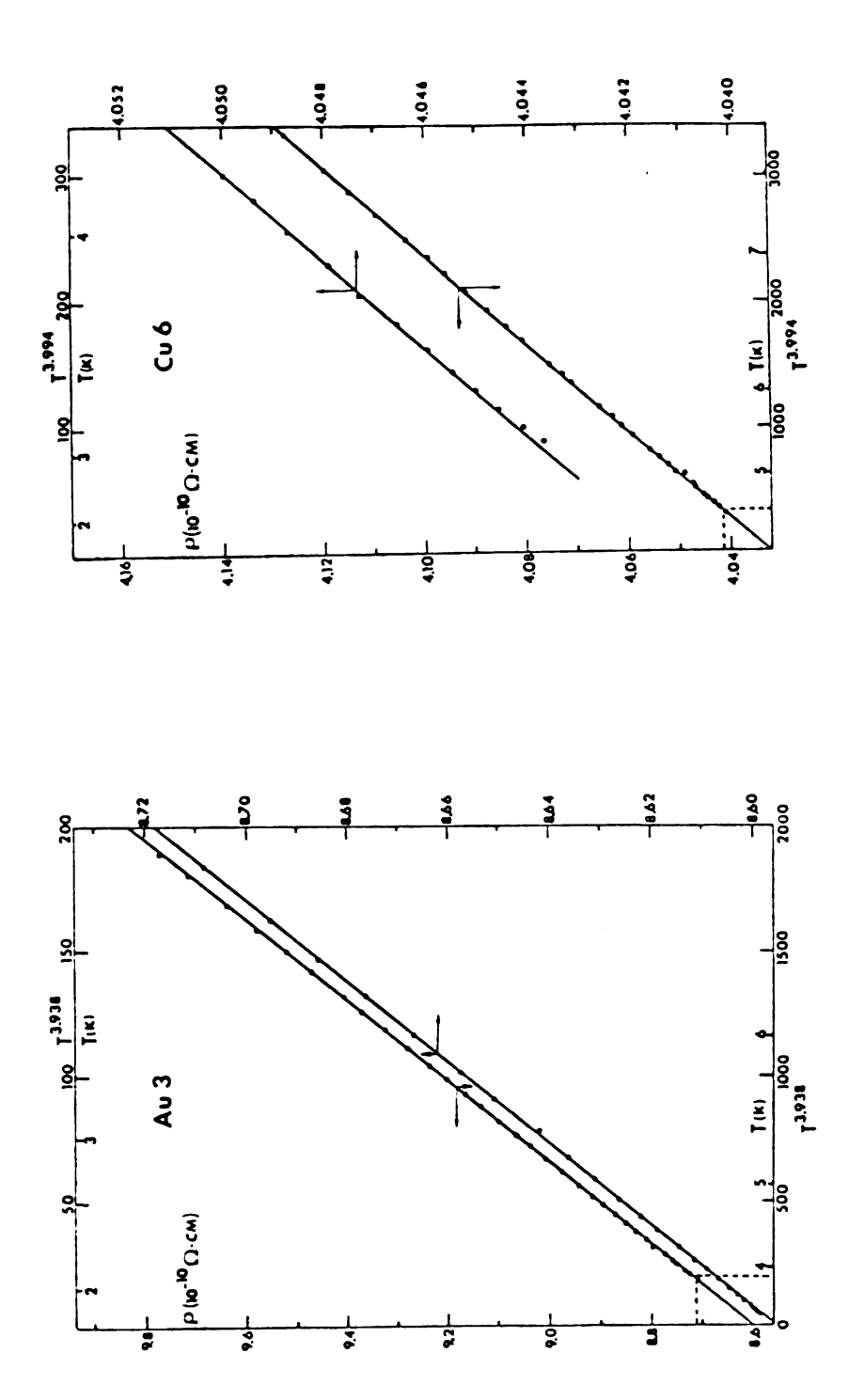


Fig. 3.1 ρ vs. \tilde{T}^4 for Ag 3 and Cu 6 (note, the ordinate for Au 3 should be multiplied by 0.9).

variables, the data do not all have the same precision. However, Fig. 3.2 shows the T^4 plots of data from one of the least as well as one of the most precise runs to show that B was a well defined quantity in each case. This figure displays a pure and an impure sample each in a strained and unstrained state to show how the slopes of the graphs, B, vary with the introduction of impurities and dislocations. For consistency in comparing B from the various runs, the fit to Eq.(3.1) was made over roughly the same range of T^4 for all runs even though some runs were made to higher and/or lower temperatures than the fitting range of $3 \lesssim T \lesssim 7.2$ K. The data were taken in even intervals in T^4 and fit without weights by least squares to Eq.(3.1). The results of these measurements are given in Fig. 3.3 which shows the values of B vs. ρ_0 for the annealed and the strained samples. To understand this figure it is helpful to identify several special values of ρ_0 and B. We define ρ_a and B_a to be the values of ρ_o and B pertaining to the annealed state and shown on the figure by the open symbols. The solid symbols refer to samples in various states of strain. The amount of strain is given in percent next to each point and is determined by summing the values $(L_{j+1}-L_{j})/L_{j}$ from each successive strain, where the L_{j} are the lengthsof the samples after each strain. Because the values of B seem to be leveling off for large strains it is helpful to estimate a limiting value B_{ϱ} for each sample which is assumed to be approached asymptotically. As expected, the values of \boldsymbol{B}_{a} exhibit a behavior similar to a Caplin-Rizzuto plot as shown by the straight line of large dashes. This behavior is generally understood in terms of the anisotropy model as discussed previously. A more striking feature of Fig. 3.3 is the behavior of B vs. ρ_0 for the strained samples. The decrease in B due to

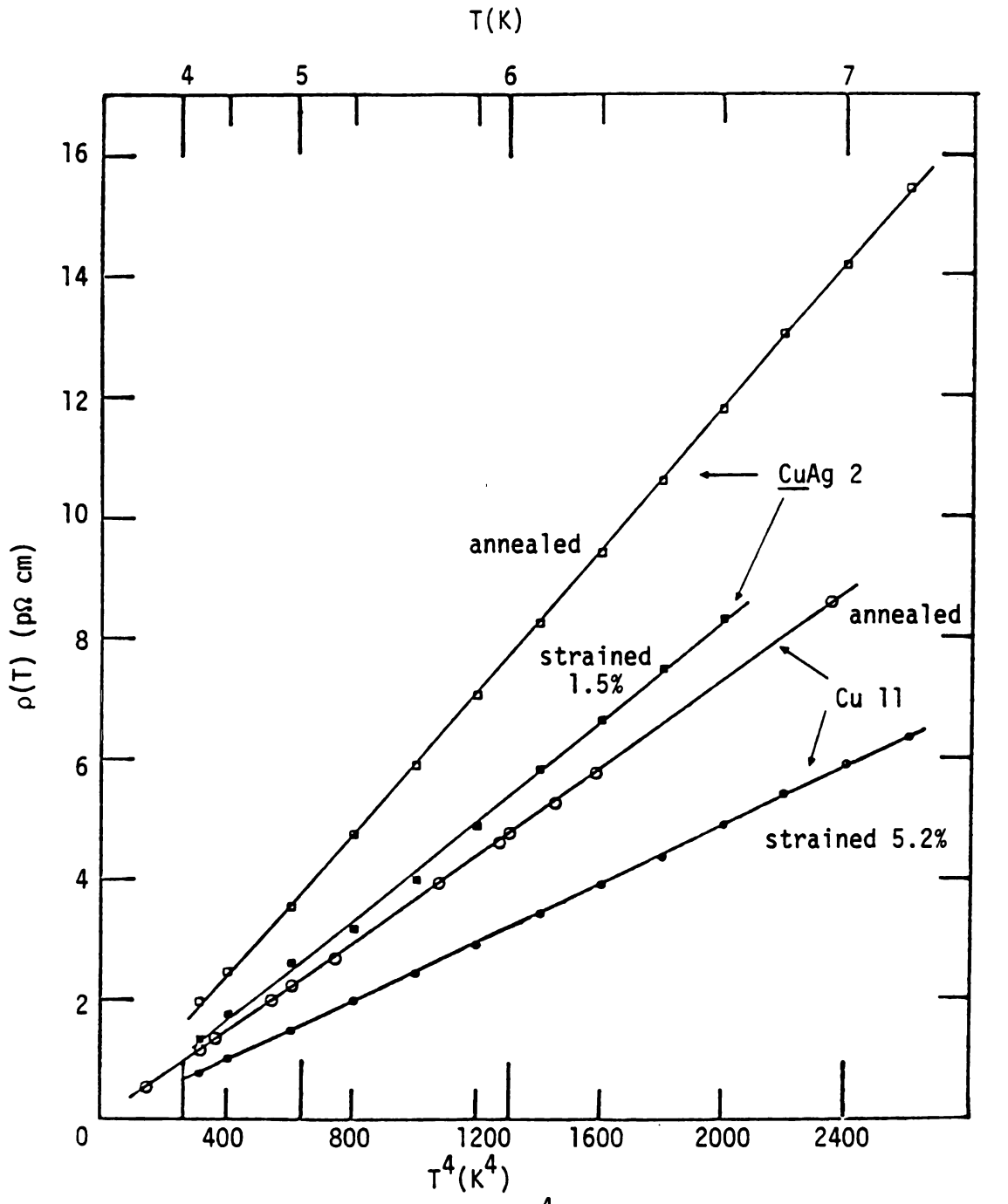
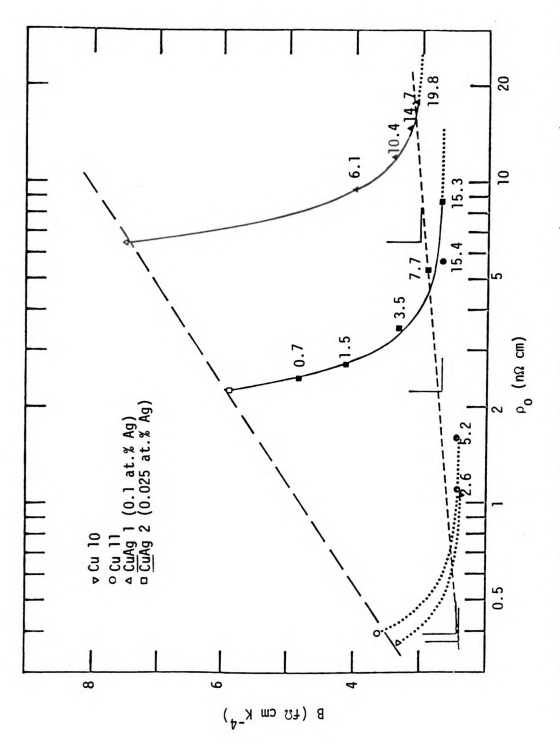


Fig. 3.2 $\rho(T) = (\rho_{Total} - \rho_{o})$ vs. T^{4} for annealed and strained states of Cu 11 and CuAg 2. The strained Cu 11 and CuAg 2 shown are examples of worst and the best precision in this series of runs.



B vs. ρ_0 for Cu and dilute CLAg alloys in annealed (open symbols) and strained (solid symbols) states with strain shown in percent. See text for explanation of various lines and curves. . Fig. 3.3

straining is in keeping with the findings of Rowlands and Woods (1978) for several other metals (Al, Pd, and Ag at higher temperatures). Again, this is explicable in terms of the anisotropy model.

The initial rapid drop in B due to the introduction of dislocations provides evidence of a rather large effect on the distribution function. This implies that by introducing dislocations one produces a large increase in the ratio of small to large angle scattering which, we have seen in Chapter 1, produces a much smaller relaxation time on the necks compared to the bellies. The saturation of B for larger strains indicates the distribution function is no longer changing. However, it is uncertain how closely the dislocation dominated distribution function mimics the ideal phonon dominated distribution function in a perfect pure metal. The line of short dashes going through the points (ρ_a, B_g) indicated by the set of small coordinate axes has a small slope implying that the dislocation dominated distribution function is only weakly dependent on initial impurity.

The small sets of axes suggest an alternative way to plot the data. It seems reasonable that the more impurity a sample has initially, the more dislocations must be added to effect the same change in the electron distribution function. Thus, we might define a more meaningful parameter $x = \rho_0/\rho_a$ which scales the residual resistivity obtained after adding dislocations by the initial resistivity. We can also define a parameter $y = B - B_g/B_a - B_g$ which essentially shifts the zero of B to B_a and scales it by the total change in B. When this is done one finds that the data for the two alloys fit a simple equation with only one free parameter

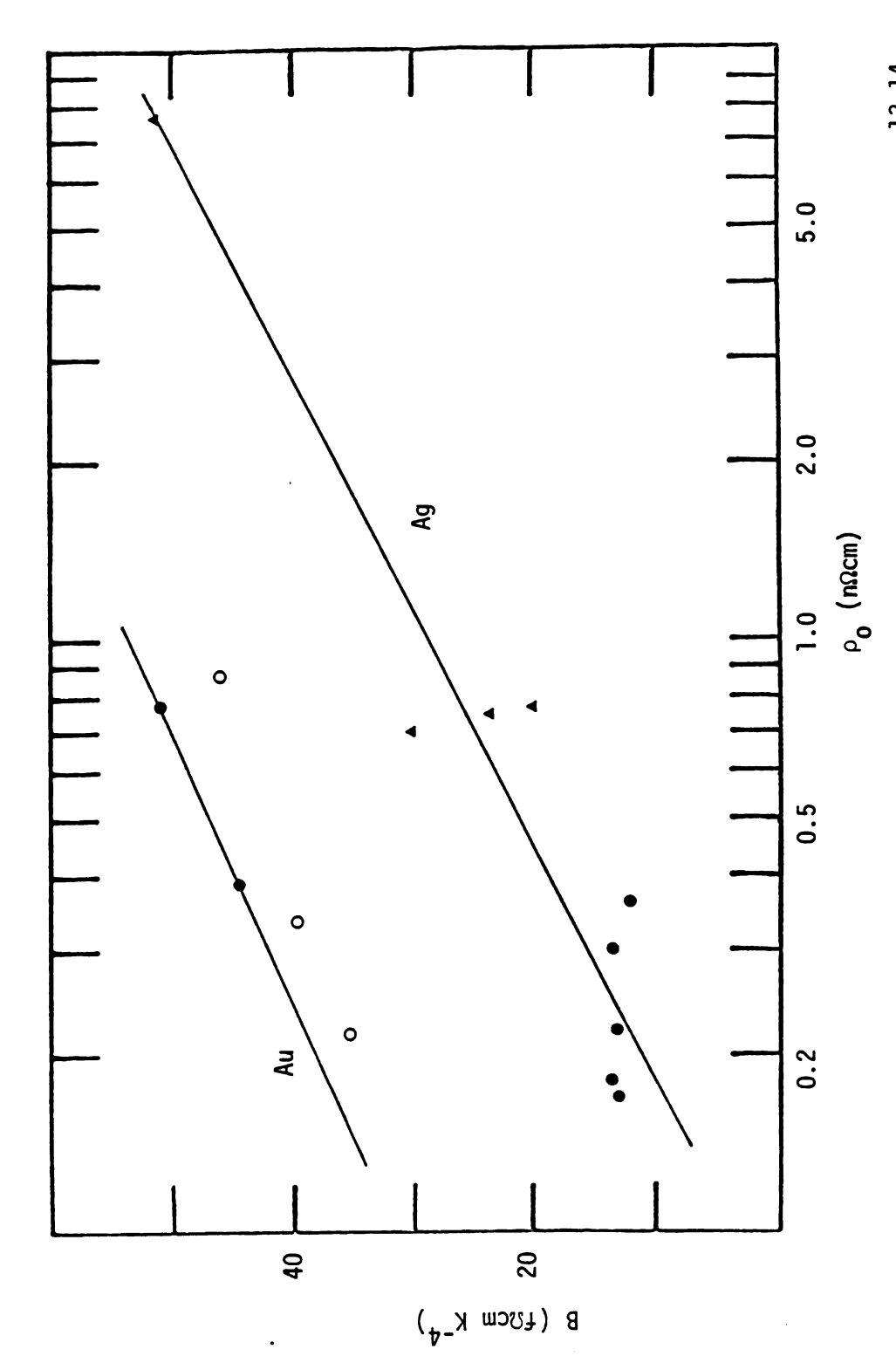
$$y = x^{-V} \tag{3.2}$$

For both alloys $v = 4.0\pm0.1$ produced the best fit. The degree of fit can be seen in Fig. 3.3 where the solid lines were drawn according to this equation.

At this stage it is unclear why the value of v should be the same for both samples. Nor do we understand why it has the value four. However, the existence of such a simple function is at least intriguing.

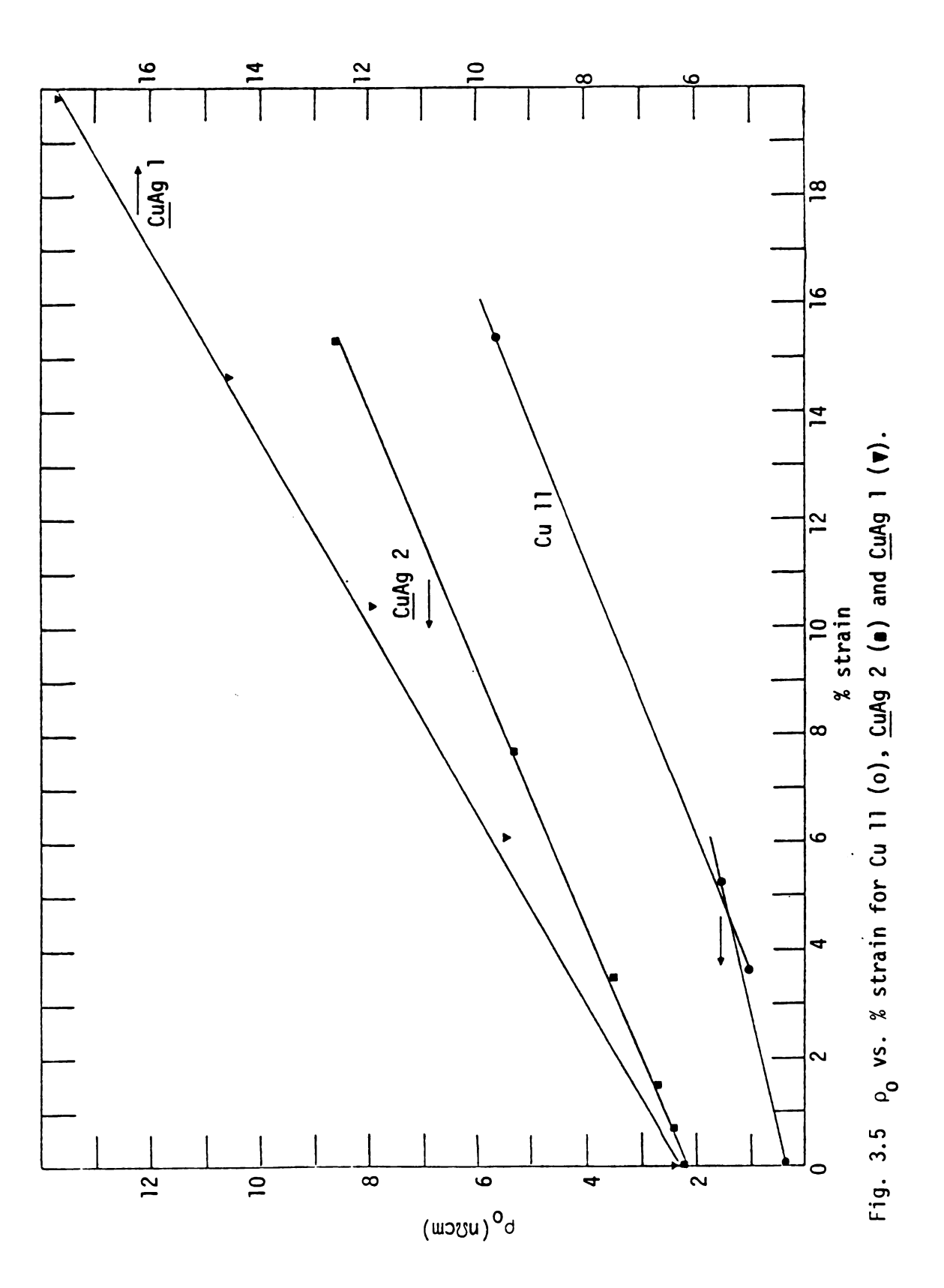
Unfortunately the pure samples Cu 10 and Cu 11 were given initial strains which were too large to allow this equation to be checked for them. However, the values of B_a and B_ℓ are known so the dotted curves were drawn according to Eq.(3.2), assuming v = 4.

The sample dependence of the values of B for Cu and Au published in K. and Ag published in B.C. and K. are now explicable from Fig. 3.3 on an empirical level. Figure 3.4 shows published results for Au and Ag. The results for Au include some unpublished values (open circles). These samples had significant Kondo minima which adds some uncertainty to these values. In addition, they were polycrystalline and of much smaller dia-Therefore they probably had been given more unintentional strain during handling especially since they were measured before the effects of strain on $\rho(T)$ were appreciated. Nevertheless, as a group they show the same upward trend with ρ_{o} . First we notice the general upward trend for increased impurity level (i.e. increased ρ_{O}). However, the Ag data of K. (dots) and B.C. (triangles) show marked deviations from this general trend. Due to the strong sensitivity of B to small amounts of strain, it seems likely that the very pure samples of K. and B.C. all had significant but variable ratios of ρ_d/ρ_i even in samples with nearly identical values of $\rho_0 = \rho_d + \rho_i$. For example, one sample of B.C. was measured a second time after having its potential leads reattached.



B vs. ρ for published (•) and unpublished (o) data of Koshnevisan et al. for Ag and Caplin for Ag. Fig. 3.4

When measured again, even though its ρ_Ω had increased slightly (2.7%) its value of B decreased noticeably (15%). On the basis of our results it seems highly probable that it was strained slightly in the handling between runs. The three samples of B.C. having nearly the same ρ_{Ω} would seem to lie very well on the steep portion of curves similar to those for strained Cu in Fig. 3.3. The purer samples of K, on the other hand, show a more or less constant B and would seem to lie well on the asymptotic tail of such a curve. This is reasonable because the purer the sample the greater the relative contribution of the unavoidable residual dislocations to the total ρ_0 . Of course, quite apart from their effects on the magnitude of phonon scattering, the introduction of dislocations increases the total residual resistivity. The variation of ρ_{o} with strain is shown in Fig. 3.5. It is seen to increase more rapidly with samples of lower purity. To the maximum strain introduced each curve is roughly linear. These increases in slope with impurity content may not be related to the anisotropy model. If the cores make the major contribution to ρ_{d} it is not obvious why ρ_{d} should increase more rapidly with strain in impure samples. If the strain fields make a major contribution one might expect this would only occur when the e.d.f. is impurity dominated because only then is small angle scattering important. In that case, for the larger strains, Fig. 3.3 implies the e.d.f. is already dominated on the necks by the dislocations so as to reduce the effects of small angle scattering. Thus, one would expect to see a decrease in slope in the ρ_{o} vs. strain graphs corresponding to a reduction of the strain field contribution of $\boldsymbol{\rho}_{\boldsymbol{d}}.$ Since no sign of saturation occurs there seems to be support for the calculations of Lukhvich and Karolick 68 which suggest the major contribution to $\boldsymbol{\rho}_{0}$ comes from the strongly scattering



core regions of the dislocations. The problem of accounting for the differing slopes remains. Possibly the impurities cause a larger number of dislocations to form per unit strain by preventing dislocations from moving out of the system.

B. Analysis in Terms of the Theory of Bergmann, Kaveh and Wiser

1) Reanalysis of Published Data

Just when the results of the preceding section were ready for publication Bergmann et al. 3 published a theoretical justification for the fourth power behavior. From now on we call this theory B.K.W. Recall from Chapter 1 that it is based on a fortuitous combination of T^2 e-e scattering and $T^{-4.5}$ phonon scattering. The inclusion of a T^2 term was attempted by both B.C. and K. but always in addition to a T^4 term. A fit to the form suggested by Bergmann et al. Eq.(1.63) was never attempted nor was its generalization

$$\rho = \rho_0 + AT^2 + CT^N$$
 (3.3)

A fit with two variable exponents was attempted but not published in K. because it did not give a better fit than a single exponent. In light of B.K.W. it seemed appropriate to reanalyze some of the data we published previously in K. to see if we could fit the entire temperature range rather than dividing it into two regimes as had been done.

We digress briefly to describe some aspects of the curve fitting program used in this analysis. The data were fit using a general non-linear curve fitting program called KINFIT 4 developed by J. L. Dye and V. A. Nicely in the M.S.U. department of chemistry. This program weights each data point in the fit according to the user's estimates of error in

both the independent and the dependent variable. The weighting takes into account the sensitivity of the user defined residual function (whose weighted and summed squares are to be minimized) to the estimated error of each variable at each point. This function F has a value F_i at the i^{th} point which, in this case, is just the difference of the measured resistivity and the fitting curve at the i^{th} temperature. The weighting of each point is given by

$$W_i = 1/\sigma_{F_i}^2 \tag{3.4}$$

where

$$\sigma_{F_i}^2 = \left(\frac{\partial F}{\partial x}\right)_i^2 \sigma_{X_i}^2 + \left(\frac{\partial F}{\partial y}\right)_i^2 \sigma_{y_i}^2$$
 (3.5)

where $\mathbf{x_i}$ and $\sigma_{\mathbf{x_i}}^2$ are the independent variable and its variance at the ith point and similarly for the dependent variable y. The program uses an iteration procedure to find the best fit. During each iteration, the computer uses the most recent form of the fitting function to calculate the next set of weights $\mathbf{W_i}$. This program was superior to that used in K. in that it supplied more information. Besides the "best fit" parameters and their standard deviations, it provided the following information: The sum of the residuals squared, the <u>multiple correlation coefficients</u>, $\mathbf{P_{ij}|k...}$ $\mathbf{R_i}$ is a measure of the total correlation of a given parameter, that is, to what extent variations of this parameter can be compensated by the simultaneous variations of the other parameters and still maintain a good fit within the scatter of the data. The $\mathbf{P_{ij}|k}$ are a measure of how strongly the ith and jth parameters are correlated such that one can compensate for variations in the other while the other parameters

k... are held constant. The program also supplies a complete list and plot of the residuals at each point. These are useful in detecting systematic deviations of the data from the curve.

The standard deviations of the parameters (called the marginal standard deviations) include the correlation effects so they represent the span of values a parameter can take while allowing the others to compensate so as to retain the same goodness of fit. Thus, even though the parameters in these fits show sizeable correlation, the data are sufficiently precise that the standard deviations remain small allowing us to be confident regarding the validity of the fit. Of course, large standard deviations coupled with large correlations would make the result meaningless. It should be no surprise that the highest pairwise correlations between parameters in an equation like (3.3) are the variable exponent and its coefficient. If ρ_0 is allowed to vary, it generally shows the least correlation with other parameters.

The data were fit (where applicable) to the following equations:

$$\rho = \rho_0' + BT^4 + \delta \tag{3.6}$$

B and δ adjustable

$$\rho = \rho_0' + B'T^N + \delta \tag{3.7}$$

B', N, and δ adjustable

$$\rho = \rho_0' + AT^2 + CT^{4.5} + \delta$$
 (3.8)

A, C, and δ adjustable

$$\rho = \rho_0' + A'T^2 + C'T^N + \delta$$
 (3.9)

A', C', N and δ adjustable

In these equations we have written the true residual resistivity $\rho_0 = \rho_0' + \delta$. For ρ_0' we use the resistivity measured at 40 mK for the unstrained pure metals. We then expect the adjustable parameter δ to be less than the experimental error in determining ρ_0' . For each of the fits to Eqs.(3.6) to (3.9), the quantity S defined by

 S^2 = Sum of residuals squared/number of degrees of freedom

was calculated to give a measure of the goodness of fit. Note that in their original publication Khoshnevisan et al. 13,14 performed a variety of analyses but always kept N = 4. Equations (3.8) and (3.9), therefore, represent analyses not previously presented. However, even Eqs. (3.6) and (3.7) represent new fits because they are now being used over the entire temperature range.

Of the pure metal samples studied in K. we choose the following for further analysis. Au 3 is chosen because Fig. 1 of Khoshnevisan et al. 14 indicates that its temperature dependence can be represented to a very good approximation by a single power law from 2 to 7°. We have not included the results of Au 1 because they show a resistance minimum at $^{\circ}$ 0.3 K (note that reference 11 is in error in that the Kondo minimum ascribed to Au 3 actually applies to Au 1) and we are aware from other unpublished data on Au we have measured that the effect of the Kondo term extends to temperatures $^{\circ}$ 5 times the Kondo temperature. For the same reason we choose Cu 6 rather than Cu 1. From Khoshnevisan et al. 13 we choose AgC $_3$ which represents our best low temperature data, but which unfortunately extends only up to 4.16 K. We also analyze AgD with data ranging from 30 mK to 6.17 K. The results for the unstrained pure metal samples Cu 6, Au 3, AgC $_3$, and AgD are given in Table 3.1. The δ 's

Table 3.1 Reanalysis of published data in terms of Equations (3.8) and (3.9)

Equation	v	, A,	.°°		z	•	Temp. Range	°0
	(10 ⁻¹⁴ ncm)	(10 ⁻¹⁴ scmK ⁻²)	(10 ⁻¹⁵ GCMK ^{-N})	(10 ⁻¹⁵ ncmK ^{-N})		(10 ⁻¹⁴ ocm)	(K)	(10 ⁻⁹ acm)
ອີ ກວ່								
3.6	5.24			3.02 ± .006	~	€.0 ± .4*	0.064 - 7.53	0.404046
3.7	3.68			4.15 ± .09	3.84 ± .01	4.3 ± .3*		
3.8	1.18	$3.05 \pm .02$	0.910 ± .002		4.5	11. ± 21.0		
3.9	1.01	2.68 ± .05	1.16 ± .03		4.39 ± .13	11. + 19.0		
Au 3								
3.6	12.5			49.8 ± .02	4	7.4 ± 1.3*	0.5 - 7.2	0.775110
3.7	6.6			51.9 ± .2	3.978 ± .002	2.37 ± 1.21*		
3.8	41.3	35.6 + .8	16.3 ± .07		4.5	¥9 + 19		
3.9	8.2	5.2 ± .7	45.4 + .8		4.037 ± .008	-6.87 ± 1.6*		
AgC3								
3.6	2.8			14.2 ± .03	•	2.87 ± .22	0.03 - 4.2	0.298616
3.7	2.1			18.0 ± 0.3	3.83 ± .01	1.98 + .18*		
3.8	95.0	4.68 ± .03	5.68		4.5	-1.62 ± .05*		
3.9	.53	4.38 + .07	6.31 + .13		4.44 + .01	23 + .58		

Table 3.1 (cont'd)

Reanalysis of published data in terms of Equations (3.8) and (3.9)

Equation	S (10 ⁻¹⁴ ^{(,cm})	А, А' (10 ⁻¹⁴ ксшК ⁻²)	A, A' C, C' B ($10^{-14} \text{s.cm} \text{K}^{-N}$) ($10^{-15} \text{s.cm} \text{K}^{-N}$)	8 (10 ⁻¹⁵ ocmk ^{-N})	z	6 (10 ⁻¹⁴ scm)	Range (K)	^р о (10 ⁻⁹ ис m)
Agü								
3.6	4.6			10.72 ± .19	•	3.37 ± .40	3.37 ± .40 .03 - 6.2	.219349
3.7	2.2			13.97 ± .007	2.10 ± .20			
3.8	4.0	6.51 ± .13	3.64 ± .02		4.5	-1.99 ± .39		
3.9	4.4	2.4 ± .16	9.45 ± .27		4.03 ± .01	91. ± 65.	0.03 - 6.2	.219349

marked with an asterisk represent values which lie outside the error bars for ρ_0 . For Cu 6, AgC $_3$ and AgD satisfactory values of δ occur but only for fits to Eqs.(3.8) and (3.9). For these same samples, S is reduced significantly in going from fits to Eqs.(3.6) to (3.9). For Au 3 there is not much to choose between Eqs.(3.8) and (3.9) because for this sample N \approx 4, and any attempt to raise it to 4.5 (Eq.(3.8)) for example results in a bad fit. None of the Au 3 fits give acceptable δ values. We believe this is due to some remnant Kondo resistance in this sample—despite the fact that there is no minimum.

The prime significance of Table 3.1 is to compare the fits to the various equations. It is becoming very clear that the constants A, A', and C, C' are sample and history dependent, and that one should not put too much faith in the individual values. For example, when we come to study the strained samples it will become evident that A' and C' are strongly strain dependent, and very careful experiments on well characterized samples are still very necessary to assign precise values of A' and C' to these materials. However we believe the trends are significant. As we go from Cu to Ag to Au, A and B both increase. B in particular is much larger for Au than for Cu and Ag, and all the analysis bear out that N is very close to four for Au.

The analyses in terms of Eq.(3.9) for Cu and Ag clearly show this to give the best fits. S is appreciably smaller and the δ 's are acceptable.

2) Analysis of New Data for Strained Cu

We now present our attempts to fit our strained Cu data to the less empirical forms--especially Eq.(3.9). The results for a typical sample

Cu lla are shown in Table 3.2. For this particular sample, 2.1 < T < 6.91 K and $\rho_0' = 0.392769 \pm 0.000002$ n Ω cm. δ alters the fifth digit—a not unreasonable but quite unverifiable amount. Not surprisingly, the goodness of fit parameter S becomes smaller as the number of adjustable parameters increases, but for a constant number of parameters as in Eqs.(3.7) and (3.8) there is a significantly better fit when the AT 2 term is introduced, and this is significantly improved again by letting N be an adjustable parameter in Eq.(3.9).

The results for another sample $\operatorname{CuAg2}_{\mathbf{u}}$ are shown in Table 3.3 for the two best fitting equations. This sample had data in the range 1.5 K \leq T \leq 7.96 K. This allowed us to test the effects of cutting off the points at low temperatures where some of the other samples were not measured. The effects of cutting off the lowest six points (all points below 3.7 K) of the total 26 points for equation 9 are seen to be noticeable but not severe. The change in δ is the largest relative change but the changes in the other three parameters of interest are 6% or less. The effect on A of Eq.(3.8) was large but this equation was not the best fit. The effect of dropping the highest six points in Eq. (3.9) (T > 7.0 K) was of roughly the same magnitude except, of course, in δ which changed very little due to the presence of the low temperature points. The residual resistivity can be eliminated all together if the temperature derivative is fit. To test the results of such a fit the data were differentiated by simply taking differences between successive points. This process tends to increase the scatter so the error estimates were increased appropriately. The results of these fits to the derivatives of Eqs.(3.8) and (3.9) yielded the values in Table 3.3 labeled as 8-d and 9-d. Each of these cases was also fit

Table 3.2

Typical fits to various equations for Cu lla

Equation	S (10 ⁻¹⁴ Ωcm)	A, A' (10 ⁻¹⁴ Ωcm K ⁻²)	8, 8' (10 ⁻¹⁵ Ωcm K ^{-N})	C, C' (10 ⁻¹⁵ Ωcm K ^{-N})	N	$(10^{-14} \Omega \text{cm})$
			3.66*			
3.6	2.5		3.75 <u>+</u> .03			-5.84 <u>+</u> .72
3.7	1.2		5.06 <u>+</u> .22		3.83 <u>+</u> .025	-8.24 <u>+</u> .52
3.8	.49	3.35 <u>+</u> .05		1.17 <u>+</u> .01		-1.85 ± .03
3.9	.11	2.76 <u>+</u> .19		1.62 <u>+</u> .16	4.35	-1.66 <u>+</u> .01
					<u>+</u> .05	

^{*} Slope of p vs. T⁴

Table 3.3 Fitting parameters for CuAg 2 u (ρ_0 = 3.49534 nΩcm)

Equation	\$ (40)	A, A' (fΩcmK ⁻²)	C, C'	и'	6	Range
	(fΩcm)	(TOCHK)	(TΩCMK)		(fΩcm)	
3.8	· 18	36.2 <u>+</u> .9	1.009 <u>+</u> .009		-71 <u>+</u> 7	1.5 <u><</u> T <u><</u> 7.96
3.8		24.5 <u>+</u> 1.2	1.077 <u>+</u> .007		94 <u>+</u> 17	3.7 <u><</u> T <u><</u> 7.96
3.8d		34.5 <u>+</u> 2.0	1.014 <u>+</u> .015			1.5 <u>< T ≤</u> 7.96
3.8d		29.3 <u>+</u> 2.6	1.049 <u>+</u> .017			3.7 <u>< T <</u> 7.96
3.9	7.2	46.5 <u>+</u> .9	.480 <u>+</u> .033	4.84 <u>+</u> .03	$-10.7 \pm .4$	1.5 <u><</u> T <u><</u> 7.96
3.9		43.3 <u>+</u> 3.2	.514 <u>+</u> .070	4.82 <u>+</u> .06	-6.3 ± 3.0	3.7 <u><</u> T <u><</u> 7.96
3.9		45.4 <u>+</u> 1.3	.536 <u>+</u> .059	4.79 <u>+</u> .05	-10.3 <u>+</u> .5	1.5 <u><</u> T <u><</u> 7.0
3.9d		47.5 <u>+</u> 3.0	.497 <u>+</u> .077	4.82 <u>+</u> .08		1.5 <u>< T <</u> 7.96
3.9d		47.6 <u>+</u> 7.2	.481 <u>+</u> .14	4.82 <u>+</u> .14		3.7 < T < 7.96

with and without the lowest six points. Again the values of the parameters A', C' and N agree quite well with the fits which included the residual resistivity adjustment term δ .

In Table 3.4 we show the results for several samples, for fits to Eqs.(3.8) and (3.9). In terms of Eq.(3.8) B.K.W. would say that A should increase and C decrease as the dislocation content or strain is increased. We observe, however, that with one or two exceptions both A and C decrease with increasing strain. However, this is probably an artifact of the fact that 4.5 is not the correct exponent for the phonon term. This is shown by the increase in N with strain in Eq.(3.9) which gives a much better fit. Thus, the fitting program must compensate for the incorrect exponent by decreasing A in Eq.(3.8). We might add that B.K.W. suggest that 4.5 is only an approximate value obtained from a dirty limit calculation without dislocations. We see that the exponent is actually about 4.3 for all three annealed samples. The analysis using Eq.(3.9) gives A' and N which increase with strain and C' which decreases. But now it is not sufficient to consider C' alone since N is also varying. We therefore consider what happens to $C'T^N$ at a constant temperature, as the strain is increased. The general trend in C' is to decrease as strain increases, where as N increases. These two observations mean that at 1 K C'T^N will exactly follow C': for T < 1 K C'T^N will decrease with strain at a faster rate; for T > 1 K, there will be some T at which $C'T^N$ will increase with strain. This comes out to be ~36 K for sample CuAg la. However, at such a temperature we have no reason to believe N is the same. For illustration we give $C'5^N$ in Table 3.4. Again with a minor exception it decreases with strain as predicted.

Table 3.4 Values of the fitting parameters A, A', C, C' and N for strained samples

C,5 ^N	(10 ⁻¹² ,acm K ^{-N})	1.78	.88	3.87	1.60	1.02	1.11	2.93	1.16
z		4.35 ± .05	4.71 ± .06	4.32 ± .04	4.74 ± .14	5.03 ± .15	4.75 ± .16	4.32 ± .01	4.84 ± .03
, 3 ,	(10 ⁻¹⁵ acm K ^{-N})	1.62 ± .16	.45 ± .07	3.70 ± .34	.78 ± .29	.31 ± .11	.53 ± .21	2.80 ± .08	.48 ± .03
ပ	(10 ⁻¹⁵ acm K ^{-4.5})	1.17 : .01	0.745 ± .004	2.46 ± .01	1.32 ± .02	1.09 ± .02	.98 ± .01	1.86 ± .01	1.01 ± .01
, v	(10 ⁻¹⁴ ncm K ⁻²)	2.76 ± .19	3.59 ± .35	1.43 ± .60	3.61 ± .90	5.85 ± .73	4.48 ± 1.2	3.49 ± .11	4.65 ± .09
ď	(10 ⁻¹⁴ ucm K ⁻²)	3.35 ± .05	2.42 ₺ .08	3.76 ± .20	2.22 ± .32	2.97 ± .33	2.54 ± .24	4.83 ± .09	3.63 ± .09
		Cu 11 a	v	CuAg 1 a	w	•	>	CuAg 2 a	5

The overall conclusion is that analyses according to Eq.(3.9) give a superior fit to the data and the results from it are consistent with Kaveh and Wiser's predictions. The other point of some significance is that $N \to 5$ as the strain increases. As discussed in Chapter 1, this may well be expected because the e.d.f. is dominated by dislocation scattering on the necks and thus becomes highly anisotropic, resulting in a decrease in the importance of the neck contribution to the phonon resistivity. Thus, the spherical bellies now determine the temperature dependence which is expected to obey the Bloch T^5 law.

C. <u>Electron-Electron Scattering</u>

The superior fits to the data obtained by adding a T^2 term as outlined above make it now possible to extract meaningful values of the T^2 coefficient and, assuming the T^2 term to be more than just a term in a polynomial fit, identify this term with the long sought electron-electron scattering contribution to the resistivity. This identification is given some support by the fact that the coefficients agree rather well with their predicted magnitudes. This is seen by comparing Table 1.4 with the values of A' in Tables 3.1 and 3.4.

The average values of A' show only about a factor of two variation among the three noble metals whereas the phonon resistivity coefficients show very different magnitudes getting progressively larger as their atomic mass increases. This is consistent with the fact that the usual expressions for electron-phonon resistivity at low temperatures contain $(T/\theta_D)^5 J_5(\infty)$ where θ_D is the Debye temperature and $J_5(\infty)$ = 124.4 is the low temperature limit of the J_5 Debye integral. The vaules of C in the given units for Cu 6, AgC₃ and Au 3 respectively are roughly

0.91, 5.7 and 16.3. The values of θ_D in order are 315 K, 215 K and 170 K thus the values of $C\theta_D^5$ in appropriate units are 2.8, 2.6 and 2.3-all roughly the same magnitude. The e-e term on the other hand is roughly proportional to $n^{-5/3}$ where n is the electron density. This comes from the usual formulas for the e-e resistivity which contain a factor $(nE_F)^{-1}$ where E_F is the Fermi energy $(E_F \propto n^{2/3})$. The values of n for Cu, Ag and Au respectively are 8.47, 5.86 and 5.9 $(10^{22} \text{ cm}^{-3})$. We find the e-e coefficients A' for the same three samples to be roughly 27, 44 and 52 in the appropriate units. We find the magnitudes of A'n^{5/3} to be 9.5, 8.4 and 10 which, again, are seen to be about the same, demonstrating the rough validity of the $n^{5/3}$ scaling factor.

We must consider what factors may influence the coefficient A'.

That is, although it seems reasonable to say

$$\rho(T) = \rho_{ee}(T) + \rho_{p}(T) \tag{3.10}$$

We must exercise a bit of care in making an exact identification of ρ_{ee} with A'T 2 and of $\rho_p(T)$ with C'T N . A' will exhibit some variation if the other terms in the fit are varied due to a certain amount of correlation between the terms. This was seen to cause the different responses of A and A' to strain already discussed. By allowing N to be a variable parameter we feel that the term C'T N provides a much better representation of the phonon term $\rho_p(T)$. To the extent that C'T N completely represents $\rho_p(T)$ we can probably be assured that A'T 2 completely represents $\rho_{ee}(T)$. However, it is almost certain that $\rho_p(T)$ is not exactly given by C'T N over the entire temperature range. Thus, phonon scattering may have some small effect on the value of A'. Comparison of the value A' = 26.8 (fΩcm K $^{-2}$) for Cu 6 with the value from

the low temperature data of K. is instructive. That value of 34.8 (f Ω cm K^{-N}) was obtained for a single power fit to data from 0.064 to 2.15 K with an exponent of 2.03. It is likely that this value is higher because the fit also included a small contribution from $\rho_p(T)$ at the upper part of the range. This is given support if we consider that the C'T^N term for Cu 6 has a value of 24.3 f Ω cm at 2 K which is non-negligible compared with the value of 107.2 f Ω cm for the A'T² term. In addition, it seems clear on the basis of our evidence and the predictions of B.K.W. that there is no unique value for the magnitude of ρ_{ee} since it seems to depend on the relative amounts of dislocation and impurity scattering.

Having said this, it remains desirable to try to eliminate any significant phonon contribution by going to the lowest temperatures with high precision. The experimental methods and difficulties of such measurements were outlined in Chapter 2 for high purity samples of Ag and Cu having RRR values of ~20,000 and ~13,000 respectively. We will call these Ag_{20} and Cu_{13} . Figure 3.6 shows the results of these measurements for Ag_{20} . The solid curve with the solid data points from the second run on Ag_{20} (Ag-run 2) was determined by the differential method previously described and is, therefore, given by

$$\frac{1}{\rho_0} \frac{d\rho}{dT} \tag{3.11}$$

The dashed curve is the integral of the solid curve and is proportional to $\rho(T)$. The actual values of $\rho(T)$ can be obtained by multiplying the vertical scale with units by $1.5 \times 10^{-11}~\Omega \text{cmK}$. It is obvious that if we were in a pure $\rho - \rho_0 = AT^2$ regime the solid curve should be a straight line through the origin. It is also obvious that this is not the case. The strange behavior at the lowest temperatures (which we will briefly

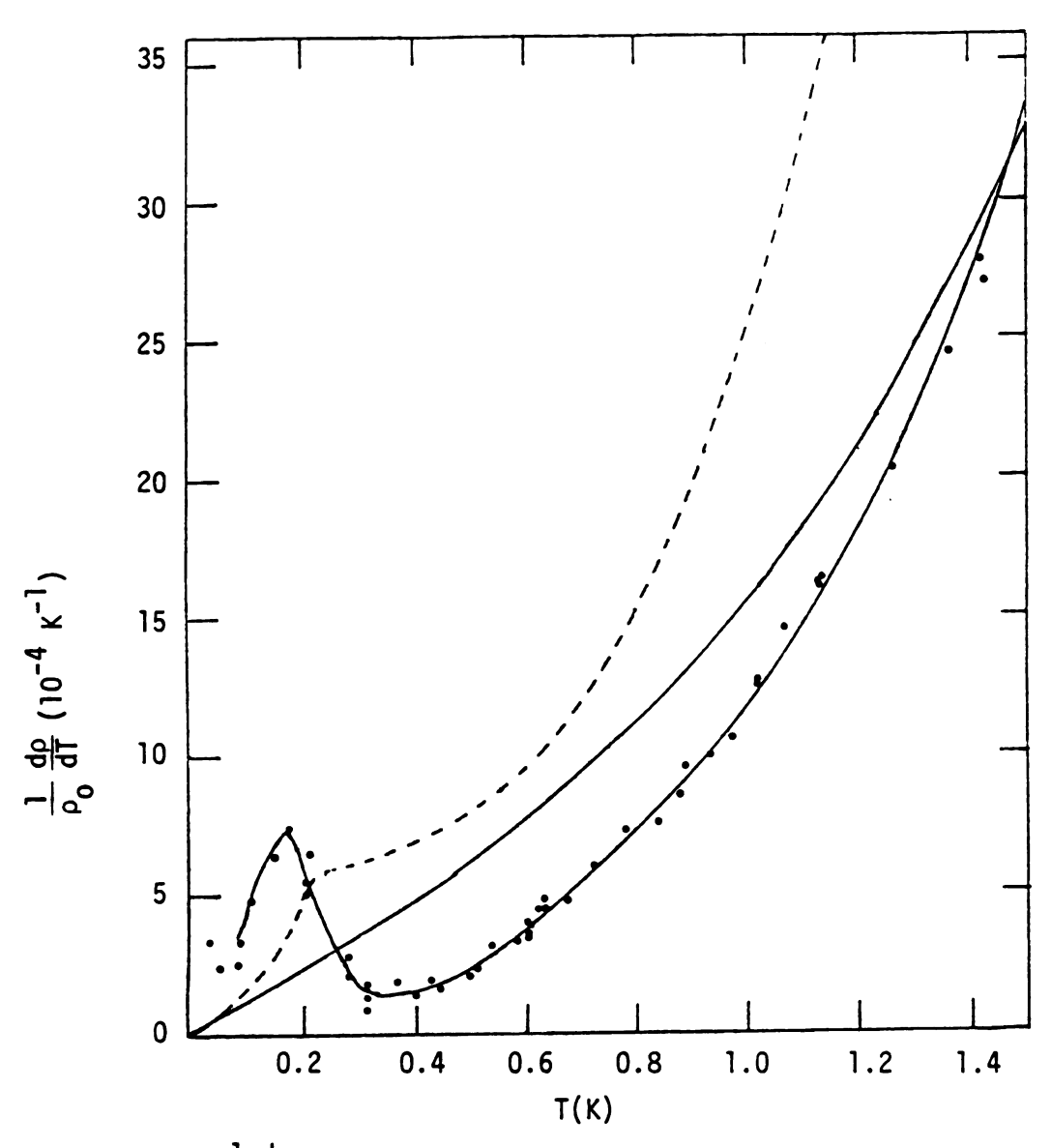
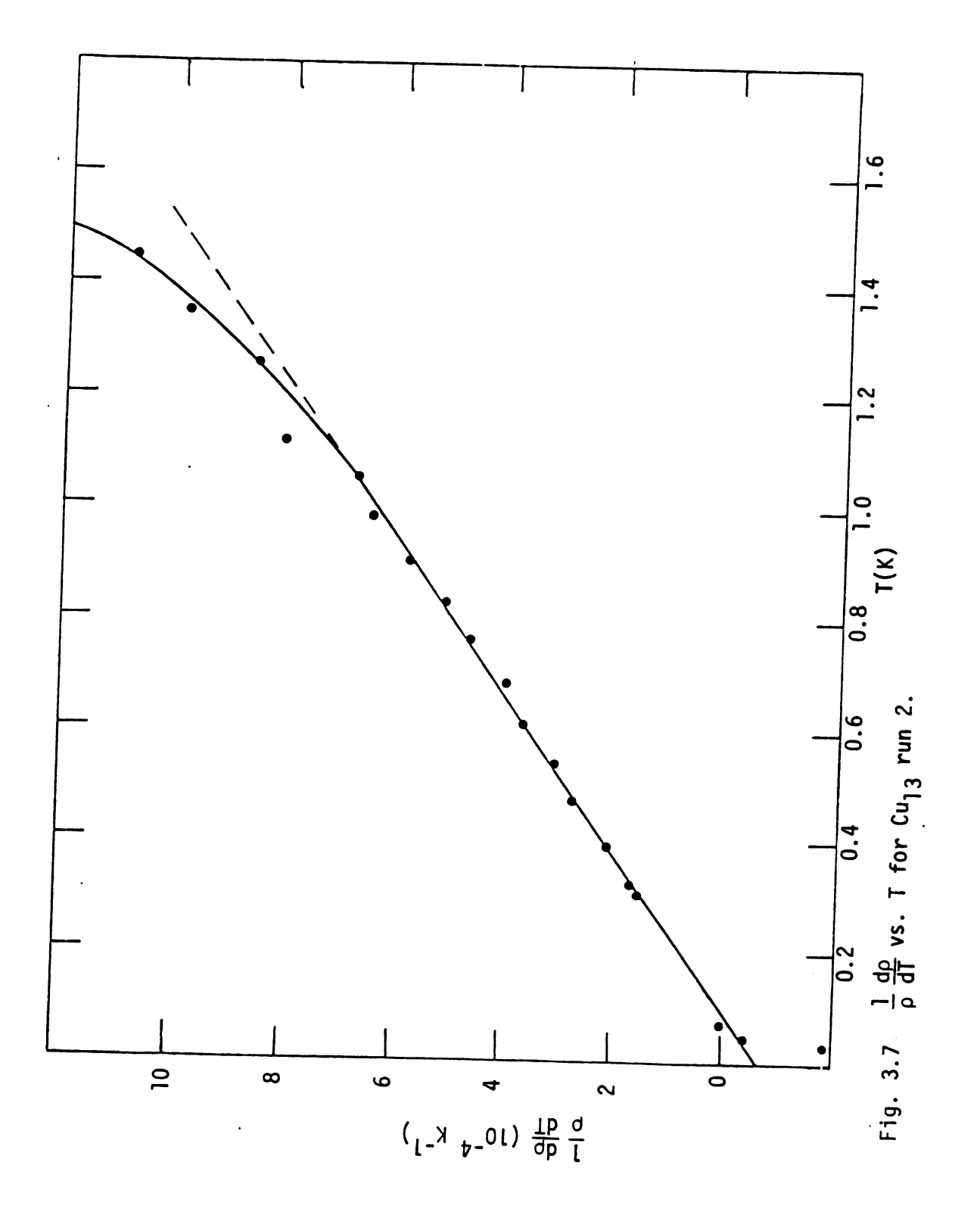


Fig. 3.6. $\frac{1}{\rho}\frac{d\rho}{dT}$ vs. T for Ag₂₀, run 1 (o) and run 2 (•). Dashed line $\rho(T)$ (ρ_0 times integral of solid curve through data). Other solid line is the derivative of Eq.(3.9) with parameters from fit to AgC₃ divided by ρ_0 from Ag₂₀.

consider seperately) destroys any hope of seeing a straight line through the origin below 0.5 K. Above this temperature the resistivity is obviously increasing more rapidly than T^2 . If we go back to our analysis of the Ag samples of K., say AgC_3 , we find the ratio $\rho_p/\rho_{ee} \cong 0.14$ at 1 K. Suppose we require $\rho_p/\rho_{ee} \le 5\%$, then we would be restricted to temperatures below 0.65 K. For comparison we have plotted the derivative of the Eq.(3.9) fit to the AgC_3 data which has been divided by the ρ_0 of Ag_{20} for scaling purposes. At our present level of ~1 ppm precision for such samples it appears it would be possible to obtain the T^2 coefficient to better than 10% from measurements below ~0.6 K if there were no peculiar behavior in this region. It is also clear why the fits to the less precise Ag data published in K. below 1.5 K yielded exponents around 2.5 rather than 2.

Copper provides better hope of isolating the true T^2 term because it has a smaller phonon term at temperatures below 1 K. Indeed Cu_{13} has provided the best evidence of an isolated T^2 term in the noble metals. Figure 3.7 shows the second and probably best run of this sample (Currun 2) when superconducting shields were placed around the sample, reference and solder terminals as described in Chapter 2. The graph shows a rather good straight line fit to about 1.1 K. Taking figures from Table 3.1 for Cu 6 we see that at 1 K we might expect the phonon contribution to be ~4%. However, because of the extreme purity of this sample it is likely that the phonon term is a bit smaller due to the effects of residual dislocations than in the less pure Cu 6. The slope of this curve is just $2A\rho_0^{-1}$ where A is the T^2 coefficient yielding a value of $4.8 \times 10^{-14}~\Omega cm~K^{-2}$ for A, with an estimated ~10% error due to uncertainties in ρ_0 . These uncertanties arise because in the differential



method of measurement ρ_0 is not determined and, due to the extremely low resistance of the sample, the determination of ρ_0 for the RRR measurement by the method described in Chapter 2 is not very precise. Comparison of this value with the values of A' for strained samples would indicate support for the assumption of a significant dislocation component to ρ_0 since only the strained samples had values as large as this. To be fair, however, we must mention the fact that the straight line does not intercept the origin as it should for a pure T² resisitivity. Although it comes near the origin one cannot force it through the origin and yet maintain a good fit. This problem is probably related to the apparent negative values of dp/dT at the very lowest temperatures.

D. Anomalous Behavior at Ultra-low Temperatures

Due to the very peculiar and unexpected behavior of the ultra-pure Ag₂₀ sample below 0.6 K when it was run the first time (Ag--run 1) we suspected possible experimental problems because we were using a new sample holder. These data are shown by the open circles in Fig. 3.6. During this run Cu₁₃ was used as a reference but not measured itself. During Ag--run 2 we qualitatively reproduced the results of the first run even though we had improved the sample holder. The points from Ag--run 1 are fewer in number and slightly less precise especially above 0.5 K due to problems with temperature control. Nevertheless, they seemed to exhibit differences from the data of Ag--run 2 beyond their error. (The degree of reproducibility below 0.5 K is indicated by the two points at about 0.22 K.) The two most marked differences are the apparently greater height of the peak at ~0.17 K and the small negative values around 0.5 K. If these negative values are real, the actual resistivity

for Ag-run 1 would have a slight resistance minimum. The existence of the peak was again verified by taking several points (not shown) in the vicinity of the peak during the second run on Cu_{13} ($\operatorname{Cu-run}$ 2)--the run using superconducting shields. The results of our first run on Cu_{13} are even more strange at lowest temperatures (see Fig. 3.8). Cu-run 1 was made during Ag-run 2 where, after measuring Ag_{20} using Cu_{13} as a reference, the roles were reversed and Cu_{13} was measured with Ag_{20} as reference. Although the set-up was optimized for measuring the Ag_{20} this was more a matter of convenience and we do not feel it was detrimental to the results. The negative and positive values shown below 0.2 K were checked on several successive days of the run and each time the behavior was the Although the errors are rather large due to the necessity of making small temperature differentials at such low temperatures, there seems to be no doubt that on cooling below 0.2 K the apparent values of dp/dT swing rather sharply upward and then abruptly go negative. The transition occurs between 35 and 28 mK but we have no values within this range during this run. As seen in Fig. 3.7 when measured on a second run (Cu-run 2) this sample did not show the same positive peak before going negative but seems to make a smooth transition to negative values below ~70 mK. Unfortunately there are not many points in this region. The first negative point occurs at ~40 mK. At this temperature the values were positive on the previous run. In Cu-run 2 the Cu_{13} and Ag_{20} samples had been physically interchanged so that Cu_{13} used a different thermometer than Cu-run 1. Both had been recently calibrated and would not be expected to differ by more than 1 or 2 mK. Another possible source of error is that if dp/dT is actually varying as rapidly indicated in Fig. 3.8 then the use of finite differentials could cause appreciable

error. However, the failure to obtain similar qualitative features, save the fact that $d\rho/dT$ ultimately goes negative, makes it impossible to say more at this stage. We have been unable to ascribe these differences to anything associated with the fact that the samples had been interchanged. In both positions there did not seem to be any possible thermal path through the samples to cause thermal electric problems. The only thermal path was through the potential and current leads whose thermal conductivity is extremely small. However at this point we cannot be completely confident this low temperature behavior is real in the Cu_{13} sample. In the Ag_{20} sample, on the other hand, we have greater confidence that the peak in $\text{d}\rho/\text{d}T$ is real. Up till now no one has so closely scrutinized the resistivity of such pure samples at these temperatures.

Assuming the Cu data are real, the rather wild behavior found in Cu-run l and even the somewhat milder behavior of Cu-run 2 do not seem explicable in terms of the usual Kondo type mechanism because the Kondo minimum normally relies on the fact that the magnetic scattering contribution decreases with T while the phonon term increases. In this case, the phonon term is insignificant. The transition from negative to positive dp/dT and hence, the resistance minimum, is quite sharp. It would seem the electron-electron term is not strong enough to cause such a sharp transition unless the magnitude of the negative slope from the magnetic term were itself decreasing quite rapidly.

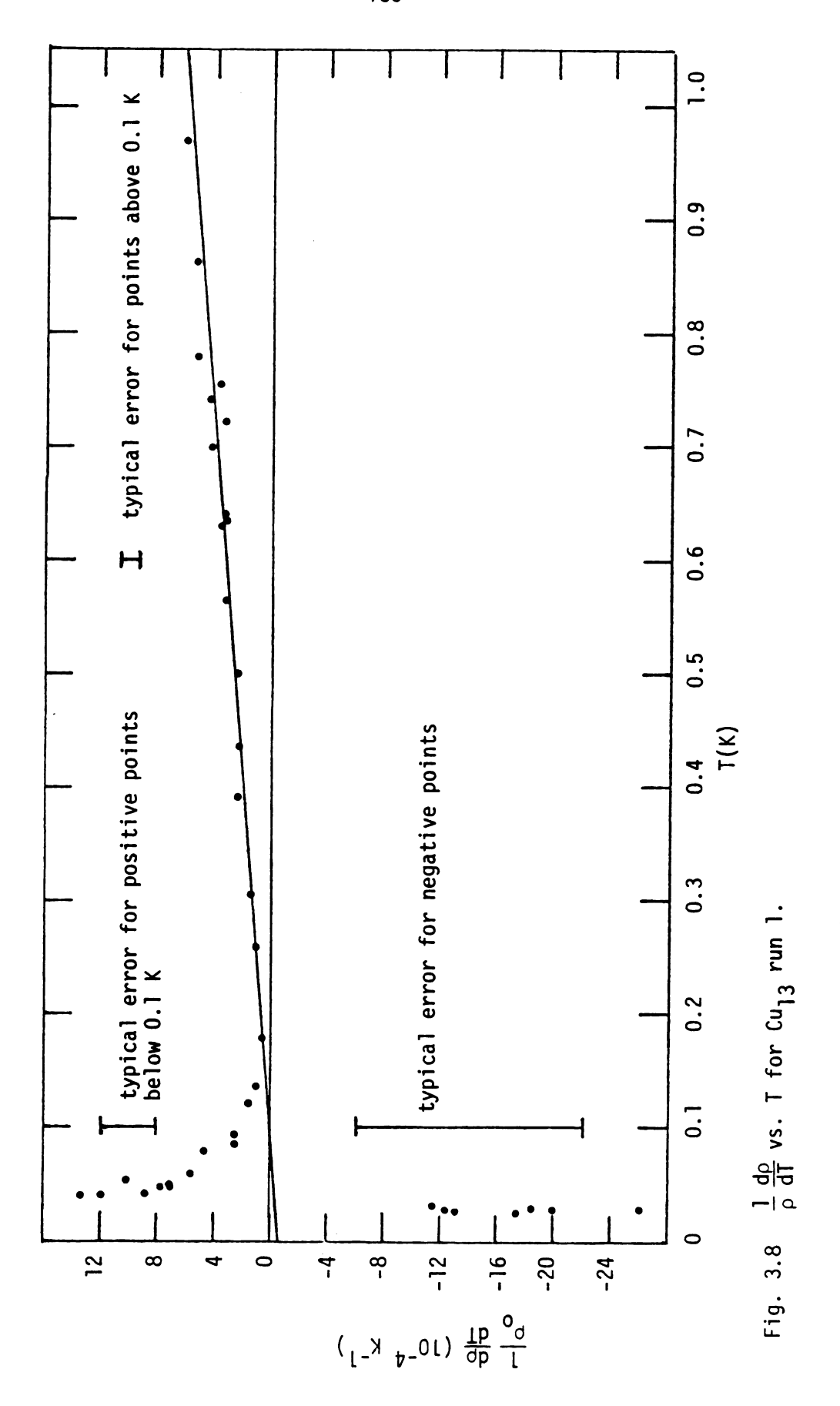
Supposing the peak in the Ag data is real it is difficult to say what might be the cause because the sample is of such high purity that we don't know what impurities are present. However, taking the liberty to engage in pure speculation, we might guess this is due to long range interactions between trace amounts of magnetic impurities. The shoulder

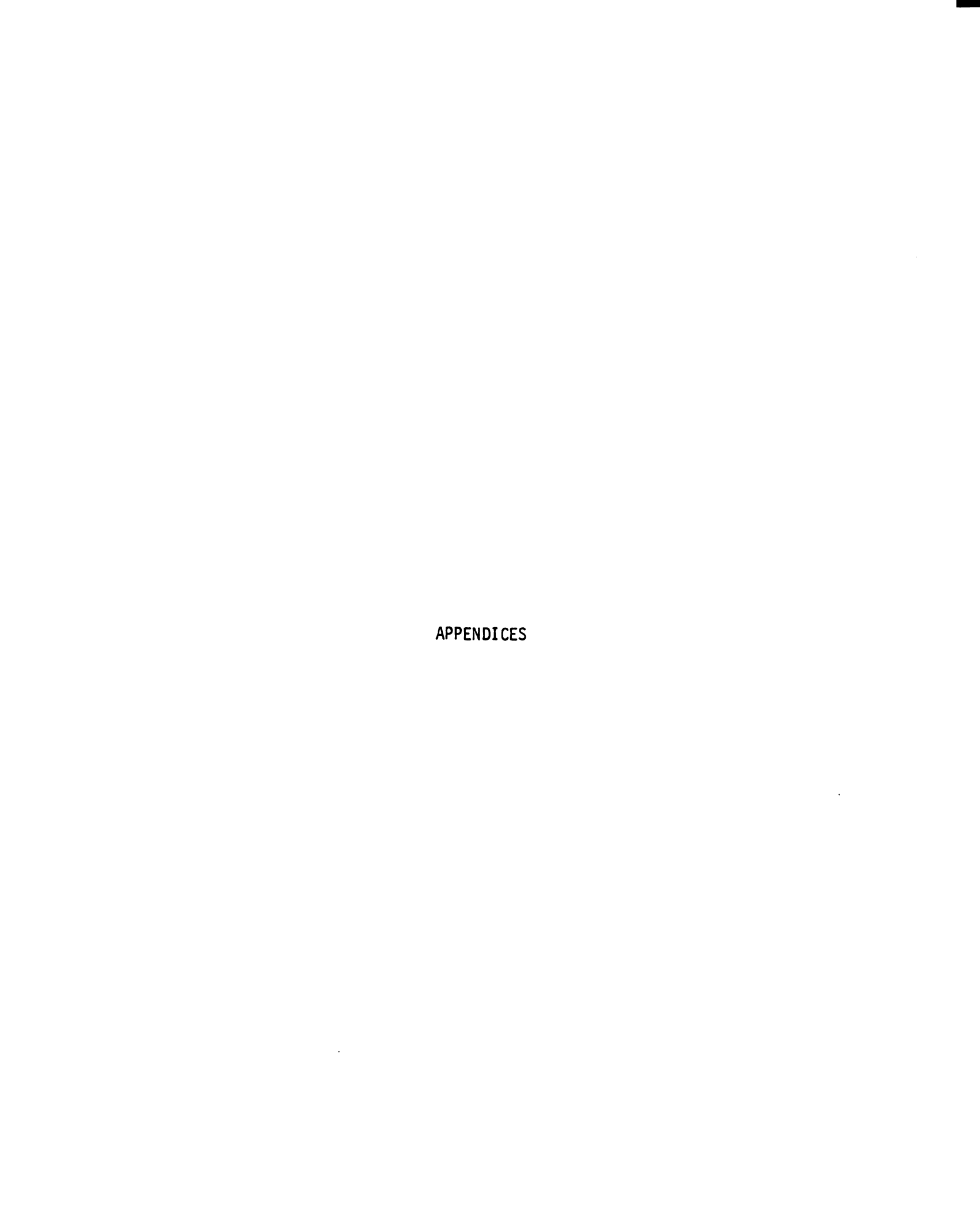
in the dashed resistivity curve in Fig. 3.5 is qualitatively similar to resistivity curves of spin glasses at low temperatures. This leads us to hypothesize the existence of some type of collective behavior of magnetic impurities. Although such magnetic interactions would be expected to be extremely weak, the large electron mean free path might allow the impurities to "see" each other at sufficiently low temperatures. Consider an impurity concentration of one part per billion. This implies a mean impurity seperation of ~1,000 atomic diameters or ~4,000 Å. This is much smaller than the ~1 mm mean free paths of the conduction electrons. At low enough temperatures the interaction energy may become greater than $k_{\rm R}T$. Then some type of collective behavior may be possible. Excitations of this system might be able to scatter the electrons and contribute a strong temperature dependence due to the freezing out of the higher energy excitations as the temperature is lowered in a manner analogous to the freezing out of the higher excitations of the collective motion of atoms in the lattice, i.e. the phonons. The shoulder in the resistivity would indicate a temperature where the longer range interactions were being destroyed by thermal energy leaving the temperature dependence of $\rho(T)$ to the traditional mechanisms we have discussed. At this point all one can say is that this behavior is interesting but requires much more work before more can be said. We do know that up till now no one has looked with such precision, at such low temperatures at samples of such high purity. Perhaps we should not be too surprised if we find the unexpected when we explore the previously inaccessible.

Summary and Conclusion

The work we have presented demonstrates with high precision the interplay of various scattering mechanisms with the temperature dependent part of the resistivity $\rho(T)$ at liquid He⁴ temperatures. It is the first investigation detailing precisely the strong effects of dislocation scattering on $\rho(T)$ at these temperatures. In addition, we have give substantial support to the predictions of Bergmann et al. concerning the origins of the T⁴ behavior of $\rho(T)$ as being due to the combination of electron-electron scattering and electron-phonon scattering. Of particular interest is the agreement of our data with their prediction that electron-electron scattering will increase with the introduction of dislocations as opposed to the already known $^{34}, ^{35}$ decrease of the phonon contribution. These predictions are based on the anisotropy of relaxation times in k-space which our data show plays a crucial role in determining the form of $\rho(T)$.

Finally, we have obtained good evidence in very pure copper for the isolation of the elusive T^2 electron-electron contribution to $\rho(T)$ by performing very precise measurements to ultra-low temperatures. In addition, we have uncovered some tantalizing new behaviors in silver and copper at the very lowest temperatures.





APPENDIX A

THERMOELECTRIC RATIO MEASUREMENTS ON STRAINED CU

When we made the series of measurements of electrical resistivity in the strained copper samples we also measured the thermoelectric ratio defined by

$$G = \frac{I}{\dot{O}}$$

where I is the current necessary to generate a sufficient voltage across the samples resistance to cancel the thermal voltage generated by the flow of heat Q along the sample. G is positive if I and Q are in the same direction. Figure A-1 - A-3 contain the data for samples Cull. CuAg2 and CuAg1 respectively, that is, in decreasing order of purity. Each figure contains all of the strainings. The common feature to all three samples is seen to be a value of G which increases with strain while showing a decreasing temperature dependence. Straight lines are drawn through the points in each case although in the more strained samples there is noticeable curvature even on the scale of these figures. Because the graphs do not include T = 0, the linear extrapolations to zero were calculated and are plotted in Figure A-4 which is a Nordheim-Gorter type of plot of G(T=0) vs. $^{1}/_{\rho_{0}}$. The actual values of ρ_{0} are along the top and ρ_0^{-1} along the bottom horizontal axis. Note, the "zero" intercept is on the right. This intercept determines the so called characteristic value of G for dislocations at T = 0. This value

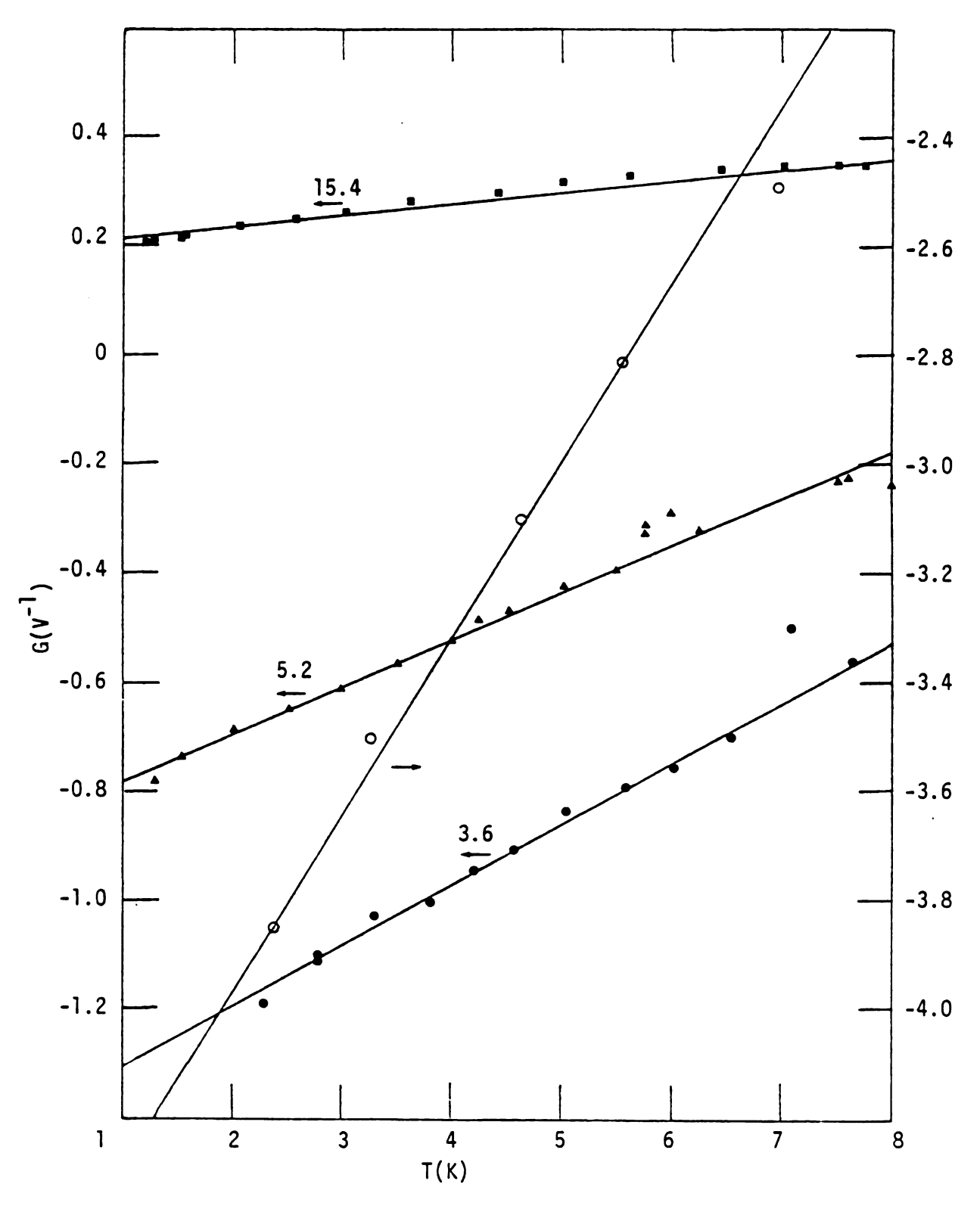
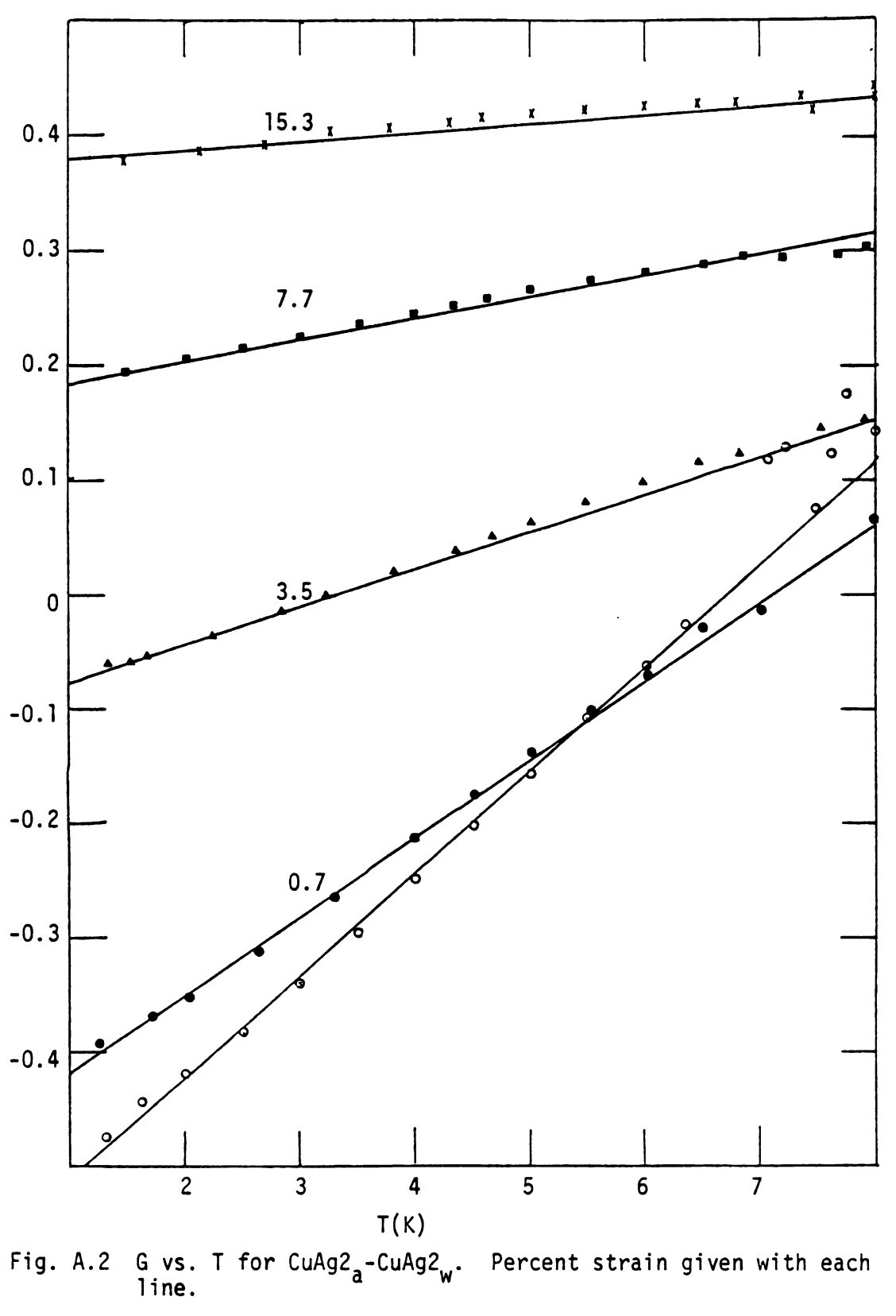


Fig. A.1 G vs. T for \underline{Cu} 11_a -Cu 11_u . Percent strain give with each line.

.



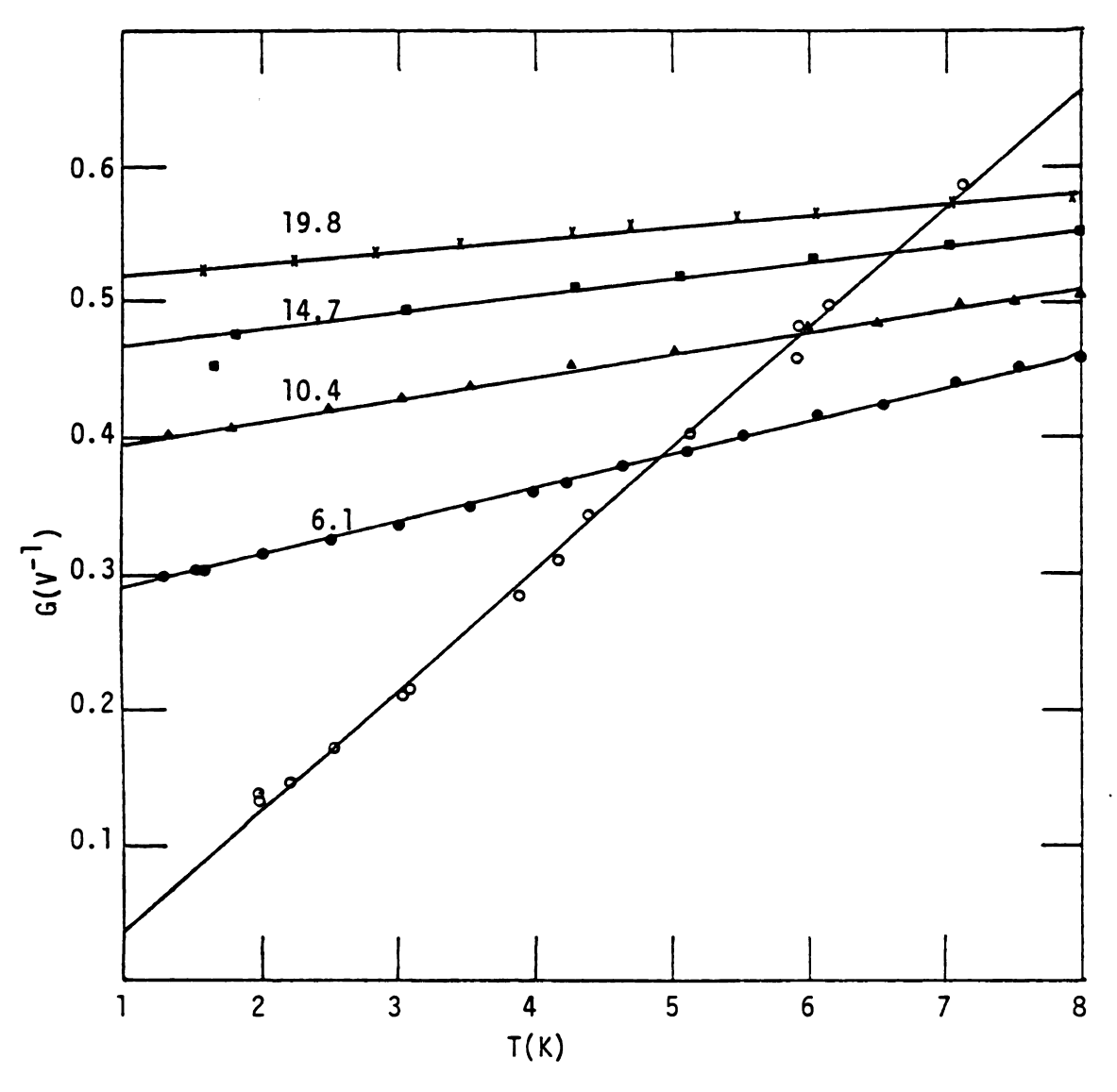


Fig. A.3 G vs. T for CuAgl_a-CuAgl_v. Percent strain given with each line.

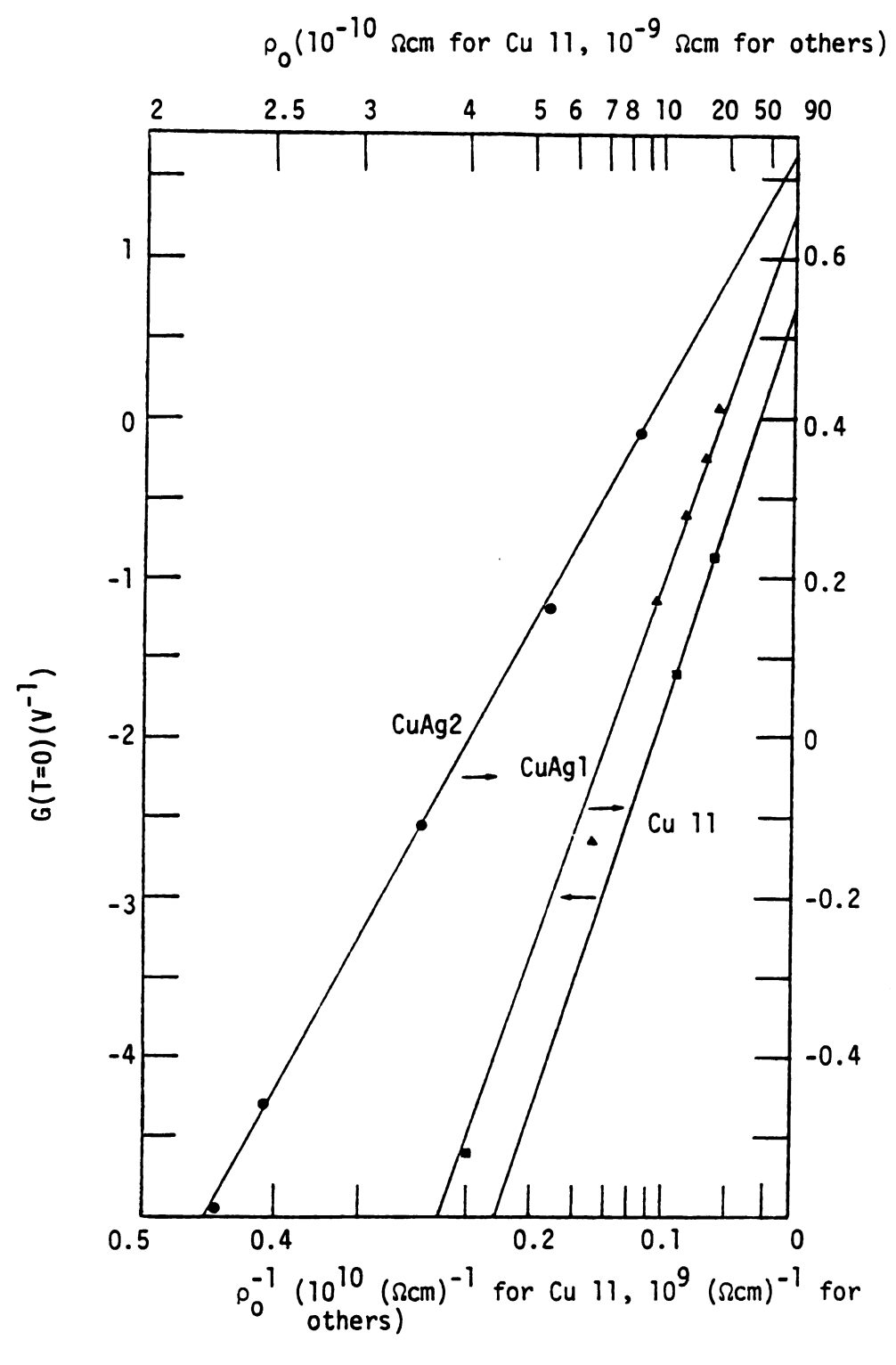


Fig. A.4 A Nordheim Gorter type of plot of ρ_0^{-1} vs. G(T=0). The horizontal axis has reciprocal ruling (note the zero on the right).

is $\sim +0.7 \text{V}^{-1}$ and is in agreement with that calculated from Pearson's 69 result for the characteristic thermopower S of dislocations in Cu by using the relation

$$S = GL_0T$$

where L_0 is the Lorentz ratio.

A similar plot (not shown) for the three annealed samples, allows us to determine the characteristic G for the Ag impurity in Cu and gives a value of $\sim +0.4 \text{ V}^{-1}$ at T = 4K. This is in fair agreement with the value 0.6 V⁻¹ calculated from determinations of the characteristic thermopower of Ag in Cu by Guenault.⁷⁰

APPENDIX B

DERIVATION OF USEFUL EXPRESSIONS FOR SUPERCONDUCTING TRANSFORMERS AND PARALLEL INDUCTORS USED IN SQUID CIRCUITS

The basic equation relating magnetic flux $\boldsymbol{\varphi}$ and current I in an inductor is

$$\phi = LI \tag{B.1}$$

where L is the inductance. We now apply this definition to the superconducting transformer connected to the SQUID signal coil (refer back to Fig. 2.3b for circuit diagram). We use the property of a closed superconducting circuit that the total magnetic flux enclosed remains constant. We assume initially it is zero for simplicity but this does not affect the validity of the derivation. Assuming no flux lines can link the primary and SQUID coils, the current I_T in the primary coil L_1 produces a flux through the secondary coil windings given by MI_T . Where M is the mutual inductance between the primary and secondary transformer coils. This must be cancelled by flux $(L_S + L_2)I_S$ generated in both L_S and L_2 by the induced current I_S so that the total flux is zero. This means

$$MI_T - (L_S + L_2)I_S = 0$$
 (B.2)

The current I_S induces a flux MI_S back in L_1 so that the net flux in L_1 is reduced and given by $L_1I_T - MI_S$. By Eq.(B.1) we define the effective inductance L_e at the primary terminals to be the net flux through the primary coil divided by the primary current. That is

$$L_{e} = \frac{L_{1}I_{T}^{-MI}S}{I_{T}}$$
 (B.3)

The definition of the mutual inductance in terms of a dimensionless constant called the coupling constant or coefficient of coupling is

$$M = k \sqrt{L_1 L_2}$$
 (B.4)

Using this definition and solving Eq.(B.2) for I_S in terms of I_T we obtain from Eq.(B.3)

$$L_{e} = L_{1} \left(1 - \frac{k^{2}L_{2}}{L_{S}^{+}L_{2}} \right)$$
 (B.5)

We want to maximize the ratio r of the current through the SQUID I_{S} to the total signal current I_{T} thus from Eqs.(B.2) and (B.4) we have

$$r = \frac{I_S}{I_T} = \frac{M}{L_S + L_2} = \frac{k \sqrt{L_2 L_1}}{L_S + L_2}$$
 (B.6)

This can be rewritten to eliminate L_1 using (B.5)

$$r = \sqrt{\frac{k^2 L_e L_2}{[L_s + L_2(1 - k^2)](L_s + L_2)}}$$
 (B.7)

We assume the value of $L_{\rm e}$ is fixed by the desired time constant of our measuring curcuit. $L_{\rm S}$ is also a fixed value. Thus the maximization condition is ${\rm dr/dL_2}$ = 0. Evaluating the derivative is straightforward an yields

$$\frac{dr}{dL_2} = \frac{r}{2} \left(\frac{1}{L_2} - \frac{a}{L_S + aL_2} - \frac{1}{L_S + L_2} \right)$$
 (B.8)

where $a = (1-k^2)$. The requirement that Eq.(B.8) be zero implies the quantity in parethesis vanishes. This allows us to solve for L_2^i the value of L_2 which will yield maximum r.

$$L_2' = \frac{L_S}{\sqrt{a}} = \frac{L_S}{\sqrt{1-k^2}}$$
 (B.9)

Now we can go back to find the corresponding value of L_1 , we solve Eq.(B.5) for L_1

$$L_{1} = \frac{L_{e}(L_{S} + L_{2})}{L_{S} + aL_{2}}$$
 (B.10)

Substituting L_2^1 for L_2 we get

$$L_1' = L_e \frac{L_S(1 + \frac{1}{\sqrt{a}})}{L_S(1 + \sqrt{a})} = \frac{L_e}{\sqrt{a}} = \frac{L_e}{\sqrt{1 - k^2}}$$
 (B.11)

Substituting L_1^1 and L_2^1 into the expression for r we find

$$r_{\text{max}} = \sqrt{\frac{L_e}{L_S}} \frac{k}{1 + \sqrt{1 - k^2}}$$
 (B.12)

Let us determine what the ratio $r' = I_S/I_T$ is if a shunting inductance is used to create the desired L_e . We refer to the circuit diagram of Fig. 2.3a. If I_T is the total signal current, it must divide into currents I_S through L_S and I_P . Since the two inductors form a closed superconducting loop we will require the total flux in the loop to be zero as before. This implies the magnitude of the flux generated in each coil must be the same or

$$L_{\varsigma}I_{\varsigma} = L_{p}I_{p} \tag{B.13}$$

Adding $\mathbf{L}_{p}\mathbf{I}_{S}$ to both sides we obtain

$$(L_p + L_S)I_S = L_pI_T \tag{B.14}$$

since $I_T = I_S + I_P$. Thus we find

$$r' = \frac{L_p}{L_p + L_s} = \frac{L_e}{L_s}$$
 (B.15)

Now we define the ratio of ratios r and r'

$$W = \frac{r}{r'} = \frac{I_S(transformer)}{I_S(choke)}$$
 (B.16)

If W > 1 the transformer would be mathematically superior to the parallel inductor although it might not be practically superior unless W >> 1. We immediately obtain

$$W = \sqrt{\frac{L_S}{L_e}} \frac{k}{1 + \sqrt{1 - k^2}}$$
 (B.17)

APPENDIX C

THERMOMETRY PROGRAM FOR HP67 PROGRAMMABLE CALCULATOR

Purpose:

The purpose of this program is to calculate the temperature given the resistance of a resistance thermometer $(R\rightarrow T)$ or to give the resistance corresponding to a given temperature $(T\rightarrow R)$. The latter case is simpler if the manufacturer has already done a calibration and given coefficients for the equation

$$\log R = \sum_{i=0}^{n} A_{i} (\log T)^{i}$$

Basic Method:

To do the T+R conversion the given polynomial is simply evaluated in the part of the program with Label B. Of course, for a given thermometer the proper coefficients and the order of the polynomial must be stored in the memory registers.

The R+T conversion requires finding the inverse function.

To do the R \rightarrow T conversion (which is the one usually desired in the laboratory) the program uses the last temperature calculated (initially it uses 4°) as a starting point to do a Newton-Raphson method of finding the zero of a function. The function being the difference between the actual resistance entered by the user and calculated resistance at the trial point $R(T_{last})$.

The general formula for the Newton Raphson method is $X_{i+1} = X_i - \frac{f(X_i)}{f'(X_i)} \text{ where } f \text{ is the function whose zero}$ is to be found, f' is its derivative. In this method $\left|f(X_{i+1})\right| < \left|f(X_i)\right| \text{ so by iteration one approaches zero.}$

We define $t \equiv \log T$, $r(t) = \sum_{i} A_{i}^{t}i$

Memory Allocations for the HP67.

0-9 hold the polynomial coefficients.

 $A \rightarrow n$ the order of the polynomial.

 $B \rightarrow log R$ the value of R entered from keyboard.

$$C \rightarrow \frac{df}{dt} = \frac{dr}{dt}$$
 where $f = r - \log R$, $t = \log T$.

 $D \rightarrow r(t)$ and $f = r(t) - \log R$.

 $E \rightarrow \log T \equiv t$.

I → current value of index.

<u>Operation</u>

Read in program card and appropriate data card. For cryocal #2844 thermometer the data includes the 10 coefficients and stores n=9 in memory A while storing log 4° in memory E.

To use for $R \rightarrow T$ conversion just enter thermometer resistance in ohms and push A. To use $T \rightarrow R$ conversion enter T, push B.

Below is the actual HP67 program which can be keyed in manually and stored on a magnetic card for future use.

Step	Code	Operation	Comment
001	312511	f LBL A	entry point A
002	3153	L06 ₁₀	
003	3312	STO B	
004	312503	LBL 3	
005	322211	65B a	call subroutine a
006	322212	65B b	call subroutine b
007	3413	RCL C	
800	3415	RCL E	<u> </u>
009	71	X	† ~
010	3414	RCL D	
011	3412	RCL B	
012	51		
013	3314	STO D	
014	51		
015	3413	RCL C	
016	81	<u>:</u>	
017	3315	STO E	
018	83	•	this is the test value
019	00	0	for convergence. Can be
020	08	8	changed if necessary
			· ·

HP67 Program cont'd.

Step	Code	Operation	Comment
021	3414	RCL D	
022	3564	ABS	
023	3281	X>Y	
024	2203	GTO 3	
025	3415	RCL E	
026	3253	10 ^X	
027	3422	RTN	
028	312512	LBL B	Entry point B
029	3153	log ₁₀	
030	3315	STO E	
031	322211	GSB a	
032	3414	RCL D	
033	3253	10 ^X	
034	3522	RTN	
035	322511	LBL a	subroutine entry point a
036	3411	RCL A	
037	3533	STI	٠
038	00	0	ine to calc
039	41	†	• • • • • • • • • • • • • • • • • • •
040	312501	LBL 1	. .
041	3424	RCL(i)	subroutine to calc
			v.

HP67 Program cont'd.

Step	Code	Operation	Comment
042	61	+	
043	3415	RCL E	
044	71	x	
045	3133	DSZ	
046	2201	GTO 1	
047	3400	RCO O	
048	61	+	
049	3314	STO D	
050	3522	RTN	***************************************
051	322512	LBL b	subroutine entry point b
052	3411	RCL A	
053	3533	STI	
054	00	0	
055	41	†	
056	312502	LBL 2	
057	3424	RCL(i)	
058	61	+	
059	3534	RCI	
060	41	†	
061	41	†	
062	01	1	

HP67 Program cont'd.

Step	Code	Operation	Comment
063	3251	X=Y	
064	2213	GTO C	
065	51		
066	81	:	-1
067	71	x	logR)
068	3415	RCL E	
069	71	x	calc. derivative
070	3133	DSZ	r
071	2202	GTO 2	
072	312513	LBL C	calc
073	3554	R∧	t ot
074	3313	STO C	Subrout.
075	3522	RTN	subr
076	84	R/S	

LIST OF REFERENCES

REFERENCES

- 1. W. E. Lawrence, Phys. Rev. B 13, 5316 (1976).
- J. E. Black, Can. J. Phys. <u>56</u>, 708 (1978).
- A. Bergman, M. Kaveh and N. Wiser, J. Phys. F 10, L71 (1980).
- D. Shoenberg and D. J. Roaf, Phil. Trans. Roy. Soc. <u>255</u>, 85 (1962).
- 5. J. M. Ziman, Adv. Phys. 10, 1 (1961).
- N. W. Ashcroft and N. O. Mermin, <u>Solid State Physics</u>, Holt, Rinehart and Winston, (1976).
- 7. J. M. Ziman, Phys. Rev. 121, 1320 (1961).
- 8. J. Kondo, Prog. Theor. Phys. <u>32</u>, 37 (1964).
- 9. F. J. Blatt, <u>Physics of Electronic Conduction for Solids</u>, McGraw-Hill, Inc., (1968).
- 10. J. S. Dugdale, <u>The Electrical Properties of Metals and Alloys</u>, Edward Arnold, (1977).
- 11. A. C. Ehrlich and J. T. Schriempf, Sol. State Commun. <u>14</u>, 469 (1974).
- 12. W. Royall and J. D. Gavenda, Phys. Rev. B 3, 3577 (1971).
- 13. M. Khoshnevisan, W. P. Pratt, Jr., P. A. Schroeder, S. D. Steenwyk, and C. Uher, J. Phys. F 9, L1 (1979).
- M. Khoshnevisan, W. P. Pratt, Cr., P. A. Schroeder, and S. D. Steenwyk, Phys. Rev. B 19, 3873 (1979).
- 15. E. R. Rumbo, J. Phys. F <u>6</u>, 85 (1976).

- 16. B. Barnard and A. D. Caplin, Commun. Phys. 2, L23 (1977).
- 17. A. J. Barber and A. D. Caplin, J. Phys. F 5, 679 (1975).
- 18. T. Dosdale and G. J. Morgan, J. Phys. F 4, L32 (1974).
- 19. Z. S. Basinski, J. S. Dugdale and A. Howie, Phil. Mag. 8, 1989 (1963).
- R. A. Brown, J. Phys. F <u>7</u>, L95 (1977).
 Ibid., 1283.
 Ibid., 1477.
- 21. V. F. Gantmakker, V. A. Gusparov, G. I. Kulesko, and N. N. Matveer, Sov. Phys. JEPT 36, 925 (1973).
- 22. Y. K. Chang and R. J. Higgins, Phys. Rev. B 12, 4261 (1975).
- 23. P. G. Klemens, Can. J. Phys. 34, 1212 (1956).
- 24. J. M. Ziman, Electrons and Phonons, Oxford University Press, (1960).
- 25. J.H.J.M. Ribot, J. Bass, H. VanKempen and P. Wyder, J. Phys. F <u>9</u>, L117 (1979).
- 26. B. Blumenstock, Ph.D. Thesis, Michigan State University (1980)
 Appendix.
- H. VanKempen, J. S. Lass, J.H.J.M. Ribot and P. Wyder, Phys. Rev. Lett. <u>37</u>, 574 (1976).
- 28. J. A. Rowlands, C. Durvury, and S. B. Woods, Phys. Rev. Lett. <u>40</u>, 1201 (1978).
- 29. B. Levy, M. Sinvani and A. J. Greenfield, Phys. Rev. Lett. <u>43</u>, 1822 (1979).
- 30. C. W. Lee, Ph.D. Thesis, Michigan State University (1980).
- 31. J. Bass, Adv. Phys. <u>21</u>, 431 (1972).
- 32. M. R. Cimberle, G. Bobel and C. Rizzuto, Adv. Phys. 23, 639 (1974).
- 33. M. Kohler, Z. Phys. 126, 495 (1949).

- 34. J. A. Rowlands and S. B. Woods, J. Phys. F (1976).
- 35. J. A. Rowlands and S. B. Woods, J. Phys. F 8, 1929 (1978).
- 36. M. Kaveh and N. Wiser, J. Phys. F 10, L37 (1980).
- 37. M. Kaveh and N. Wiser, Phys. Rev. Lett. 266, 35 (1971).
- 38. W. R. Cox and J. D. Gavenda, Phys. Rev. B <u>3</u>, 3577 (1971).
- 39. J. F. Kos, Phys. Stat. Sol. (b) 52, 389 (1972).
- 40. J. F. Kos, Can. J. Phys. <u>51</u>, 1002 (1973).
- 41. A. Bergman, M. Kaveh, and N. Wiser, Phys. Rev. Lett. <u>32</u>, 606 (1974).
- 42. A. D. Caplin and C. Rizzuto, J. Phys. C (London) 3, L117 (1970).
- 43. A. D. Caplin and C. Rizzuto, Aust. J. Phys. 24, 309 (1971).
- 44. M. R. Brett and J. E. Black, Can. J. Phys. <u>55</u>, 521 (1977).
- 45. A. Bergman, M. Kaveh, and N. Wiser, Sol. State Commun. <u>34</u>, 369 (1979).
- 46. D. H. Damon, M. P. Mathur, and P. G. Klemens, Phys. Rev. <u>176</u>, 867 (1967).
- 47. E. R. Rumbo, J. Phys. F <u>3</u>, L9 (1973).
- 48. T. Dosdale and G. J. Morgan, J. Phys. F <u>4</u>, 402 (1974).
- 49. C. A. Kukkonen and H. Smith, Phys. Rev. B <u>6</u>, 4466 (1972).
- 50. W. E. Lawrence and J. W. Wilkins, Phys. Rev. B <u>6</u>, 4466 (1972).
- 51. M. Kaveh and N. Wiser, Phys. Lett. 51A, 89 (1975).
- 52. P. Haussler and S. J. Wells, Phys. Rev. 152, 675 (1966).
- 53. J. F. Koch and R. E. Doezema, Phys. Rev. Lett. 24, 507 (1970).
- 54. D. Nowak and M.J.G. Lee, Phys. Rev. Lett. 1201 (1972).
- 55. H. Schmidt and E. Mann, Phys. Stat. Sol. (b) <u>94</u>, 95 (1979).
- 56. B. Lengeler, W. Schilling, and H. Wenzl, J. Low Temp. Phys. $\underline{2}$, 237 (1970).

- 57. J. S. Dugdale and Z. S. Basinski, Phys. Rev. 157, 552 (1967).
- 58. D. W. Terwilliger and R. J. Higgins, Phys. Lett. 31A, 316 (1970).
- 59. J. Imes, Ph.D. Thesis, Michigan State University, (1974).
- 60. J. L. Imes, G. L. Nieheisel, and W. P. Pratt, Jr., J. Low Temp. Phys. 21, 1 (1975).
- 61. O. U. Lounasmaa, <u>Experimental Principles and Methods Below 1 K</u>, Academic Press, Inc. (New York, 1974).
- 62. P. A. Schroeder and C. Uher, J. Low Temp. Phys. 29, 487 (1977).
- 63. D. L. Edmunds, W. P. Pratt, Jr., and J. A. Rowlands, Review of Scientific Instruments (in press).
- 64. R. P. Gifford, R. A. Webb and J. C. Wheatley, J. Low Temp. Phys. 6, 563 (1972).
- 65. R. L Powell, A. F. Clark and R. R. Fickett, Phys. Kondeno Materie 9, 104 (1969).
- 66. F. R. Fickett, Mat. Sci. Engr. <u>14</u>, 119 (1974).
- 67. Y. Yaeli and S. G. Lipson, J. Low Temp. Phys. 23, 53 (1976).
- 68. A. A. Lukkvich and A. S. Kovolich, Phys. Met. Metall. <u>45</u>, 161 (1979).
- 69. W. B. Pearson, Phys. Rev. 119, 549 (1960).
- 70. A. N. Guenault, <u>Thermoelectricity in Metallic Conductors</u>, ed.
 F. J. Blatt and P. A. Schroeder (Plenum Press, New York, 1978)
 p. 39.